ILLUMINATING MECHANISMS OF NUCLEAR AND MITOCHONDRIAL HEME DYNAMICS

A Dissertation Presented to The Academic Faculty

By

Mathilda M. Willoughby

In Partial Fulfillment
Of the Requirements for the Degree
Doctor of Philosophy in the
School of Chemistry and Biochemistry

Georgia Institute of Technology
August 2023

ILLUMINATING MECHANISMS OF NUCLEAR AND MITOCHONDRIAL HEME DYNAMICS

Approved by:

Dr. Amit Reddi, Advisor
School of Chemistry and Biochemistry
Georgia Institute of Technology

Dr. Raquel Lieberman
School of Chemistry and Biochemistry
Georgia Institute of Technology

Dr. Loren Williams
School of Chemistry and Biochemistry
Georgia Institute of Technology

Dr. Matthew Torres
School of Biological Sciences
Georgia Institute of Technology

Dr. Adegboyega Oyelere
School of Chemistry and Biochemistry
Georgia Institute of Technology

Date Approved: June 20, 2023

ACKNOWLEDGEMENTS

This work would not have been possible without the support, advice, and patience of my advisor Professor Amit R. Reddi. The author would also like to thank her thesis committee members, Professors Loren Willliams, Raquel Lieberman, Adegboyega Oyelere, and Matthew Torres, for their unwavering support and encouragement.

The author would also like to acknowledge past and current Reddi Lab Group members. They have provided immense and valuable feedback and support both inside and outside of the lab. In addition, she is thankful for the lifelong friendships she has made throughout this time.

Last, this work could not have been completed without the encouragement and moral support from her husband, Matthew Richardson, and parents, Ross and Mary Ellen Willoughby.

TABLE OF CONTENTS

LIST OF TABLES

LIST OF FIGURES

LIST OF SYMBOLS AND ABBREVIATIONS

*A*600	Absorbance units at 600 nanometers
AD	Alzheimer's Disease
ALA	5-aminolevulinic acid
ALAD	Aminolevulinic acid dehydratase
ALAS	Aminolevulinic acid synthase
AMP	Ampicillin
ANOVA	Analysis of variance
ARV1	ARE2 Required for Viability
AS	Ammonium Sulfate
ATCC	American Type Culture Collection
Aβ	Amyloid Beta
BMH2	Brain Modulosignalin Homolog
BY4741	Strain of *Saccharomyces cerevisiae*
C. elegans	*Caenorhabditis elegans*
Ccs1	Copper chaperone
CIP	Alkaline Phosphatase, Calf Intestinal
CISDY	ECFP-IsdX1-Linker-ISD-EYFP
CL	Cardiolipin
Cnm1	Contact nucleus mitochondria
CO	Carbon monoxide
CPOX	Coproporphyrinogen oxidase

CRZ1	Calcineurin-responsive zinc finger
Ctt1	Catalase
Cyt b_{562}	Cytochrome b_{562}
Cyto	Cytosol
Dap1	Damage response protein
DFP-rhodol	Deoxygenated difluoropiperidine-rhodol
DMSO	Dimethyl sulfoxide
DNA	Deoxyribonucleic acid
Dnm1	Dynamin-related GTPase
E. coli	*Escherichia coli*
eCFP	Enhanced cyan fluorescent protein
eGFP	Enhanced green fluorescent protein
ER	Endoplasmic Reticulum
Erg	Ergosterol
ERMES	ER-mitochondria encounter structure
EV	Empty Vector
eYFP	Enhanced yellow fluorescent protein
FABS	Fatty acid binding protein
FDR	False Discovery Rate
FECH	Ferrochelatase
fL	femtoliters
FLVCR	Feline Leukemia Subgroup C Cellular Receptors

FRET	Fluorescence resonance energy transfer
G418	Geneticin
GAPDH	Glyceraldehyde 3-phospate dehydrogenase
Gem1	GTPase EF-hand protein of Mitochondria
GO	Gene Ontology
GPD	Glycerol-3-phosphate dehydrogenase
GSH	Reduced glutathione
GSH-S	Glutathione S-transferase
H_2O_2	Hydrogen peroxide
Hap1	Heme activator protein
Hb	Hemoglobin
HBP	Heme binding protein
Hem15	Ferrochelatase
H-FluNox	Small Molecule Heme Sensor
HMC	High Molecular Weight Complex
Hmx1	Heme oxygenase 1
HO	Heme oxygenase
HPLC	High-Performance Liquid Chromatography
HRG	Heme responsive gene
HS1	Heme Sensor 1
HS1-M7A	Heme Sensor Mutant M7A
HS1-M7A-bisALA	Heme Sensor Mutant M7A, H102A
HXT11	HeXose Transporter

IM	Inner membrane
IMS	Inner membrane space
Isd	Iron-regulated surface determinant
JMP	John's Macintosh Project
KAN	Kanamycin
KanMX4	Gene marker for selection of library deletion mutants
K_d	Dissociation constant
kDa	Kilo Daltons, protein molecular weight units
L	Liter
LB	Lysogeny Broth
LEU	Leucine
LH	Labile heme
LRO	Lysosome-Related Organelle
MAMs	Mitochondrial associated membranes
MAPR	Membrane-associated progesterone receptor
MCS	Membrane Contact Site
Mdm	Mitochondrial Distribution and Morphology
MEF	Mouse embryo fibroblast
MFS	Major facilitators superfamily
mg	Milligrams
Mgm1	Mitochondrial Genome Maintenance
MICOS	Mitochondrial Contact Site and Cristae Organizing System

Mito	Mitochondria
Mito-ER	Mitochondria-Endoplasmic Reticulum
Mito-Nuc	Mitochondria-Nucleus
Mkate2	Monomeric Katushka 2
mL	Milliliter
Mmm1	Maintenance of Mitochondrial Morphology
MRP	Multidrug resistance protein
NADPH	Nicotinamide adenine dinucleotide phosphate
NAT	Nourseothricin Sulfate
nm	Nanometer
nM	Nanomolar
NOS	Nitric oxide synthase
NPC	Nuclear Pore Complex
Nuc	Nucleus
OD	Optical Density
OD_{600}	Optical Density at 600 nm
OE	Over Expression
OM	Outer membrane
ORF	Open reading frame
PAGE	Polyacrylamide Gel Electrophoresis
PANTHER	Protein analysis through evolutionary relationships
PBG	Porphobilinogen
PBGD	Porphobilinogen deaminase

PBS	Phosphate buffered saline
PC	Phosphatidylcholine
PCBP1	Poly(rC)-binding protein
PCR	Polymerase Chain Reaction
PE	Phosphatidylethanolamine
P. falciparum	*Plasmodium falciparum*
PGRMC	Progesterone membrane receptor component
PIK	Phosphatidylinositol
PMSF	Phenylmethylsulfonyl fluoride
PPIX	Protoporphyrin IX
PPOX	protoporphyrinogen oxidase
PUT	Proline utilization
R_{max}	EGFP/mKATE2 ratio when 100 % of sensor is heme bound
R_{min}	EGFP/mKATE2 ratio when 0 % of sensor is heme bound
RNA	Ribonucleic acid
ROS	Reactive oxygen species
RPL8A	Ribosomal Protein of the Large subunit
S. cerevisiae	*Saccharomyces cerevisiae*
SA	Succinylacetone
SC	Synthetic complete medium
SCE	Synthetic complete medium with ergosterol and tween

SDS	Sodium dodecyl sulfate
SOD1	Superoxide Dismutase
Tango	Transport and golgi organization 2 homolog
TCA	Tricarboxylic acid cycle
TEF	Translation elongation factor
uL	microliter
uM	micromolar
UPLC	Ultra High-Performance Liquid Chromatography
UROD	Uroporphyrinogen decarboxylase
UROS	Uroporphyrinogen synthase
W303	Strain of *Saccharomyces cerevisiae*
WGS	Whole Genome Sequencing
WT	Wild type
Yet3	Yeast Endoplasmic Reticulum Transmembrane Protein
YPD	Yeast extract peptone dextrose
YPDE	Yeast extract peptone dextrose with ergosterol and tween
YPL+	Yeast Protein Localization Plus
Δ	Gene Deletion or Knock Out

SUMMARY

Heme is an essential yet inherently cytotoxic metallocofactor. In the field, heme has traditionally been viewed as a static cofactor, buried in enzymes. The development and availability of new technologies and unique sensors has created opportunities to understand the role of heme, its complex dynamics, and its broader role as a signaling molecule. Indeed, heme must be safely mobilized from sites of synthesis or uptake to target proteins across the cell.

Heme is a potentially toxic, hydrophobic, and pro-oxidative molecule. This necessitates the cell tightly regulates heme (synthesis, uptake, trafficking, degradation, and export) to limit detrimental interactions with off-target proteins and membranes. However, molecules and mechanisms that regulate intracellular heme bioavailability (transport, trafficking) to and within virtually every subcellular compartment are not well understood.

Herein, this thesis combines the use of fluorescent heme sensors, genetic screens, and biochemical techniques to identify and characterize heme trafficking factors that control heme bioavailability. Doing so will enhance our understanding of heme implications in diseases such as Alzheimer's, Anemias, Porphyrias, Cardiovascular, and Cancers, and the development of better and improved therapies.[1]

This comprehensive work integrates fluorescent heme sensors and genetics to probe the labile heme pool to identify and elucidate heme trafficking and heme homeostasis pathways. Specifically, we aim to further elucidate 1)

factors that aid in mitochondrial heme export, 2) factors that regulate steady-state nuclear heme availability, and 3) the relationship between heme utilization and bioavailability.

CHAPTER 1. INTRODUCTION

Heme (iron protoporphyrin IX) is an essential, yet potentially toxic cofactor, signaling molecule, and nutrient, essential for virtually all aerobic life (Figure 1).[2] Having Lewis acidity, redox activity, and hydrophobicity, this multi-faceted cofactor enables a diverse array of critical cellular functions; including electron transfer, catalysis, and gas transport.[3, 4] Interestingly, the same characteristics that are attributed to heme's essentiality and versatility also render it potentially toxic.

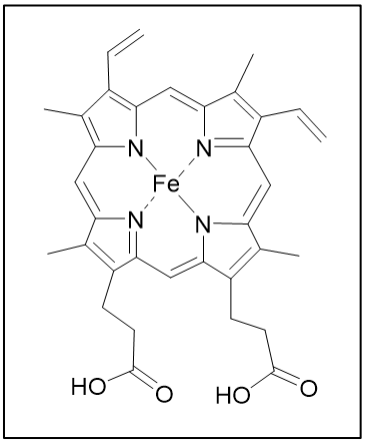

Figure 1. Heme b Chemical Structure. Heme b is the most common form of heme. Figure was generated using ChemDraw.

The redox activity and hydrophobicity of heme potentiates its ability to disrupt membrane structure, associate with and alter function of off-target proteins, and catalyze deleterious redox reactions.[4-7] In fact, defects in heme homeostasis have been implicated in several significant diseases; including cancers, neurodegenerative and cardiovascular diseases, and anemias.[1] To mitigate toxicity, the cell has developed mechanisms to manage harmful heme biosynthetic precursors and heme mobilization/trafficking. However, the molecules and

mechanisms that regulate heme bioavailability (transport, trafficking) to and within virtually every subcellular compartment are not well understood. Therefore, there is an immediate need to enhance our understanding of the mechanisms of heme trafficking and regulation. In this chapter, we will discuss a brief review of heme, its roles in cell biology and pathology, potential heme trafficking pathways, and tools to study heme bioavailability.

1.1 Heme in Cell Biology

There are four different types of heme in eukaryotes: *Heme a, heme b, heme c,* and *heme o* (Figure 2). They all contain an iron center within a porphyrin ring, however, they differ in their side chains on the ring.[2] Heme b is the most common and abundant form. Most notably, heme b is tightly bound to globins to aid in oxygen transport. *Heme a* is a cofactor in cytochrome c oxidase, an important respiratory enzyme.[2] *Heme o* is similar to *heme a* in structure but is only found in *Escherichia coli*.[2] *Heme c* is unique in that it forms a covalent interaction to hemoproteins via a thioether linkage in cytochrome c and the cytochrome bc1 complex.[2] This work is focused on protoheme (*heme b*), the most abundant form.

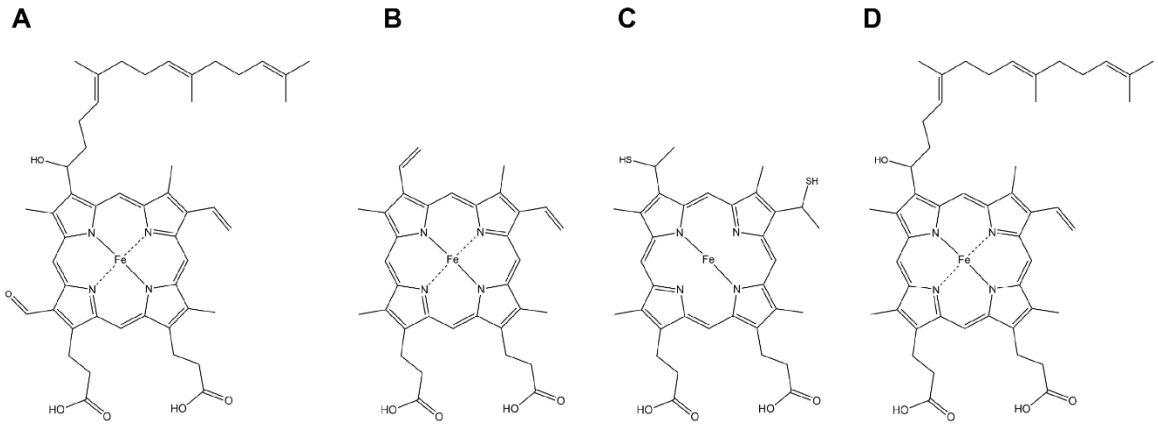

Figure 2 – Structures of Different Types of Heme. (A) Heme a, **(B)** Heme b, **(C)** Heme c, **(D)** Heme o. Figures generated using ChemDraw.

Eukaryotic heme synthesis is a highly conserved eight enzymatic-step pathway (The Shemin Pathway) and takes place between the cytosol and mitochondria.[8] The pathway begins with the condensation of glycine with succinyl-coenzyme A to produce aminolevulinic acid (ALA).[8] ALA is then exported to the cytosol for the following four steps. The final cytosolic step produces coproporphyrinogen III, which is then trafficked back into the mitochondria for the remaining biosynthetic steps. The final step is the insertion of Fe^{2+} into protoporphyrin IX (PPIX) by ferrochelatase (FECH) to produce heme b within the mitochondria matrix (Figure 3a).

Heme degradation is aided by heme oxygenase (HO). HO catalyzes the catabolism of heme into biliverdin, carbon monoxide (CO) and free iron. This reaction is oxygen-dependent and begins with the formation of a ferric heme-HO complex. In this state, the heme iron center is reduced by an electron donated from NADPH-cytochrome P450 reductase. Molecular oxygen then binds and

stabilizes the complex as the iron gains another electron and proton from cytochrome P450 and water, respectively, forming a hydroperoxide intermediate. Finally, the hydroperoxide oxygen attacks the alpha-carbon of the porphyrin ring forming biliverdin. Biliverdin is quicky converted to bilirubin by biliverdin reductase and acts in signaling (Figure 3b).[9]

Heme b is an essential cofactor for all aerobic life and is present in almost every subcellular compartment. Heme b has unique properties and can act as a cofactor, signaling molecule, and nutrient. As a protein cofactor, heme facilitates gas transport, electron transfer, and catalysis.[3, 4] For example, heme b in globins aids in oxygen transport, and heme b in cytochromes and P450s enable electron transfer.[3, 4] As a signaling molecule, transient heme binding can regulate proteins; including transcription factors, ion channels, kinases, and cell surface receptors, altering their expression, activity, or both.[10] Heme's role as a cofactor is well-studied, while heme as a signaling molecule is less understood.

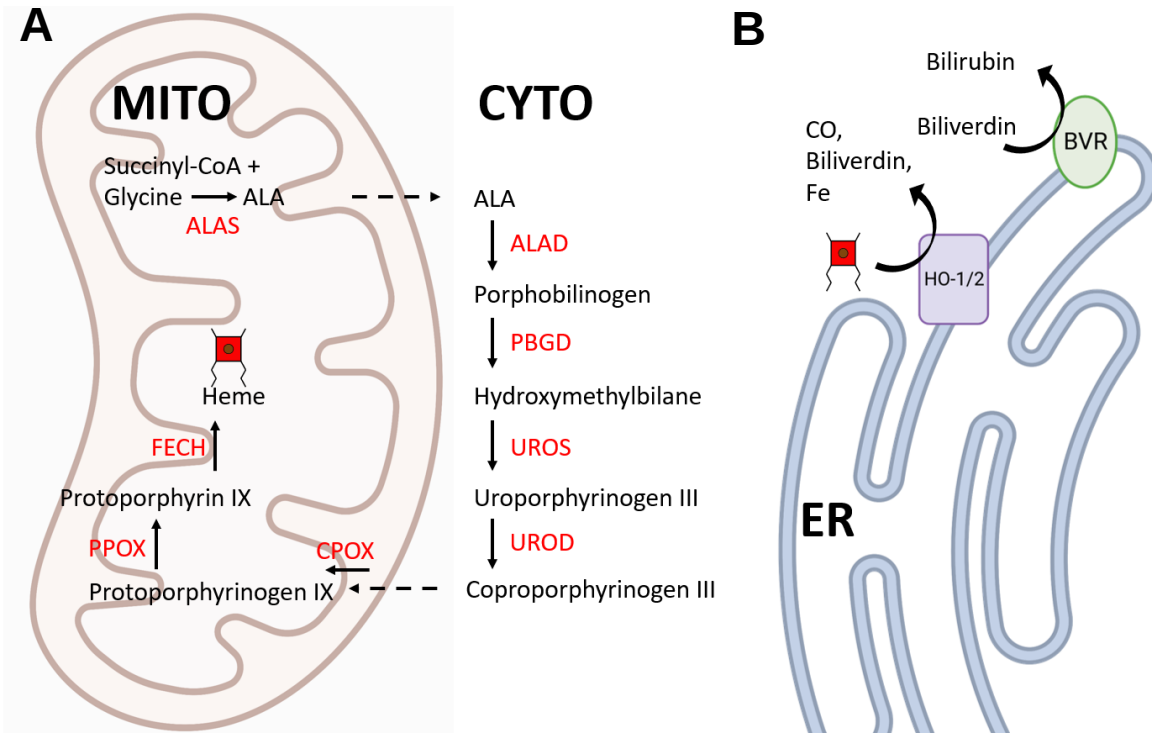

Figure 3. Heme biosynthesis and degradation in eukaryotes. (A) Heme is synthesized in eukaryotes via a highly conserved eight enzymatic step pathway called the Shemin pathway. This pathway occurs in the cytosol and mitochondria where heme is ultimately formed in the mitochondria matrix. ALAS = 5-aminolevulinic acid (5-ALA) synthase; ALAD = 5-ALA dehydratase; PBGD = porphobilinogen deaminase; UROS = uroporphyrinogen synthase; UROD = uroporphyrinogen decarboxylase; CPOX = coproporphyrinogen oxidase; PPOX = protoporphyrinogen oxidase; FECH = ferrochelatase. **(B)** Heme degradation in eukaryotes is facilitated by heme oxygenase (HO) enzyme. HO catalyzes the heme breakdown forming biliverdin, carbon monoxide (CO) and free iron. Figure was generated using BioRender and Adobe Illustrator.

1.2 Heme Mobilization and Trafficking

To begin to understand heme as a signaling molecule, we must first understand its bioavailability in the cell. In biology, heme exists in two pools: 1) an exchange inert heme pool, and 2) an exchange labile (bioavailable) pool.[11] Exchange inert heme is tightly bound to proteins and is kinetically inaccessible, while exchange labile heme is kinetically accessible and dissociable.[11] These two heme pools must be regulated to limit potential heme toxicity.

The cell has evolved mechanisms to regulate heme homeostasis. Heme concentration is tightly regulated by synthesis and degradation processes. However, mechanisms governing heme trafficking and incorporation into apo-hemoproteins following heme synthesis or cellular import at the plasma membrane are less understood. Since heme is made on the matrix side of the mitochondria inner-membrane, heme must traverse mitochondria inner- and outer-membranes for subsequent availability to the rest of the cell and delivery to apo-hemoproteins (Figure 4). Hemoproteins are all throughout the cell, including cytochromes in the mitochondria, globins in the cytosol, P450s in the ER, NADPH oxidases at the plasma membrane, and heme-regulated transcription factors in nucleus. How heme is mobilized or trafficked to these different locations is not fully understood (Figure 4).

To investigate heme regulation, we as scientists must appreciate that heme displays dual characteristics both as a transition metal and a lipid. As a result, heme trafficking may mimic that of a metal, a lipid, or a combination. Like metals, heme could be trafficked via chaperones, buffers, and transporters. For example, the progesterone membrane receptor component 1/2 (PGRMC1/2) acts as heme chaperone by accepting heme from FECH facilitating mitochondria heme export.[12] Mobilization as a lipid would require trafficking via membrane tethering complexes (ER-mitochondria encounter structure, ERMES, or mitochondria associated membranes, MAMs), lipid transfer proteins, vesicles, or organelle contact points.[2, 10, 13] These well-known pathways for lipid and metal trafficking can help researchers glean on heme trafficking and regulation throughout the cell,

beginning with its export from the mitochondria following synthesis, and further, its trafficking and availability within the nucleus. Some of the putative heme transporters and chaperones are displayed in Figure 3 and are discussed below.

1.2.1 Heme in the Nucleus

As mentioned, heme acts as a signaling molecule affecting an array of cellular activities. In the nucleus, heme regulates gene transcription by binding to transcription factors eliciting activation or inhibition. Heme signaling in this context can affect various cellular functions, including iron homeostasis, circadian rhythms, apoptosis, and cell proliferation.[10] For example, heme binds to and activates the transcription factor Hap1p, turning on genes involved in respiration.[14] Heme also interacts with transcription repressors: Bach1, Rev-erb, and p53, where upon heme binding, either destabilizes the complex, or elicits nucleolar export and/or degradation.[15-17] To regulate these critical processes, heme in the nucleus must be available for when it is needed.

1.2.2 Heme Transporters

Although heme has lipophilic properties, its carboxylate side chains limit its diffusion across membranes. Therefore, there is a need for heme transporters to aid in traversing membranes. Several heme transporters have been identified, including Feline Leukemia Subgroup C Cellular Reporters (FLVCR), heme responsive genes HRG1 and HRG4, and the multidrug resistance proteins (MRPs).[18-20] FLVCR proteins are members of the Major Facilitator Superfamily (MFS). Two splice variants of the FLVCR proteins, FLVCR1b and FLVCR1a, have

been identified in mitochondria heme export and heme import at the plasma membrane, respectively. These transporter proteins have transmembrane domains where FLVCR1a has twelve hydrophobic domains (an amount common among MFS proteins), while FLVCR1b has six predicted transmembrane domains.[21, 22] FLVCR protein expression is abundant in the brain, liver, kidney, and bone marrow of mammals.[18] Particularly, FLVCR1b is critical for erythroid differentiation presumably enabling mitochondrial heme export and delivery to globins.[18]

MRP5 is another heme transporter that was first identified in *C. elegans* critical for heme export from intestines.[20] *C. elegans* is a heme auxotroph and relies on heme uptake mechanisms to acquire heme from the environment. Heme distribution throughout the organism is dependent on export from the intestine which is an essential function performed by the MRP5 heme transporter.[20] Two additional heme transporters first identified in *C. elegans* are heme responsive genes 1 and 4 (HRG-1 and HRG-4). HRG-1 is localized to endosomal and lysosomal membranes and transports heme to the cytosol.[23] HRG-4 aids in heme uptake across the plasma membrane into the cytosol.[19]

1.2.3 Heme Buffers

In cells, the cytosol has the highest concentration of labile heme (ranging from 20 – 340 nM) compared to the nucleus and mitochondria.[24-27] Therefore, cytosolic labile heme is probably buffered by proteins to mitigate cytotoxicity. To date, several proteins have been identified as heme binding proteins and are

proposed to regulate heme homeostasis; including heme binding proteins HBP22 and HBP23, GAPDH, glutathione S-transferase (GSH-S transferase), fatty acid binding proteins (FABS), and heme oxygenase-2 (HO-2).[28-33]

HO-2 and GAPDH were recently identified as heme buffering factors. HO-2 is constitutively expressed in humans. Rather than performing its canonical heme degradative role, researchers found that HO-2 binds and buffers heme. In the absence of excess heme, they propose HO-2 regulates heme homeostasis by acting as a heme buffering factor and controls heme bioavailability.[33]

GAPDH is unique in that it is the only cytosolic protein that has been identified to bind, buffer, and traffic/deliver heme to downstream targets. In mammalian cells, GAPDH is required for heme delivery to nitric oxide synthase (NOS).[34] In Baker's yeast, GAPDH buffers cytosolic heme and regulates heme availability in the nucleus.[30]

1.2.4 Heme Chaperones

Chaperones are proteins that specifically bind and deliver small molecules or cofactors to other protein recipients. For example, Poly(rC)-binding protein (PCBP1) is metallochaperone that binds and delivers iron to the storage protein ferritin.[35] CCS1 is a protein that specifically binds and delivers copper to the Cu/Zn superoxide dismutase (SOD1) enzyme.[36, 37] Similarly, heme chaperones also exist. Progesterone Receptor Membrane Components 1 and 2 (PGRMC1/2) have been recently identified as putative heme chaperones. PGRMC1 is a heme-binding proteins and it interacts with Ferrochelatase, the terminal heme

biosynthesis enzyme, in the heme metabolon. Interestingly, PGRMC1 preferentially interacts with FECH in the “product release” conformation, and it can transfer heme to apo-proteins including cytochrome b_5. Together, this evidence highlights PGRMC1’s potential as a heme chaperone.[12]

A second isoform of PGRMC, PGRMC2, has been recently identified as a heme chaperone. As a resident ER protein, Galmozzi, et al. showed PGRMC2 is critical for heme delivery to the nucleus in adipocytes. They hypothesize PGRMC2 acquires heme from PGRMC1 to facilitate heme trafficking from the mitochondria, through the ER, and to the nucleus to affect gene transcription.[38]

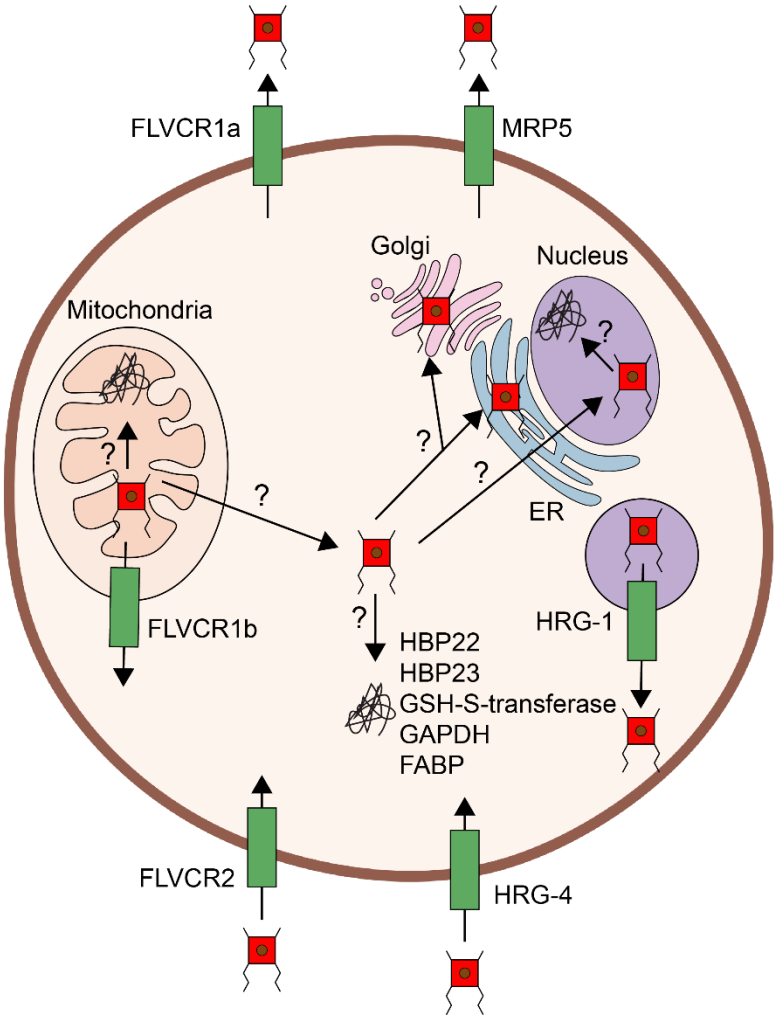

Figure 4 – Comprehensive Model of Heme Transport and Trafficking Pathways. Following heme synthesis in the mitochondria, heme must be exported and trafficked and incorporated into hemoproteins all throughout the cell. Trafficking to various locations involves transporters and chaperones. Unknown intracellular trafficking pathways are marked with a question mark. Putative transporters are labelled above at their predicted cellular location and marked as green cylinders. Their direction of transport is denoted by arrows. Putative heme buffering factors are listed as well. Figure was generated using BioRender and Adobe Illustrator.

1.3 Heme in Pathology

Heme is an essential molecule yet can also be cytotoxic. Heme's versatility and cytotoxicity are due to the same unique chemical properties such as its redox

active iron center and hydrophobic porphyrin ring. Due to these characteristics, heme has the potential to cause deleterious harm in several disease contexts.

In sickle cells and malaria, incredible amounts of toxic heme are released. This heme can cause blood vessel blockage, resulting in painful sickle cell ischemic episodes.[39] The amounts of heme released are too much for HO-mediated heme degradation to overcome. The heme toxicity stems from its ability to catalyze peroxidation reactions and hydroxyl radical production via Fenton chemistry.[40] These harmful redox reactions generate reactive oxygen species that can perpetuate lipid oxidation, DNA damage, apoptosis, and protein degradation and aggregation.[40] Apart from its redox activity, heme can aggregate with membranes, altering their structure and permeability.[7] Further, the heme released in malaria infections can alter immune function and trigger sepsis.[41, 42]

Further, mis-regulated heme can contribute to disease states through inappropriate protein interactions. In Alzheimer's Disease (AD), heme can interact with and be sequestered by amyloid-beta (Aβ) plaques, the protein that causes AD. As a result, cells react as if they are heme starved, and heme synthesis is upregulated.[5] Further, heme-Aβ complexes exhibit peroxidase activity, resulting in oxidative damage to macromolecules. Recent data describe heme and hemoglobin decrease Aβ-mediated expression of pro-inflammatory cytokines in astrocytes.[6] In cancer, heme interacts with the tumor suppressor protein, p53p, and promotes p53 nuclear export and p53 proteasomal degradation in the cytosol.[17]

Other heme-related pathological conditions are associated with heme synthesis and belong to a family of disorders called porphyrias. Deficiencies in any of the eight heme biosynthetic enzymes are associated with eight distinct types of porphyria. Defects in any of these heme biosynthetic enzymes lead to the accumulation of photo-sensitive porphyrin intermediates that result in skin lesions on the patient.

Another example of heme pathology is in the context of infectious diseases. Pathogenic bacteria have sophisticated pathways to satisfy their iron requirements. For example, bacteria can siphon iron from human hosts using siderophores. However, in humans, heme represents the major form of iron. Taking advantage of this, bacteria have evolved to use heme as an iron source and have established unique heme uptake and degradation pathways to survive.[25] These specific heme acquisition pathways can be studied, and heme-based therapeutics may be designed.

1.4 Probing the Labile Heme Pool

The insufficient knowledge regarding heme trafficking has been primarily due to the lack of tools to provide adequate molecular specificity, spatial and temporal resolution, and sensitivity. Current approaches towards studying heme trafficking include traditional biochemical assays. These approaches utilize HPLC, affinity chromatography, or mass spectrometry to identify heme trafficking factors based on the heme-binding ability.[43, 44] Identifying heme-binding proteins in this fashion may give false positive results. Due to heme's hydrophobic properties, it

easily associates with hydrophobic pockets of proteins regardless of if it is a true heme binding protein. A genetics approach is an additional tool to study heme trafficking. In this approach, a variety of heme-dependent processes are measured in gene deletion mutants and compared to a wild type where all genes are present.

A powerful tool to study labile heme is the use of heme sensor probes. Heme probes such as hemoprotein peroxidase reporters, small molecule heme probes, and fluorescent sensors have been reported to probe heme in several contexts and organisms.[45-47]

Enzymatic peroxidase-based reporters have been developed to study subcellular heme distribution. A horseradish peroxidase reporter has been recently developed, where enzymatic activity of the reporter is dependent on heme. This robust reporter is genetically encoded and can be targeted to different compartments.[45]

A second approach to study heme is the use of small molecule fluorescent probes. These probes are activity-based fluorescent probes that can monitor fluctuations of labile heme. For example, H-FluNox is a probe that detects labile heme using biomimetic N-oxide deoxygenation (heme dependent reaction) which produces DFP-rhodol, a fluorescent molecule.[46]

Further, several FRET-based sensors have also been reported. The CISDY sensor developed by Song, et al. contains heme binding domains, IsdX1 and IsdC, and ECFP and EYFP fluorescent proteins at the N- and C-termini, respectively.[48]

This probe is designed such that heme binding induces heterodimerization of IsdX1 and IsdC, resulting in an increase in the FRET efficiency between ECFP and EYFP.[48] Similarly, quenched fluorescence heme reporters have also been designed. The CHY biosensor developed by Abshire et al. was designed to study labile heme in the malaria parasite, *Plasmodium falciparum* (*P. falciparum*). CHY contains a heme binding domain rich with Histidine residues flanked by ECFP and EYFP FRET pairs. In the apo state, this sensor exhibits FRET. However, when bound with heme, FRET energy transfer from the donor is quenched.[47]

1.4.1 First Generation Heme Sensor 1 (HS1)

Our lab has developed ratiometric fluorescent heme sensors that can be targeted to cytosolic, mitochondria matrix, and nuclear locales (Figure 5A). These sensors are called HS1, and they provide enhanced capability to study heme trafficking dynamics in space and time within living organisms. These tri-domain sensors were engineered so that exchangeable heme binds to the cytochrome b_{562} (cyt b_{562}) domain of the sensor (Figure 5A). Upon heme binding, eGFP fluorescence is quenched through FRET, while mKATE2 fluorescence is unaffected by heme and therefore serves as an internal standard (Figure 5B and C, respectively).[27] Altogether, HS1 acts as an excitation-emission ratiometric probe where eGFP fluorescence is heme-dependent, and mKATE2 fluorescence is heme-independent. Normalizing eGFP fluorescence to mKATE2 fluorescence therefore allows for heme detection and response independently of sensor concentration.

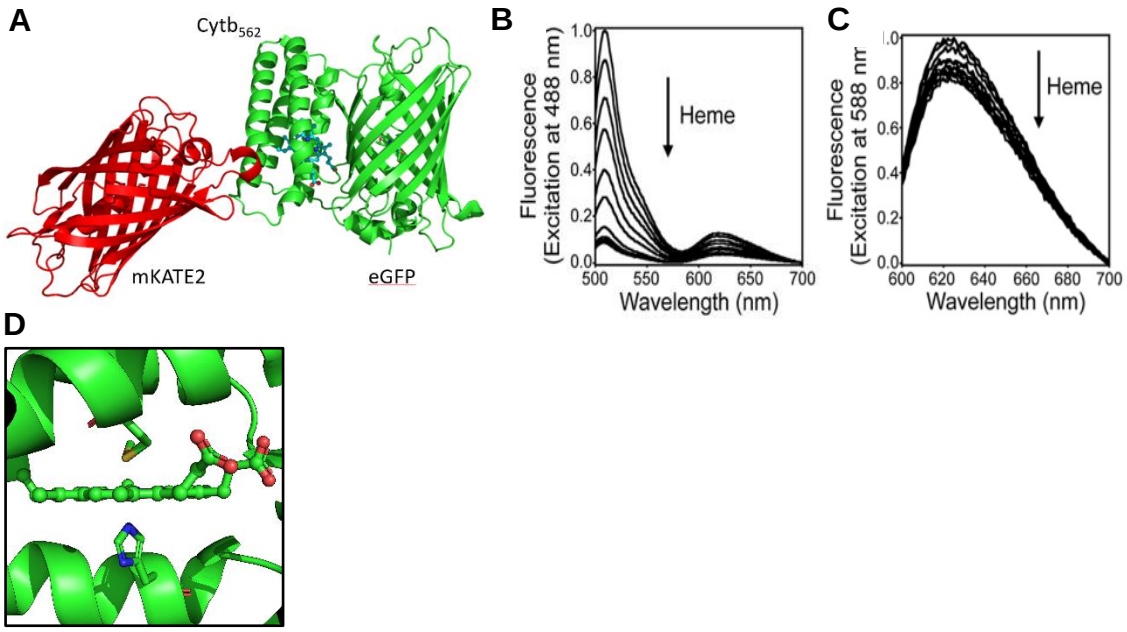

Figure 5. Design and heme-dependent fluorescence properties of the heme sensors. (A) Moleculear model and design principles of the heme sensor, HS1. Model is derived from the X-ray structures of mKATE (PDB 3BXB) and CG6 (PDB 3U8P). Ferric heme-dependent changes in the normalized fluorescence emission spectra of HS1 at pH 8.0 upon excitation of **(B)** EGFP (ex. 488 nm) and **(C)** mKATE 2 (ex 588 nm). **(D)** Heme binds to the Cyt b562 domain of the sensor and is coordinated by Methionine 7 and Histidine 102 residues. Permission statement. Figure B, C, and D previously published in *Hanna, D. A.; Harvey, R. M.; Martinez-Guzman, O.; Yuan, X.; Chandrasekharan, B.; Raju, G.; Outten, F. W.; Hamza, I.; Reddi, A. R. Heme dynamics and trafficking factors revealed by genetically encoded fluorescent heme sensors. Proceedings of the National Academy of Sciences* ***2016****, 113 (27), 7539-7544. DOI: 10.1073/pnas.1523802113.*

Heme binding to HS1 is coordinated by His102 and Met7 of Cyt b_{562} interactions with the heme-iron center (Figure 5D). HS1 has high affinities for ferrous and ferric heme (with dissociation constants in the sub-nanomolar range) and is 100 % saturated with the analyte. To better detect changes in labile heme, a sensor with moderate heme affinity, poised at ~ 50 % saturated would be more suitable. HS1-M7A is a mutant HS1 sensor where the Met7 heme coordinating residue of Cyt b_{562} is mutated to an alanine residue. HS1-M7A heme dissociation constants for ferric and ferrous heme are 2 uM and 25 nM, respectively.[27] This

sensor is poised a ~ 20 – 50 % saturated with heme. Therefore, HS1-M7A is better suited for monitoring labile ferrous heme.

Indeed, these sensors have already contributed invaluable knowledge regarding labile heme (LH) trafficking and dynamics and have been employed to identify and characterize heme homeostatic factors like GAPDH, and heme homeostasis in different stress conditions.[27, 30, 49]

1.5 Scope of Thesis

Heme is an essential yet inherently cytotoxic metallocofactor. Heme has traditionally been viewed as a static cofactor, buried in enzymes. However, with the development of new technologies, the field is beginning to appreciate and understand the dynamics of heme and its role as a signaling molecule.

This versatile molecule is synthesized in the mitochondria matrix and must be trafficked to disparate cellular locations. Despite being essential for all aerobic life, heme and its biosynthetic precursors may act as toxins producing deleterious reactive oxygen species and altering protein and membrane functions. In addition, it can catalyze the production of deleterious reactive oxygen species and alter protein and membrane functions. These potentially detrimental heme characteristics demand that cells carefully orchestrate heme synthesis and trafficking throughout the entire cell. To exit the mitochondria, heme must traverse mitochondria inner and outer membranes before reaching the cytosol or be handed off to chaperones or other molecules aiding in heme distribution.

Unfortunately, the molecules and mechanisms that regulate mitochondrial heme export and heme bioavailability (transport, trafficking) to and within virtually every subcellular compartment are not well understood. Regulation of nuclear bioavailable heme is of specific interest. In the nucleus, heme acts as a dynamic signaling molecule where it regulates transcription factors in response to environmental changes and stress. Therefore, there is an immediate need to decipher the mechanisms regulating mitochondrial and nuclear heme dynamics, specifically, mitochondrial heme export and nuclear heme availability.

Herein, we used genetically encoded fluorescent heme sensor to identify determinants of mitochondrial heme export and steady state nuclear heme, in addition to exploring the relationship between heme utilization and heme bioavailability.

In this thesis, I have elucidated mechanisms that affect mitochondrial heme export and trafficking to the nucleus. I have investigated the effects of mitochondria inner membrane structure on heme homeostasis. Abolishing the mitochondria contact site and cristae organizing system (MICOS) by removing the core subunit component, Mic60, resulted in altered heme biosynthesis, but not heme trafficking or bioavailability. This work has provided new insights regarding the regulation of heme biosynthetic machinery and the importance of mitochondrial architecture in this pathway.

Further, I established a system to elucidate PGRMC/DAP1 complementary roles in nuclear heme trafficking in both mammals and yeast. I studied the only

PGRMC homolog in yeast, Dap1. PGRMCs/Dap1 are recognized as hemoproteins able to transfer heme, however, the mechanisms are not clear. Deleting DAP1 in yeast abolishes heme trafficking to the nucleus. This phenotype was rescued by yeast DAP1 or mammalian PGRMC1 expression experiments. These observations give significance to our Dap1 deletion yeast system.

This work also has characterized for the first time the yeast gene Ygr127w as a determinant of mitochondrial heme export and nuclear trafficking. Ygr127w shares 26 % amino acid sequence identity with both human Tango2 and *C. elegans* Hrg-9 genes. In Tango2 deletion mutants, nuclear heme trafficking is abolished, and steady state mitochondrial heme is elevated. Similarly, heme sequestration in heme-enriched organelles (like mitochondria or lysosome-related organelles) was seen in other organisms, such as *C. elegans* and human cells with Tango2 deletions. Mutations in Tango2 represent a rare genetic disease in humans. Zebrafish with mutant Tango2 experience symptoms like that of human Tango2 disease states; including, encephalopathy, cardiac arrhythmias, and rhabdomyolysis. Our studies identifying yeast Ygr127w as a human Tango2 homolog, and as a heme homeostatic factor have expanded the broader knowledge about Tango2-related diseases and heme homeostasis implications using yeast as a model organism.

This thesis also utilized an unbiased genetic high throughput screen to identify determinants of steady state nuclear heme availability. The *S. cerevisiae* haploid gene deletion library was transformed with nuclear-targeted high and low affinity heme sensors. Yeast mutants with altered heme availability were identified

and validated. The low affinity heme sensors revealed 183 mutants with high nuclear heme and 314 mutants with low nuclear heme. The high affinity heme sensors revealed 86 mutants with low nuclear heme. Several of these 86 candidates were validated, however, none were able to be complemented. I hypothesize epigenetics or post-translational modifications are contributing to the observed low heme in these mutants.

Finally, I investigated the relationship between heme utilization and heme bioavailability. To limit heme toxicity, cells only produce the heme that will be utilized for specific processes, while excess heme is degraded or stored in a benign form.[50] This reasoning is not entirely true due to the existence of the labile heme pool. This begs the question: How do cells balance or regulate heme utilization and bioavailability? How are these two aspects optimized within the cell? Taken together data from previously published works, I found that the expression of half of the known yeast hemoproteins are regulated by the transcription factor Hap1p. Hap1p mutants that are defective in transcription activity caused an increase in the labile heme pool, while minimally affecting the total heme levels. Decreasing the need for heme does not result in a comparative or synergistic change in the bioavailable heme. Further, Hap1p regulates heme by controlling the expression of heme buffering proteins, including catalase. Finally, I observed that with higher levels of free heme, hydrogen peroxide toxicity was reduced.

Overall, using genetically modified yeast (GMY) models and genetically encoded heme sensors, my work, in collaboration with others has identified several

factors that facilitate mitochondrial heme export, nuclear heme trafficking, and steady state nuclear heme. I also investigated the broader relationship between heme utilization and bioavailability in yeast. The combination of tools and yeast systems we evaluated and demonstrated here may potentially be extended to and for the future to study mammalian heme trafficking factors and related heme homeostatic diseases.

CHAPTER 2. MITOCHONDRIAL HEME EXPORT AND NUCLEAR HEME TRAFFICKING FACTORS REVEALED BY GENETICALLY ENCODED FLUORESCENT HEME SENSORS

2.1 Preface

Chapter 2 is separated into four parts (2.4, 2.5, 2.6, and 2.7). Each part focuses on a specific pathway or protein involved in mitochondrial heme export and trafficking to the nucleus. While each part is distinct, they all relate thematically and are therefore discussed within this chapter.

2.2 Thesis Attribution Statement for Chapter 2.

Portions of this chapter are adapted from published work:

"Sun, F.*, Zhao, Z.*, Willoughby, M. M., Shen, S., Zhou, Y., Shao, Y., . . . Chen, C. (2022). HRG-9 homologues regulate haem trafficking from haem-enriched compartments. *Nature*, *610*(7933), 768-774."[51]

"Dietz, J. V., Willoughby, M. M.,…Khalimonchuk, O. (2021). Mitochondrial contact site and cristae organizing system (MICOS) machinery supports heme biosynthesis by enabling optimal performance of ferrochelatase. *Redox Biology, 46*, 102125."[52]

2.3 Introduction

After its synthesis in the mitochondria, heme must be distributed throughout the cell. Therefore, heme mobilization of newly synthesized heme begins with mitochondrial export. To exit the mitochondria, heme must traverse mitochondria inner and outer membranes before reaching the cytosol or be handed off to chaperones or other molecules aiding in heme distribution.[20, 53] Multiple pathways for such trafficking have been investigated and hypothesized.

One possibility for newly synthesized heme distribution is via a heme metabolon complex. Metabolons facilitate the channeling of substrates within a biochemical pathway.[54] These complexes serve to 1) reduce or prevent competition for metabolites by intersecting pathways, 2) increase flux, and 3) protect cells from reactive metabolic intermediates.[55] For example, enzymes in the TCA cycle form a metabolon, as these enzymes are intermediary in several metabolic pathways such as glycolysis, the urea cycle, corrinoid synthesis, and fatty acid metabolism.[56-60]

Several components of heme biosynthesis exist in such a complex: including 5-aminolevulinic acid (5-ALA) synthase (ALAS), protoporphyrinogen oxidase (PPOX), and ferrochelatase (FECH), the first, seventh, and last enzymes in the pathway, respectively. Other proteins involved in iron metabolism have also been identified in this heme metabolon, thus representing the convergence of iron and porphyrin metabolism, coordinating heme and iron availability for optimal heme synthesis. This work will investigate two heme metabolon-interacting

proteins, Mic60p and Progesterone Receptor Membrane Component 1 (PGRMC1) and it's yeast homolog, Damage Response Protein 1 (Dap1p) for their roles in heme trafficking (in section 2.4 and 2.5, respectively). Mic60p and PGRMC1 were reported to be associated with FECH, the terminal heme biosynthetic enzyme.[12] We hypothesize PGRMC1, along with the yeast homolog, Dap1p, and Mic60p interactions with FECH are significant and may facilitate mitochondrial heme export in yeast.

A second pathway for heme trafficking is through inter-organelle membrane contact sites (MCS) or tethers. MCSs are physical contacts between two membrane-bound organelles and are critical for signaling and transfer of various phospholipids.[13, 61-65] Trafficking of heme via membrane tethering proteins would limit inappropriate protein interactions and is an attractive route for this redox active, hydrophobic molecule. In fact, previous work has shown mitochondria-ER membrane contact sites, ER Mitochondria Encounter Structures (ERMES), facilitate nuclear heme trafficking.[66] Here, we investigate putative mitochondria-nuclear tethering proteins recently described by Eisenberg-Bord et al. in nuclear heme trafficking.[67]

Lastly, the yeast gene and its human homolog, Transport and Golgi Organization 2 (TANGO2), Ygr127w, will be probed for its implications in heme homeostasis and mitochondria-nuclear heme trafficking. The function of Tango2 in humans is still unclear, however, as its name suggests, it has been implicated in maintaining Golgi structure and function.[68, 69]

Overall, we investigate the effects of potential mitochondria-nuclear protein tethers and heme metabolon-interacting proteins in mitochondria-nuclear heme export.

2.4 Mitochondrial Contact Site and Cristae Organizing System (MICOS) Machinery Support Heme Biosynthesis

2.4.1 Introduction

Components of the Mitochondrial Contact Site and Cristae Organizing System (MICOS) were identified as interaction partners with the terminal and rate-limiting heme biosynthetic enzyme ferrochelatase (FECH) in mammalian cells.[12] MICOS is a complex consisting of eight known proteins responsible for maintaining mitochondrial cristae inner membrane (IM) architecture and contact sites between the inner and outer mitochondrial membranes.[70-72] Further, MICOS has been reported to facilitate the bidirectional transport of hydrophobic molecules including phosphatidic acid and coenzyme Q biosynthetic intermediates.[73, 74] Even more recently, five of the eight MICOS subunits (Mic60, Mic19, Mic26, Mic27, and Mic12) were identified as physical interacting partners of the terminal heme biosynthetic enzymes FECH in mammalian cells and Hem15 in yeast cells.[52] Deleting MIC60 has been reported to abolish expression of all the MICOS subunits.[75] Therefore, to investigate the significance of MICOS-Hem15 interactions on heme homeostasis, MIC60 deletion and HEM15 overexpression (OE) yeast strains were used in this work.

2.4.2 Results

2.4.2.1 Mitochondrial Contact Site and Cristae Organizing System (MICOS) Machinery Supports Heme Biosynthesis

To investigate if MICOS influences mitochondrial heme export, rates of heme transport across the mitochondria IM were assessed. The high-affinity, genetically encoded heme sensors (HS1) targeted to cytosolic, mitochondrial matrix, and nuclear organelles were used to compare rates of heme transport in WT and MIC60 deletion (*mic60Δ*) cells. In this experiment, heme synthesis is first inhibited using the heme biosynthesis inhibitor succinylacetone (SA). SA specifically inhibits the 5-ALA dehydratase (ALAD) enzyme, also known as Porphobolinogen Synthase (PGBS), the second enzymatic step in the heme biosynthesis pathway. The inhibitor is then removed and allows heme synthesis to be re-initiated. Trafficking of the newly synthesized heme is represented by monitoring changes in the HS1 GFP/mKATE2 sensor ratio (R) as a function of time. In other words, mitochondria matrix, cytosol, and nuclear heme sensor occupancy (% Heme Bound) is calculated, and monitored over time.[66] The fractional saturation of the HS1 sensors (% Heme Bound) is calculated by considering R relative to the HS1 fluorescence ratio when the sensor is 0 % (R_{min}) and 100 % (R_{max}) bound (Equation 1). R_{min} and R_{max} values are determined by parallel samples maintained in media with or without succinylacetone, respectively. This assay revealed heme trafficking rates to the cytosol- and

nuclear-targeted sensors in WT cells were comparable to the *mic60Δ* mutant (Figure 6A and B, respectively).

$$\%\ Heme\ Sensor\ Bound = \frac{(R - R_{min})}{(R_{max} - R_{min})} \qquad \text{Equation 1}$$

Total heme levels were then analyzed in the different yeast mutants. To measure total heme levels, a porphyrin fluorescence assay was used. This assay is dependent on the inherent fluorescent properties of protoporphyrin IX. After lysing the yeast cells overnight in an oxalic acid solution, samples volumes are split where one set is treated with excessive heat to remove the iron from heme to produce the fluorescent protoporphyrin IX molecule, and the other set is left at room temperature. The samples at room temperature (un-boiled) serve as a control representing the background protoporphyrin levels in the cells. The fluorescent spectra fingerprint for protoporphyrin IX is unique, having two distinct emission peaks at ~ 608 and 665 nm wavelengths. The fluorescence intensity at either 608 or 665 nm is recorded, and a standard heme curve is used to calculate the total heme concentration per yeast cell. This experiment revealed Mic60p does not affect total heme levels (Figure 6C). It is possible that alterations in Mic60p alone do not reveal a phenotype. Therefore, yeast with altered Mic60p and Hem15 expression were used. After performing the total heme assay in yeast strains with or without Mic60p and with or without Hem15 overexpression, we found that total heme levels are only minimally affected (Figure 6D).

Despite total heme levels being unaltered, a stark difference in the background porphyrin levels was observed. The protoporphyrin emission spectra

revealed elevated total porphyrin levels in *mic60Δ* strains compared to WT strains (Figure 6E). This observation is only seen in strains lacking Mic60p and is independent of Hem15 overexpression.

Lastly, we steady state labile heme distribution was analyzed using strains expressing the HS1 sensors localized to the cytosol and mitochondrial matrix. To measure steady state labile heme, strains with the sensor expression or empty vector (EV) plasmids were cultured overnight. The next day, cultures were harvested, and the same amount of yeast cells were analyzed in a plate reader, exciting the GFP and mKATE sensor domains and collecting emission wavelengths specific to GFP and mKATE. We found Mic60 and Hem15 overexpression does not affect steady state labile heme distribution (Figure 6F).

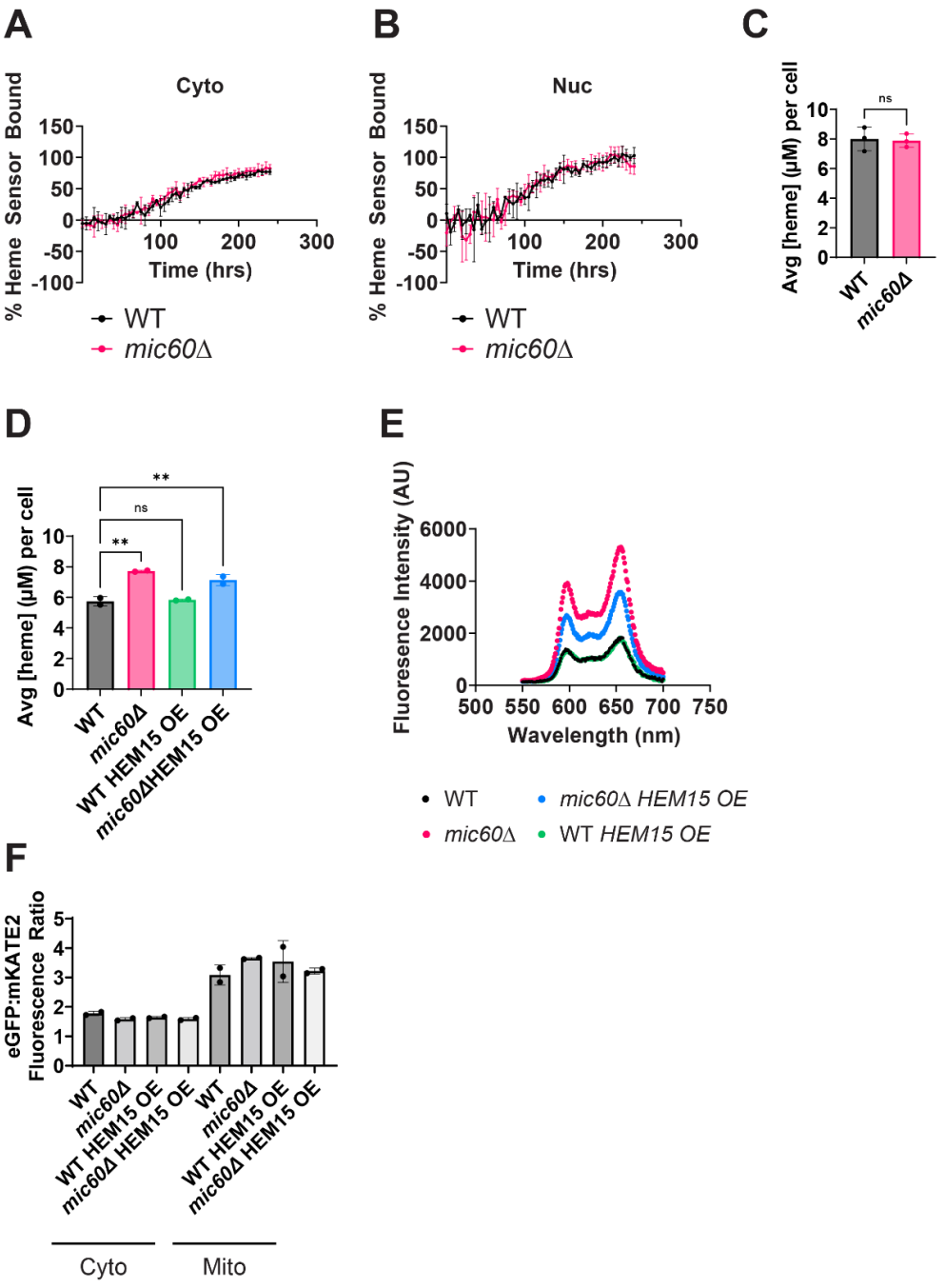

Figure 6. *mic60Δ* Yeast Cells Have Altered Porphyrin Levels. Heme trafficking dynamics to the cytosol **(A)** and nucleus **(B)** of WT and *mic60Δ* yeast. Total heme content in WT and *mic60Δ* yeast **(C)** with and without HEM15 OE **(D).** **(E)** Fluorescence spectra of steady-state total porphyrinogens from oxalic acid-digested cell extracts. **(F)** Cytosolic and Mitochondrial steady state labile heme. Each *dot* represents a biological replicate. The significance is indicated by asterisks using one-way **(C)** and two-way **(D)** ANOVA for multiple comparisons with Dunnett's post hoc test: ** $p < 0.01$, ns, not significant. Figures A – E are originally published in Dietz, J. V.; Willoughby, M. M.; Piel, R. B.; Ross, T. A.; Bohovych, I.; Addis, H. G.; Fox, J. L.; Lanzilotta, W. N.; Dailey, H. A.; Wohlschlegel, J. A.; et al. Mitochondrial contact site and cristae organizing system (MICOS) machinery supports heme biosynthesis by enabling optimal performance of ferrochelatase. *Redox Biology* **2021**, *46*, 102125. DOI: https://doi.org/10.1016/j.redox.2021.102125

2.4.3 Discussion

As a Hem15-interacting protein and a determinant of mitochondria inner membrane structure, Mic60p, is an important protein to probe for its role in heme homeostasis and mitochondrial heme export. The results show that Mic60p does not affect heme transport but affects the levels of heme biosynthesis precursors. Without Mic60p, yeast experience significantly elevated porphyrin levels. These findings parallel work done in collaboration with Dietz, et al 2021.[52] Dietz, et al. identified Mic60p as an important mediator for optimal Hem15 activity. *mic60Δ* cells overexpressing Hem15 had defects in Hem15 activity. These strains also displayed respiratory growth defects.[52] Using UPLC, Dietz, et al. separated and identified which porphyrin precursors were contributing to heightened porphyrin signal. They found 8-, 7-, 6-, 5-, and 4-COOH porphyrins were increased in cells lacking Mic60p.[52] This increase is not due to general defects in metabolite transport.[52] Taken together, my work in collaboration with Dietz, et al. suggest substrate availability may be a factor responsible for the limited Hem15 activity seen in *mic60Δ* cells overexpressing Hem15.

Heme synthesis intermediates can be toxic due to their inherent redox activity. Dietz, et al. further evaluated oxidative damage and stress by measuring aconitase levels in *mic60Δ* strains. Aconitase levels in WT and *mic60Δ* cells were similar, however, aconitase specific activity was significantly decreased in strains lacking Mic60p.[52] Another sign oxidative stress observed in *mic60Δ* Hem15 overexpression cells was a hypersensitivity to acute oxidative insults that were

rescued with supplementation of the antioxidant *N*-acetylcysteine.[52] Taken together, loss of MICOS negatively affects Hem15 activity and results in the accumulation of potentially toxic porphyrin precursors that may cause oxidative damage. Our work, together, provides a better understanding of the regulation of heme biosynthesis.

2.5 The Progesterone Receptor Membrane Component 1 (PGRMC1) has a Conserved Role in Mitochondria-Nuclear Heme Trafficking

2.5.1 Introduction

PGRMC1 and its isoform PGRMC2 were both identified as FECH interacting partners in differentiated murine erythroleukemia (MEL) cells.[12] PGRMCs are relatively small, ~25 kDa, and belong to the membrane-associated progesterone receptor (MAPR) family. As the name suggests, PGRMCs were first recognized as progesterone binding proteins, however, their involvement in progesterone signaling is unclear. While the precise role of PGRMC1 are yet to be determined, it has been implicated in various cellular functions, including cholesterol metabolism, endocytosis, intracellular signal transduction, and iron metabolism.[76-81] Among these functions, PGRMC1 has repeatedly demonstrated the ability to bind heme.[82-84]

PGRMC1 and PGRMC2 have been proposed as heme chaperone proteins.[12, 38] Piel et al show that purified PGRMC1 can donate heme to apo-cytochrome b_5, and that PGRMC1 strongly interacts with FECH when FECH is in its product release (open) conformation. In addition, they observed in vitro that

FECH activity is lowered in the presence of PGRMC1. Their work suggests PGRMC1 may regulate FECH activity by controlling heme release.[12] PGRMC2 is also hypothesized to be a heme chaperone. In adipocytes, PGRMC2 has been shown to facilitate nuclear heme availability.[38]

Yeast has only one member of the MAPR family, named Damage Response Protein 1 (Dap1). Dap1p is homologous to PGRMC1/2 and is also characterized as a heme binding protein. Further, Dap1p has been hypothesized as a potential heme chaperone delivering heme to the P_{450} enzyme Erg11 which is involved in ergosterol biosynthesis.[77, 82] On the contrary, other reports document Dap1p's ability to bind heme is critical for ergosterol synthesis, but not necessarily its interactions or a potential chaperoning activity involving Erg11.[85]

In this section, we investigate PGRMCs' role as a potential heme trafficking factor in yeast by studying the homolog Dap1p. In yeast, Dap1p is the only MAPR protein, therefore, yeast could be an extremely useful organism for directly probing the role of MAPR proteins in heme homeostasis. Further, if PGRMCs' role in heme homeostasis is conserved in the yeast Dap1p homolog, we can use the yeast Dap1p system to study this pathway and PGRMC1 function more in depth.

2.5.2 Results

2.5.2.1 PGRMC1/DAP1 Facilitate Mitochondria-Nuclear Heme Trafficking

To investigate if the roles of PGRMC1/2 in heme homeostasis are conserved, the yeast homolog Dap1p was probed. First, a growth test was

performed to answer if PGRMC1 can rescue the known *dap1Δ* inhibitory growth phenotype on the anti-bacterial agent fluconazole. Fluconazole is an inhibitor of Erg11p while Dap1p is an activator or Erg11. Therefore, *dap1Δ* strains experience a heightened sensitivity to fluconazole where fluconazole is toxic to *dap1Δ* strains. Indeed, growth of *dap1Δ* strains expressing an EV plasmid was significantly diminished on agar plates containing 10 ug/mL fluconazole (Figure 7A). As expected, DAP1 expression rescued the growth defect on fluconazole (Figure 7A, indicated by *dap1Δ* + DAP1). Similarly, PGRMC1 expression also rescued *dap1Δ* growth in the presence of fluconazole (Figure 7A, indicated by *dap1Δ* + PGRMC1).

Next, the affects of Dap1p on heme trafficking were investigated by performing a heme trafficking kinetics assay previously described in section 2.4.2 and published by Martinez-Guzman, et al.[66] This experiment revealed cytosolic heme trafficking is unaffected by Dap1, while nuclear heme trafficking is abolished in the absence of Dap1 (Figure 7B and C, respectively). Further, the absence of mitochondrial-nuclear heme trafficking in *dap1Δ* yeast cells can be rescued by expressing *DAP1* or *PGRMC1* episomally (Figure 7C). Interestingly, there is not an observed effect on steady state nuclear or mitochondrial heme homeostasis due to Dap1 (Figure 7D).

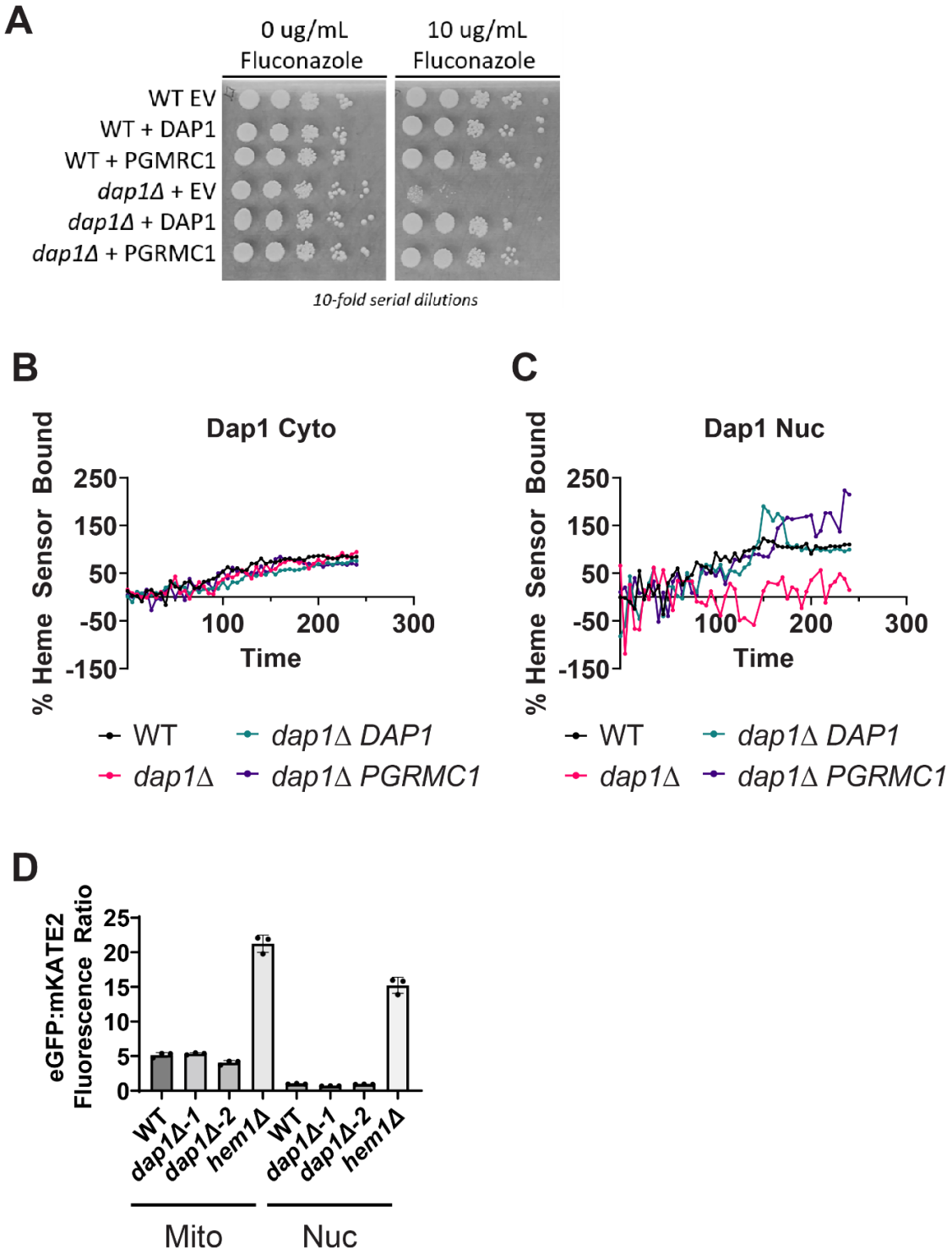

Figure 7 - Dap1 Regulates Nuclear Heme Trafficking Dynamics. (A) Spot test of WT and *dap1Δ* strains with DAP1, PGRMC1, or EV plasmids on agar plates with and without 10 ug/mL fluconazole. Heme trafficking dynamics to the cytosol **(B)** and nucleus **(C)**. **(D)** Steady State mitochondrial and nuclear heme in WT, *dap1Δ*, and *hem1Δ* yeast strains.

2.5.3 Discussion

After investigating Dap1p's role in heme homeostasis I conclude Dap1 facilitates mitochondrial-nuclear heme trafficking, but not steady state labile heme in yeast. In addition, Dap1's heme trafficking ability is conserved in higher organisms. Expression of the mammalian homolog, PGRMC1, was able to rescue both *dap1Δ* nuclear heme trafficking and fluconazole growth phenotypes. The Dap1p/PGRMC1-dependent nuclear heme trafficking phenotype supports its hypothesized role as a heme chaperone and is consistent with other reports. Galmozzi et al showed that PGRMC2 is critical for heme delivery to the nucleus in adipocytes. Heme delivery by PGRMC2 in this context affected gene transcription and physiology.[38]

Piel et al. showed PGRMC1 interacts with FECH and can transfer heme to downstream apo-hemoproteins. Further, PGRMC1 interacts with FECH preferentially when FECH is in an open conformation state. This specific interaction suggests PGRMC1 may facilitate product release from FECH (a rate-limiting step) and heme delivery to downstream targets. If PGRMC1/Dap1p functions as a true chaperone, they are expected to deliver heme to a specific downstream target. If PGRMC1/Dap1p are bound to FECH, how is heme delivered to downstream targets eventually ending up in the nucleus? Galmozzi et al hypothesize PGRMC1 transfers heme to the ER-localized PGRMC2 in adipocytes.[38] This model does not apply to yeast since Dap1p is the only MAPR protein. Therefore, there must be a different protein that Dap1p delivers heme to for ultimate availability in the nucleus.

Overall, this work established PGRMCs' role in heme homeostasis is conserved in yeast. This *dap1Δ* yeast system can be used in future experiments to further understand PGRMCs/Dap1p's roles in mitochondria heme export and subsequent nuclear heme trafficking.

2.6 Membrane Contact Sites Serve as a Potential Mechanism for Nuclear Heme Trafficking

2.6.1 Introduction

Another alternative yet far less studied mechanism for heme trafficking is by membrane contact sites (MCS). MCSs are physical contacts between two membrane-bound organelles and have key properties. The MCS tether involves proteins that fulfill specific roles and a defined lipid composition that supports MCS function.[13] Due to heme's lipophilic properties, it is possible modes of heme trafficking mimic that of mitochondrially derived lipids like cardiolipin (CL) and phosphatidylethanolamine (PE).[10] Mechanisms of mobilization of lipophilic molecules would include MCS between different organelles and vesicular transport.[10]

Indeed, mitochondrial heme export has been demonstrated through Endoplasmic Reticulum (ER)-mitochondrial encounter structures (ERMES).[66] ERMES are one type of mitochondrial-ER contact site and is composed of four proteins (Mmm1, Mdm12, Mdm10, and Mdm34).[86-88] These tethers are highly dynamic and have also been identified in aiding in the transfer of lipids and regulation of iron homeostasis.[89-91] Martinez-Guzman et al. identified GTPases

that regulate ERMES directly (Gem1) and indirectly (Dnm1 and Mgm1), and these ERMES regulatory factors modulate nuclear heme transport.[66]

Further, investigators have also observed nuclear heme trafficking rates are up to 25 % faster than trafficking rates to the cytosol and mitochondria compartments.[66] This observation suggests heme trafficking to disparate cellular locations occurs simultaneously, rather than sequentially, and that distinct trafficking pathways exist. Taking this into account, there must be a more direct pathway for heme getting to the nucleus that bypasses the cytosol. Trafficking via Mito-ER contact sites like ERMES is a possible route that would allow for faster trafficking rates to the nucleus.

Another possible and more direct route to the nucleus is through mitochondria-nuclear membrane contact sites. Such sites have been hypothesized but have only recently been shown.[67, 92] In yeast, Eisenberg-Bord identified candidate tethering proteins involved in mitochondria-nuclear organelle interactions. Using fluorescence microscopy, they demonstrated specific areas of contact between the two organelles. They uncovered a role for the protein Ybr063c, now designated as Cnm1 (contact nucleus mitochondria 1), as a tether on the nuclear membrane.[67] This section investigates Ybr063c and two other candidate tethers (Yet3 and Ysc83) described by Eisenberg-Bord et al for their potential roles in mitochondria-nuclear trafficking.

2.6.2 Results

2.6.2.1 Candidate Mitochondria-Nuclear Tethering Proteins Do Not Affect Heme Trafficking Kinetics

We first monitored heme trafficking kinetics to cytosol, mitochondria, and nuclear compartments using the pulse-chase assay described previously in this thesis and published by Martinez-Guzman et al.[66] Trafficking rates in WT, gene deletion, and gene overexpression strains were monitored. If these genes encode proteins that positively facilitate mitochondria-nuclear heme trafficking, we expect deletion mutants to have slower or abolished rates to the nucleus, and overexpression mutants to have faster rates to the nucleus. Interestingly, Ybr063c, Yet3, and Ysc83 did not affect heme trafficking rates. The kinetic traces of mutant yeast strains overlay with the WT kinetic curves for all the mutants and compartments tested (Figure 8).

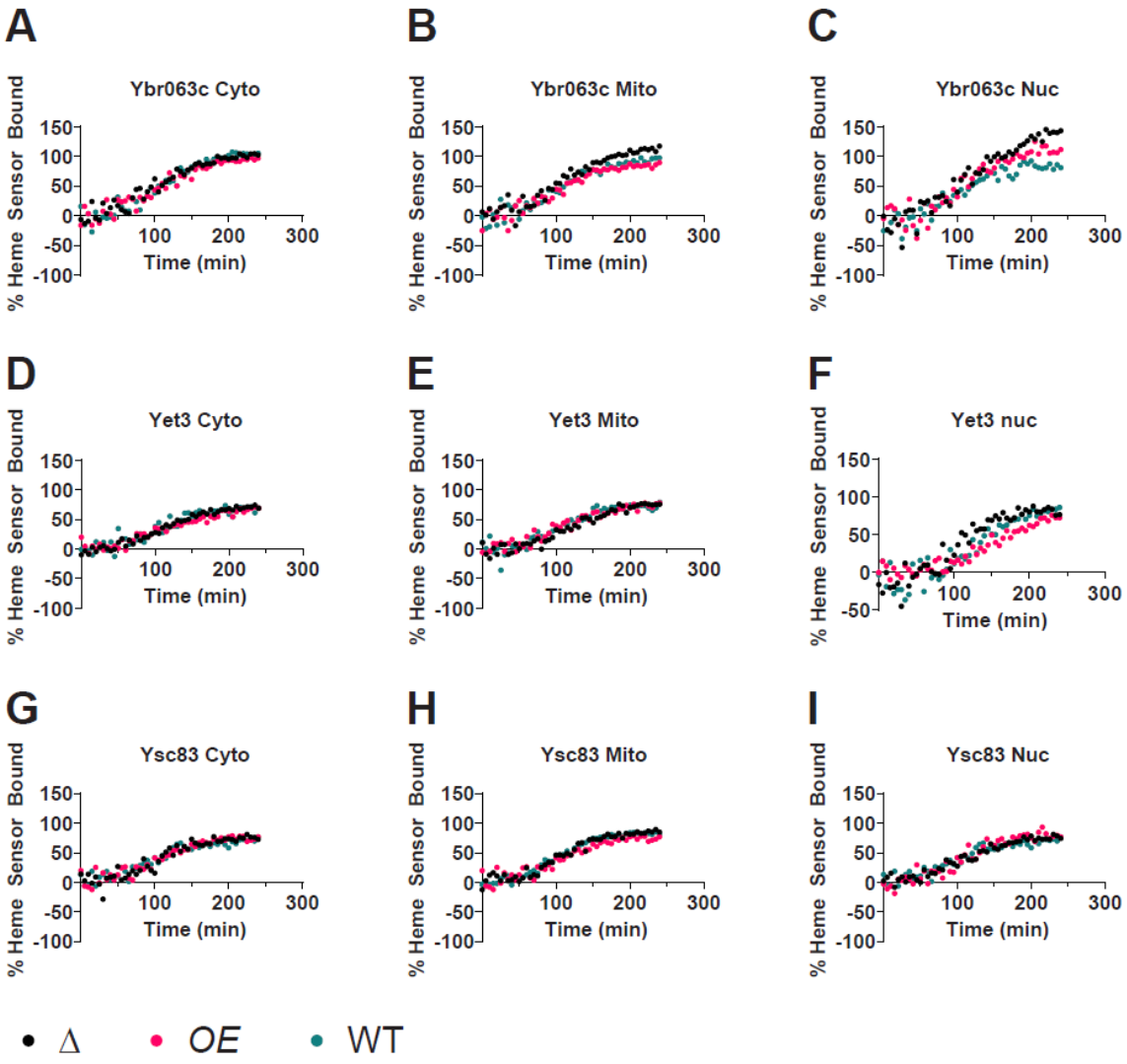

Figure 8 - Trafficking Dynamics in Different Mitochondria-Nuclear Tethering Protein Yeast mutants. Heme trafficking was monitored to the cytosol, mitochondria matrix, and nucleus in WT, and deletion and overexpression yeast mutants of Ybr063c **(A-C)**, Yet3 **(D-F)**, and Ysc83 **(G-I)**.

2.6.2.2 Yet3 Overexpression Affects Steady State Labile Heme Levels

Steady state heme homeostasis in the same yeast strains was probed (Figure 9). In contrast with the kinetics assay, to observe steady state heme levels, yeast cultures were grown overnight to mid-exponential phase before measuring the sensor fluorescence. Ybr063c does not affect steady state labile heme levels

(Figure 9A). *Ysc83Δ* yeast have significantly more cytosolic heme compared to WT, while mitochondria and nuclear heme levels were not affected (Figure 9B). Strains lacking Yet3 has a small decrease in cytosolic heme without affecting mitochondrial and nuclear heme (Figure 9C). Finally, overexpressing Yet3 resulted in significant heme distribution changes. Yet3 overexpression strains have significantly less cytosolic heme and more nuclear heme relative to WT strains (Figure 9D). In contrast, mitochondrial heme was minimally perturbed by Yet3 overexpression (Figure 9D).

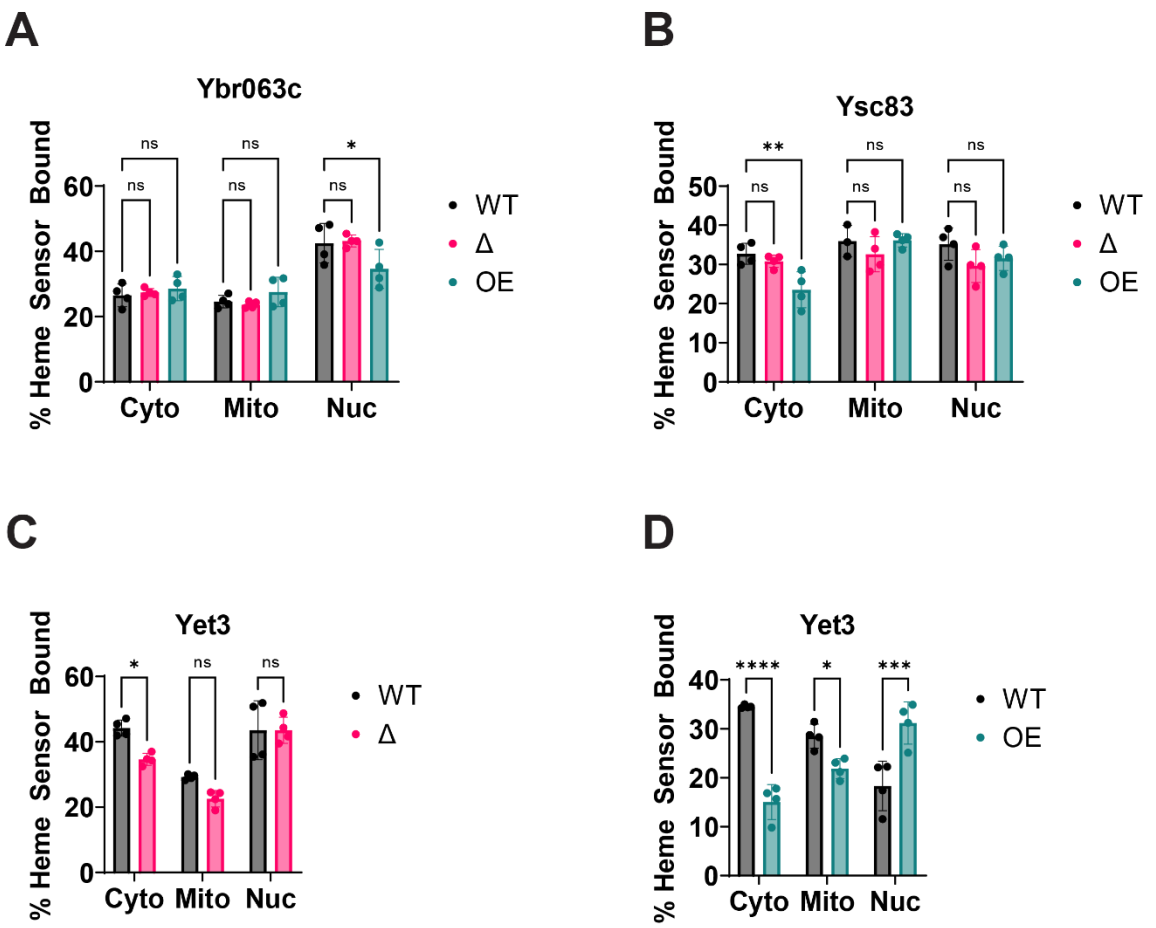

Figure 9 - Steady State Heme Distribution in Mitochondria-Nuclear Tethering Protein Yeast Mutants. Intracellular heme distribution in Ybr063c **(A)**, Ysc83 **(B)**, and Yet3 mutants **(C, D)**. Each *dot* represents a biological replicate. The significance is indicated by asterisks using a two-way ANOVA for multiple comparisons with Dunnett's post hoc test: * $p < 0.05$, ** $p < 0.01$, **** $p < 0.0001$, ns, not significant.

2.6.3 Discussion

Heme trafficking via mitochondria-nuclear tethering proteins serves as a direct route for nuclear heme trafficking. Mobilization through a membrane contact site would protect the cell from off-target heme interactions and its deleterious redox and hydrophobic properties. The effects of candidate mitochondria-nuclear

tethering proteins identified and described by Eisenberg-Bord, et al (Ybr063c, Ysc83, and Yet3) on heme homeostasis were probed.[67]

Interestingly, neither of the proteins affected heme trafficking dynamics to either the cytosol, mitochondria, or nucleus. Probing steady state heme levels revealed significant heme distribution alterations in Yet3 overexpression mutants. Yet3 overexpression yeast strains had significantly less cytosolic and more nuclear heme levels compared to WT strains. This observation is consistent with expectations of a mitochondria-nuclear tether facilitating nuclear heme transport would look like. If a protein positively affects mitochondria-nuclear trafficking, we expect less heme in the cytosol and more in the nucleus in overexpression mutants. However, we did not observe the opposite effect in strains lacking Yet3. Instead, *yet3Δ* strains did not affect steady state nuclear heme, and only minimally affected cytosolic and mitochondrial heme. A phenotype was only observed in the Yet3 overexpression mutants. One explanation for this is protein abundance. It is possible that native Yet3 protein abundance is low, and deleting Yet3 would not have a significant effect. While overexpressing Yet3 has a greater and observable effect since the cells would be expressing significantly more Yet3 protein than normal.

Ybr063c, Ysc83, and Yet3 have all been identified as mitochondria-nuclear tethering proteins, however altered heme levels was only observed in the Yet3 mutant. There are several explanations for this. Different membrane tethers perform different functions. It is possible that Ybr063c, Ysc83, and Yet3 are involved in specific tether structures each performing specific functions.

Eisenberg-bord et al describe Ybr063c expression and mitochondrial-nuclear tethering is increased in the presence of phosphatidyl choline (PC).[67] Ybr063c tethers may facilitate PC trafficking exclusively, and not heme. The tethers consisting of Ybr063c and Ysc83 may be involved in trafficking of other molecules other than heme.

2.7 Yeast Ygr127w/Tango2p Facilitates Mitochondrial Heme Export and Nuclear Heme Trafficking

2.7.1 Introduction

Tango2p is a protein in humans whose specific function is unknown. Mutations in the human Tango2 gene are classified as a rare autosomal recessive genetic disorder.[93] Patients with this disease experience a plethora of symptoms, including episodes of metabolic crisis and arrhythmias.[94-97] Drosophila cells depleted of Tango2p cause Golgi membranes to fuse with the endoplasmic reticulum (ER), where ER-to-Golgi transport and retrograde signaling is significantly delayed.[68, 69] In addition, recent reports show Vitamin B supplementation can alleviate Tango2-related disease symptoms in *Drosophila* and human cells and is currently a treatment regime for patients.[98] Investigators suggest Tango2 may affect lipid metabolism where Vitamin B supplementation restores lipid homeostasis.[98]

Since heme is hydrophobic like a lipid, it is possible Tango2 could regulate heme in a similar way. Further, the human Tango2 protein sequence is 26 % identical to the yeast gene Ygr127w (which will be referred to as Tango2 in the rest

of this work) and the *C. elegans* gene called HRG-9. Due to high sequence identity of the human Tango2 gene and yeast Ygr127w, we can use *ygr127wΔ* (*tango2Δ*) yeast to investigate its potential role in heme homeostasis and to further understand Tango2-related human diseases.

2.7.2 Results

2.7.2.1 Yeast Transport and Golgi Organization 2 (TANGO2) and Homologs Regulate Mitochondrial Heme Export and Mitochondrial-Nuclear Heme Trafficking Dynamics

Deletion of yeast *tango2* results in delayed growth that is not complemented by the heme biosynthetic precursor 5-aminolevulinic acid (ALA) (Figure 10A). *tango2Δ* strains have slightly less total heme than wild-type yeast (Figure 10B). Heme distribution in these cells was probed using genetically encoded fluorescent heme sensors. Deletion of Tango2 results in a slight, yet significant decrease in cytosolic labile heme (Figure 10C). The mitochondrial heme sensor showed a drastic reduction in sensor ratio, indicative of more labile heme, in *tango2Δ* yeast (Figure 10D). Perturbed heme homeostasis was also shown by altered Hap1p and Catalase activity. Yeast lacking Tango2, have enhanced catalase expression and activity (Figure 10E). Further, the heme trafficking dynamics assay revealed heme trafficking to the nucleus was severely reduced in *tango2Δ* cells (Figure 10H), while trafficking to cytosolic and mitochondria compartments were unaffected (Figure 10F, G, respectively).

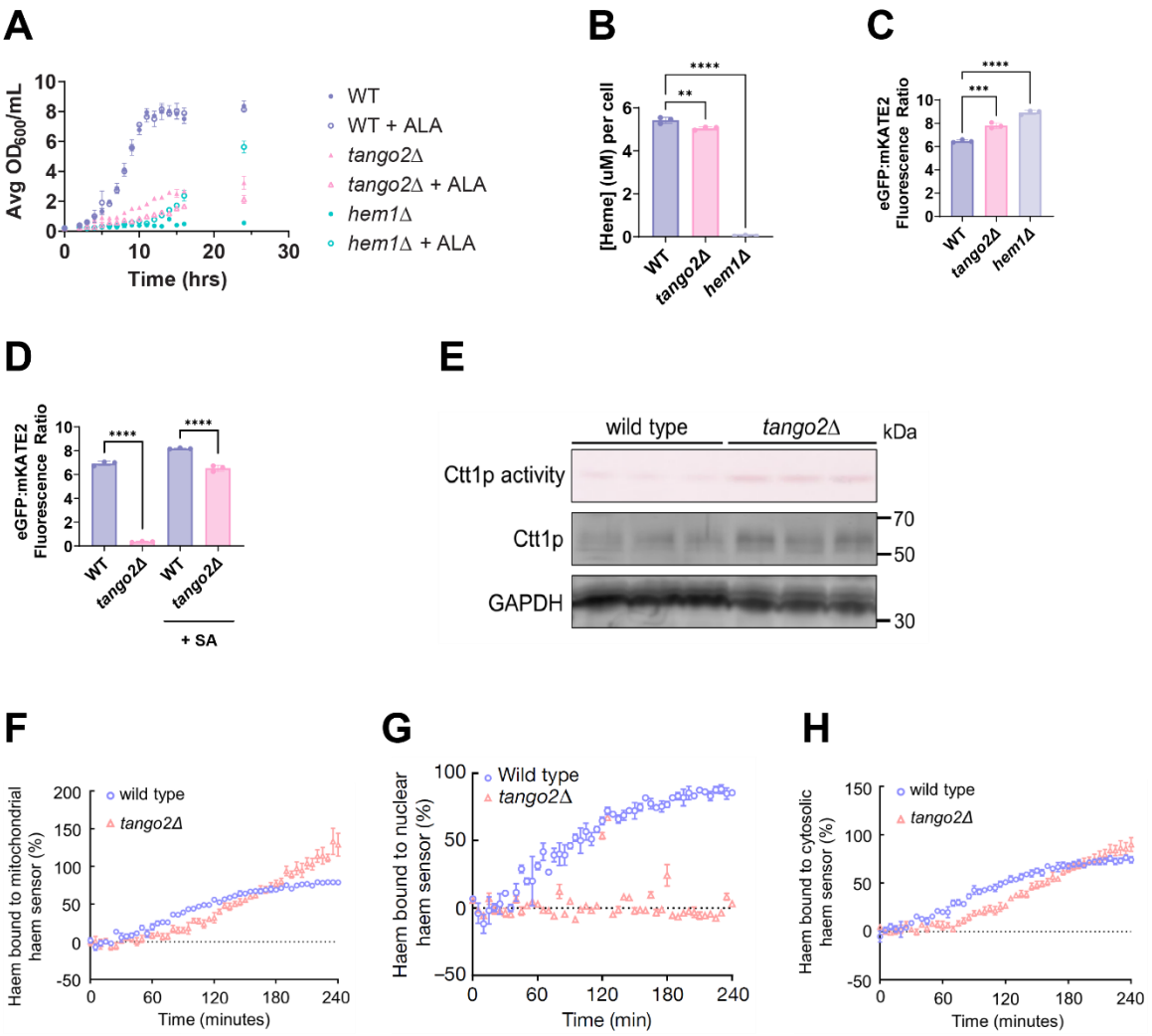

Figure 10 - Yeast Tango2p Regulates Mitochondria Heme Export. **(A)** Growth test of WT, *hem1Δ*, and *tango2Δ* yeast treated with and without 5-aminolevulinic acid (ALA). **(B)** Total Heme content in WT, *hem1Δ*, and *tango2Δ* yeast. The EGFP/mKATE2 fluorescence ratio for cytosolic **(C)** and mitochondria **(D)** heme sensors in wild-type and *tango2Δ* yeast cells treated with or without 0.5 mM succinylacetone (SA). **(E)** Catalase expression and activity in WT and *tango2Δ* yeast. Dynamics of heme trafficking to the cytosol **(F)**, mitochondria **(G)**, and nucleus **(H)** nuclei of wild-type and *tango2Δ* yeast cells. Each *dot* represents a biological replicate. The significance is indicated by asterisks using a two-way ANOVA for multiple comparisons with Dunnett's post hoc test: ** $p < 0.01$, **** $p < 0.0001$.

2.7.3 Discussion

This work shows the yeast Tango2p affects heme homeostasis. Yeast lacking Tango2 have altered steady state labile heme cellular distribution, Hap1p

activity, and defects in mitochondrial-nuclear heme trafficking. The work described here suggests Tango2p facilitates mitochondria heme export and subsequent trafficking to the nucleus. Homologs in different organisms have reported similar results. The *C. elegans* homolog, Hrg-9, is localized to intestines and facilitates heme export from lysosome related organelles (LORs).[51] Similarly, mitochondria fractions from mammalian cells lacking Tango2 have increased heme compared to WT mitochondria fractions.[51] Sun, et al. also demonstrated Tango2 stimulates heme transfer from mouse mitochondria livers to apo-myoglobin. Due to Tango2p's low ferrous and ferric heme affinities with dissociation constants estimated to be 15.4 uM and 38.7 uM, respectively, Tango2 is only able to transfer heme from heme-enriched environments.[51] Altogether, my work in collaboration with Sun et al., support a conserved role for Tango2 in heme export from heme-rich compartments (either mitochondria or lysosome-related organelles, LROs). Further, Tango2 is unlikely to act as a transporter because it does not contain any transmembrane regions. Based on these observations, the mechanism in which Tango2p transfers heme mimics that of cytosolic lipid transfer proteins.[51]

In addition, *tango2*$^{-/-}$ zebrafish experienced physiological alterations that in combination resemble encephalopathy, cardiac arrhythmias, and rhabdomyolysis. These are all major symptoms of the Tango2 disease in humans.[51] Tango2's cellular location and its specific function are still unclear.[68, 93, 95, 99, 100] For the first time, my work in collaboration with Sun et al. have identified a conserved role for Tango2 homologs in heme homeostasis.[51] Performing complementation studies in yeast using yeast Tango2 and human Tango2 expression plasmids would

enhance this work and would be a great model system to study Tango2-related human diseases. In addition, testing the effects of Vitamin B_5 treatment in *tango2Δ* yeast will also be informational to further understand the relationship between Tango2 and Vitamin B_5. Further research may lead to heme-related therapies to alleviate symptoms in Tango2 disease patients.

2.8 Materials and Methods

2.8.1 Yeast Strains, Yeast Growth, and Plasmids

2.8.1.1 Yeast Strains and Growth Conditions

S. cerevisiae strains used in this work were derived from BY4741 (*MATa, his3Δ1, leu2Δ0, met15Δ0, ura3Δ0*) or W303 (*MATa/MATα, leu2-3,112 trp1-1, can1-100, ura3-1, ade2-1, his3-11,15).* ***dap1Δ***::*kan*MX4, ***mic60Δ***::*kan*MX4, and ***tango2Δ***::*kan*MX4 strains were obtained from the yeast gene deletion collection (Thermo Fisher Scientific). The barcodes flanking the KanMX4 deletion cassette of the yeast deletion collection strains were confirmed by PCR and sequenced. WT, *HEM15 OE*, *mic60Δ, mic60Δ HEM15 OE* strains in derived from W303 and were a gift from Oleh Khalimonchuk's Lab. *ysc83Δ::NAT*, *yet3Δ::NAT*, *ybr063c::NAT*, and their respective OE and WT strains were a generous gift from Maya Schuldiner's Lab. We also utilized the previously reported strain, DH001-3b (*hem1::HIS3*).[27]

Yeast transformations were performed by the lithium acetate procedure.[101] Strains were maintained at 30 ^{o}C on either enriched or yeast extract-

peptone based medium supplemented with 2 % glucose (YPD) or synthetic complete medium (SC) supplemented with 2 % glucose with appropriate amino acids to maintain selection. Culturing of *hem1Δ* cells required supplementing YPD or SC media with 50 ug/mL 5-aminolevulinic acid (5-ALA) or 15 mg/mL ergosterol and 0.5 % Tween-80 (YPDE or SCE, respectively).[102] Spot tests on fluconazole used 5 or 10 nM fluconazole (Alfa Aesar).

2.8.1.2 E. coli Strains, Media, and Growth Conditions

For cloning, sub-cloning grade chemically competent E. coli cells, strain 10G E. cloni (Lucigen), were used according to the manufacturer's specifications. All E. coli strains were cultured in Lysogeny broth (LB) with appropriate antibiotic selection (either 50 ug/mL ampicillin or kanamycin).

2.8.1.3 Plasmids

Previously described HAP1 Transcriptional Reporter and Heme Sensor Expression plasmids were used to monitor Hap1p activity and labile heme distribution and kinetics, respectively.[27]

The PGRMC1 expression plasmid was a gift from Professor Amy Medlock's lab and was transformed into *dap1Δ*::*kan*MX4 yeast. A DAP1 expression plasmid was generated by amplifying *DAP1* from yeast genomic DNA and sub-cloning it into the XbaI/SpeI sites of p413-*GPD* to produce pAR1034-3.

2.8.2 Experimental Methods

2.8.2.1 Trafficking Dynamics Measurements

Inter-compartmental heme trafficking rates were monitored as described in Martinez-Guzman, et al.[66] Triplicate 5-mL cultures expressing the HS1 heme sensors were seeded at an initial density of 0.01-0.03 *A*600 units per ml (2–6 x 10^5 cells per mL) and grown for 14 - 16 h at 30 °C, with or without 500 μM succinylacetone (SA) (Sigma-Aldrich Cat. # D1415) in SCE-LEU medium, shaking at 220 rpm until cells reached a final density with *A*600 approximately 1.0 (2 x 10^7 cells per mL). After culturing, 1 absorbance unit (~2 x 10^7 cells) of cells were collected, washed twice with 1 mL sterile ultrapure water, and resuspended in 1 mL fresh SC-LEU medium. The cells that were pre-cultured without succinylacetone provided reference values for EGFP/mKATE2 fluorescence ratios associated with maximal heme loading of HS1 (R_{max} values). The succinylacetone-conditioned cells were split into two 500 μL fractions. One fraction was treated with 500 μM succinylacetone to give EGFP/mKATE2 fluorescence ratios associated with minimal heme loading of HS1 (R_{min} values). The other fraction was left untreated so that heme synthesis could be re-initiated to give compartment-specific heme trafficking rates. HS1 fluorescence was monitored using 200 μL of 1 *A*600 unit per ml (2 x 10^7 cells per ml) cell suspension in black Greiner Bio-one flat bottom fluorescence plates (Cat. # 655076) with a Synergy Mx multi-modal plate reader. EGFP (excitation 488 nm, emission 510 nm) and mKATE2 (excitation 588 nm, emission 620 nm) fluorescence was recorded every 5 min for 4 h, with the plate being shaken at medium strength for 30 s prior to each read.

Background fluorescence of cells not expressing the heme sensors was recorded and subtracted from the EGFP and mKATE2 fluorescence values. The fractional heme saturation of the sensor was determined using the described in Equation 1 in Section 2.4.2.1.

2.8.2.2 Dap1 Yeast Spot Test on Fluconazole

Agar plates were made containing 0, 5, or 10 ug/mL fluconazole (Alfa Aesar). The fluconazole stock was made by diluting in sterile DMSO and the appropriate volume amount was added to freshly autoclaved agar media before pouring.

Overnight cultures of WT and *dap1Δ* yeast were grown to mid-exponential phase. Cultures were washed twice in sterile ultrapure water and diluted to 0.2 OD/mL stocks in sterile ultrapure water. 10-fold serial dilutions were made using sterile ultrapure water and 5 uL was spotted onto agar plates containing 0, 5 or 10 ug/mL fluconazole (Alfa Aesar). Images were taken after 3 days of growth at 30 ^{o}C.

2.8.2.3 Total Heme Quantification

Measurements of total heme were performed using a fluorometric assay designed to measure the fluorescence of protoporphyrin IX upon the release of iron from heme as previously described.[103] For all total heme measurements, ~ 1 x 10^8 cells were harvested, washed in ultrapure water, and resuspended in 500 uL 20 mM oxalic acid and stored in a closed box at 4 ^{o}C overnight (16 – 18 hours).

An equal volume (500 uL) of 2 M oxalic acid was added to the cell suspensions in 20 mM oxalic acid. The samples were split, where half of the cell suspension was transferred to a heat block set at 95 ^{o}C and heated for 30 minutes, and the other sample half was kept in a closed box at room temperature (~ 25 ^{o}C) for 30 minutes. All suspensions were then centrifuged for two minutes on a table-top microfuge at 21000 x g and the porphyrin fluorescence (ex. 400 nm, em. 608 nm) or 200 uL of each sample was measured using a Synergy mx multi-modal plate reader in black Grenier Bio-one flat bottom fluorescence plates. Heme concentrations were calculated from a standard curve prepared by diluting 500 – 1500 uM hemin chloride stock solutions in 0.1 M NaOH into ultrapure MilliQ water and from there prepared the same as the cell samples as described above. To calculate heme concentrations, the fluorescence of the un-boiled sample (representing background levels of porphyrins was subtracted from the fluorescence of the boiled sample (representing the free base porphyrin generated upon heme iron release). The cellular concentration of heme was determined by dividing the moles of heme determined in this fluorescence assay by the number of cells analyzed, to give moles of heme per cell. To convert this to a cellular concentration the moles of heme per cell were divided by the volume of a yeast cell (given to be 50 fL).

2.8.2.4 Catalase Activity Measurements in Yeast

The activity of yeast catalase were measured using methods described previously.[104, 105] Yeast cells were cultured in 10 mL SCE media for 14 - 16 hrs to mid-exponential phase. Cells were lysed using zirconium oxide beads in a Bullet Blender (Next Advance).[27] Protein concentrations were determined by the

Bradford method (Bio-Rad). To detect the catalase activity, 15 µg protein lysates were analyzed by native PAGE on a 10% Tris-glycine gel (Invitrogen). The native gel ran in Tris-Glycine buffer at 4 ^{o}C overnight (16 – 18 hrs) at 5 mAmps/20 Volts. After electrophoresis, an in-gel activity stain was utilized to measure catalase activity.[105] While the gel is washing in ultrapure water (rocking at room temperature) the staining solution was made. In brief, the catalase staining solution was prepared by mixing 1 part dopamine (20 mg/mL) and 1 part para-phenylenediamine (3.5 mg/mL) in 0.2 M potassium phosphate buffer, pH 8, 1 part 15% H_2O_2 (JT Baker), and 2 parts DMSO in the order listed. The staining solution was added directly to the gel and allowed to stain for 2 min while gently rocking by hand, followed by imaging on an Amersham Imager. There is not a de-staining or washing step before imaging.

2.8.2.5 Immunoblotting

The expression of yeast catalase was measured using methods described previously.[104, 105] Yeast cells were cultured in 10 mL SCE media for 14–16 h to mid-exponential phase. Cells were lysed using zirconium oxide beads in a Bullet Blender (Next Advance).[27] Protein concentrations were determined by the Bradford method (Bio-Rad). To detect catalase expression, 50 – 100 ug protein lysates were analyzed by SDS-PAGE. After preparing the samples, samples were boiled at 100 ^{o}C for minutes, and briefly centrifuged. Proteins in individual samples were resolved on 14 % SDS–PAGE gels (Invitrogen), run in Tris-Glycine SDS buffer at room temperature at a constant 20 mAmps. After resolving, proteins were transferred onto nitrocellulose membranes overnight at 4 ^{o}C at 20 mAmps/100

Volts for 16 – 18 hrs. Following the overnight transfer, the membrane was cut directly above the 48 kDalton marker (GeneTex, Cat. # 89424-752) for downstream GAPDH and Catalase detection. The membranes were blocked for 1 hr, rocking at room temperature in LiCOR. The blot with the lower kDalton proteins was incubated with the anti-GAPDH (Sigma Cat. # G9545) primary antibody diluted 1:1000 in LiCOR. The blot with the higher kDalton proteins was incubated with the anti-Ctt1 (Reddi Lab) primary antibody diluted 1:1000 in LiCOR. Primary antibody incubation for both blots was performed for 1 hr, rocking at room temperature. Two, eight-minute washes were performed using 1X-TBS-T, rocking at room temperature. Both blots were then incubated with the secondary antibody, Goat anti-Rb (Biotium Cat. # 20067) diluted 1:5000 in LiCOR. This incubation was performed for 1 hr, rocking at room temperature. Two, eight-minute washes were performed in 1X-TBS-T rocking at room temperature before imaging on a LiCOR Odyssey Infrared imager.

2.9.2.6 Tango2 Growth Test

Growth tests of wild-type, *hem1*Δ and *tango2*Δ cells were performed by growing 10-ml cultures for 14–16 h to mid-exponential phase. Cultures were then diluted to 0.2 *A*600 units per ml 50-mL cultures in SC media supplemented with or without 400 µg/mL ALA. Cultures were grown for 16 hr and OD600 readings were taken every hour for 16 hr using a Cary 60 UV/vis spectrophotometer (Agilent).

2.8.2.7 Steady-State Heme Measurements

To measure steady-state labile heme, wild-type, *hem1*Δ, and *tango2*Δ cells expressing the HS1-M7A heme sensors were cultured in 10 mL SCE-LEU media, with or without 0.5 mM succinylacetone, for ~14–16 hr to mid-exponential phase (*A*600 ~ 1–2). Cytosolic and mitochondrial-targeted sensors were expressed on low copy centromeric plasmids and were driven by the GPD promoter (p415-GPD). After culturing, cells were collected, washed in water, and resuspended in phosphate buffered saline (PBS) solution to a density of 10 *A*600 units per mL. Two-hundred mirolitres of the cell suspension, corresponding to 2 *A*600 units or 4 x 10^7 cells, was used to measure EGFP (excitation 488 nm, emission 510 nm) and mKATE2 (excitation 588, emission 620) HS1-M7A sensor fluorescence. Background autofluorescence of cells not expressing the sensors was recorded and subtracted from the EGFP and mKATE2 sensor fluorescence values. Fluorescence was recorded on a Synergy Mx multi-modal plate reader using black Greiner Bio-one flat bottom fluorescence plates.

CHAPTER 3. GENOME-WIDE DETERMINANTS OF STEADY STATE NULEAR HEME BIOAVAILABILITY

3.1 Introduction

Heme b is in almost every subcellular locale where it acts as a signaling molecule or a cofactor tightly embedded in various hemoproteins. The mechanisms governing heme trafficking to these different locations and made available is not well understood. Recently, our lab developed a kinetics assay to observe heme trafficking dynamics to cytosolic, mitochondrial, and nuclear compartments over time.[66] Briefly, heme synthesis is blocked with the inhibitor succinylacetone (SA), and then re-initiated by removing the inhibitor. The fractional saturation of the mitochondria matrix-, nuclear-, and cytosol-targeted HS1 sensors with heme is monitored as a function of time. This assay revealed nuclear heme trafficking rates are up to ~ 25 % faster compared to trafficking to the cytosol and mitochondria matrix. An explanation for this prioritized mobilization is heme's role as a signaling molecule where it regulates gene expression in the nucleus. When heme synthesis is re-initiated following a period of heme starvation, the cell most likely adapts first by reprogramming through gene transcription. This explains the immediate and prioritized need for heme in the nucleus.

In the nucleus, heme regulates transcription by affecting transcription factor activities. Heme activates the transcription factor Hap1p, allowing for the expression of genes involved in respiration; including cytochromes and catalases.[14] Heme also acts on transcription repressors Bach1, p53, and Rev-erb.[15-17] Bach1 regulates expression of heme oxygenase 1 (HO-1) and globin genes. The tumor suppressor p53 suppresses tumorigenesis and regulates DNA-damage repair and cell-cycle arrest.[106, 107] Rev-erb regulates the expression of genes involved in gluconeogenesis, lipid homeostasis, immune response, and the circadian rhythm.[108-110] Heme binding to these repressors destabilizes the complex and can signal for their nucleolar export and/or degradation, removing the transcription block. Heme controls a plethora of cell functions through its ability to affect transcription factor activities in the nucleus. Therefore, there is an immediate need to understand how nuclear heme bioavailability is regulated.

Faster trafficking to the nucleus suggests 1) heme is distributed simultaneously rather than sequentially, and 2) multiple pathways exist for trafficking heme. Since nuclear heme trafficking occurs faster, a more direct pathway from the mitochondria to the nucleus must exist, bypassing the cytosol. As discussed in Chapter 2, more direct trafficking pathways to the nucleus would be through mitochondria-nuclear membrane contact sites, or through the ER. Both proposed routes would provide a more direct pathway to the nucleus bypassing the cytosol altogether. To identify additional proteins and pathways that regulate steady state nuclear heme, we designed an unbiased genetic high throughput screen.

High throughput genetic screens are useful to increase understanding of biological function, stress responses, and drug mechanisms.[111] Here, using genetic screening and biochemical techniques, in combination with heme sensors, yeast gene deletion library was screened to identify yeast mutants with altered nuclear heme levels relative to WT yeast.

We expect the screen will reveal transporters, chaperones, and buffering proteins. Transporters would be localized at the nuclear membrane, possibly facilitating nuclear heme import/export. The screen may also reveal chaperones that deliver heme from other organelles like the cytosol and mitochondria to the nucleus. These proteins would have both nuclear and cytosol or mitochondria localization. Finally, if acting as a nuclear heme buffering protein, we expect these proteins to be strictly localized to the nucleus. Further, nuclear import and export of proteins occurs via nuclear pore complexes. These complexes consist of several subunits. Heme could be trafficked similarly or via a chaperone protein that relies on this pathway.

3.2 Results

3.2.1 Development of a High Throughput Screen for Nuclear Heme Availability Using Low- and High-Affinity Heme Sensors

The commercially available yeast deletion library consists of 5154 yeast gene deletion mutants (Thermo Fisher). These 5154 genes are non-essential, and the gene deletion mutants are viable despite lacking any one of these genes. This library was transformed with low- and high-affinity heme sensors (HS1-M7A and

HS1, respectively) targeted to the nucleus. Transformations were performed using lithium acetate, microtiter plates, and a liquid handling robotics system (BioTek Precision XS).[112] HS1-M7A and HS1 sensors were successfully expressed in 4820 and 4810 mutants, respectively. The libraries were screened for altered HS1-M7A or HS1 sensor fluorescence ratios in the nucleus, relative to WT strains. Sensor ratio values were converted to % Heme Sensor Bound values for each mutant (described previously in Equation 1). Mutant frequencies with a given % Heme Sensor Bound value are displayed in the histograms below (Figure 11A and B). HS1-M7A sensor ratios were z-scored using Equation 2 where u is the mean sensor ratio of all yeast mutants within a given 96-well plate, x is the mean ratio for a given yeast mutant, and s is the mean standard deviation of sensor ratios within a given 96-well plate. Finally, the statistical significance of the mutant z-score relative to the WT z-score was calculated using JMP software. This data is summarized in the Volcano Plot in Figure 11C. Further, using the % Heme Sensor Bound values from the HS1 screen, statistical significance of the mutant % bound values relative to WT values were calculated using JMP software and results are summarized in Figure 10D.

$$Z\ score = \frac{u-x}{s} \qquad \text{Equation 2}$$

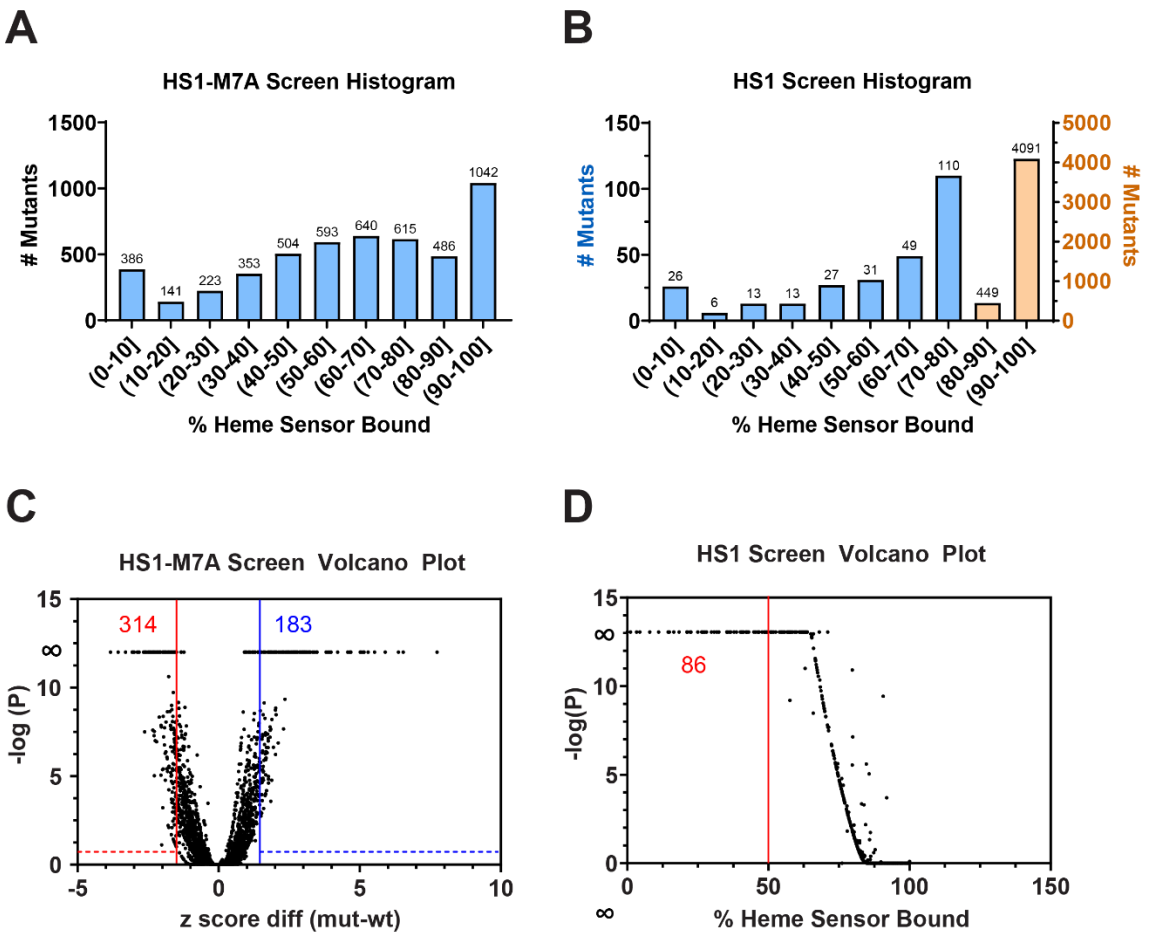

Figure 11 – High Throughput Genetic Screens Reveal Mutants with Altered Nuclear Heme. Histograms showing the frequency of mutants with a given % Heme Sensor Bound value from screening with HS1-M7A **(A)** or HS1 **(B)** nuclear-targeted heme sensors. Volcano plots of z-scored mutant ratios from screening with HS1-M7A sensors **(C)** and % Heme Sensor Bound mutant values from screening with HS1 sensors **(D)**, where P-values were calculated relative to WT.

3.2.2 Deletion Mutants with Low Nuclear Heme Revealed by Screening with the HS1-M7A and HS1 Sensors

Screening with HS1-M7A revealed 314 and 183 yeast mutants with significantly lower or higher nuclear heme compared to WT, respectively (Figure 11C). To determine if any of these genes were representative of a particular biological function or localized to a compartment, genes were submitted to the

online **P**rotein **A**nalysis **T**hrough **E**volutionary **R**elationships (PANTHER) classification system to curate and identify the statistically significant hits from the screen. Referring to the False Discovery Rate values (FDR) in Tables 1 and 2, there was not a particular biological function or localization that was significantly enriched within these gene lists (Table 1 and 2, respectively).

Table 1. GO Biological Process of Mutants with Significantly Low Heme

GO Biological Process	Fold Enrichment	Raw P-value	FDR
organonitrogen compound metabolic process (GO:1901564)	1.43	2.24E-05	5.48E-02
organic substance catabolic process (GO:1901575)	1.82	2.17E-05	1.06E-01
cellular component assembly (GO:0022607)	0.48	1.50E-03	4.08E-01
protein modification process (GO:0036211)	1.61	1.62E-03	4.16E-01
organonitrogen compound catabolic process (GO:1901565)	1.83	1.47E-03	4.23E-01
carbohydrate derivative transport (GO:1901264)	4.08	1.43E-03	4.35E-01
cellular response to extracellular stimulus (GO:0031668)	2.67	1.34E-03	4.37E-01
ATP transport (GO:0015867)	5.21	1.93E-03	4.48E-01
protein modification by small protein removal (GO:0070646)	4.44	1.85E-03	4.51E-01
regulation of biological process (GO:0050789)	1.33	2.20E-03	4.68E-01
organophosphate ester transport (GO:0015748)	3.39	7.67E-04	4.68E-01
cellular response to external stimulus (GO:0071496)	2.67	1.34E-03	4.69E-01
nucleotide transport (GO:0006862)	4.21	2.41E-03	4.70E-01
mRNA processing (GO:0006397)	0.11	2.38E-03	4.84E-01
macromolecule modification (GO:0043412)	1.55	2.19E-03	4.87E-01
RNA processing (GO:0006396)	0.4	9.97E-04	4.87E-01
response to nutrient levels (GO:0031667)	2.45	2.80E-03	4.88E-01

Table 2. GO Cellular Component of Mutants with Significantly Low Heme

GO cellular component complete	Fold Enrichment	Raw P-value	FDR
cytoplasm (GO:0005737)	1.11	2.79E-03	1.00E+00
Sin3-type complex (GO:0070822)	5.1	4.99E-03	1.00E+00
ESCRT complex (GO:0036452)	5.86	7.89E-03	1.00E+00
Set1C/COMPASS complex (GO:0048188)	8.79	8.74E-03	1.00E+00
histone methyltransferase complex (GO:0035097)	8.79	8.74E-03	1.00E+00
dolichyl-phosphate-mannose-protein mannosyltransferase Pmt1p-Pmt2p dimer complex (GO:0097582)	23.45	9.47E-03	1.00E+00
bounding membrane of organelle (GO:0098588)	1.51	9.96E-03	1.00E+00
Rpd3L complex (GO:0033698)	5.21	1.12E-02	1.00E+00
histone deacetylase complex (GO:0000118)	2.88	1.50E-02	1.00E+00
ESCRT II complex (GO:0000814)	15.63	1.54E-02	1.00E+00
dolichyl-phosphate-mannose-protein mannosyltransferase complex (GO:0031502)	9.38	3.05E-02	1.00E+00
microtubule cytoskeleton (GO:0015630)	0.16	3.17E-02	1.00E+00
Rpd3L-Expanded complex (GO:0070210)	3.61	3.25E-02	1.00E+00
peroxisomal membrane (GO:0005778)	3.01	3.26E-02	1.00E+00
microbody membrane (GO:0031903)	3.01	3.26E-02	1.00E+00
intracellular anatomical structure (GO:0005622)	1.05	3.36E-02	1.00E+00
spliceosomal complex (GO:0005681)	< 0.01	3.41E-02	1.00E+00
Golgi membrane (GO:0000139)	2	3.43E-02	1.00E+00
late endosome (GO:0005770)	2.47	4.29E-02	1.00E+00
Cul3-RING ubiquitin ligase complex (GO:0031463)	6.7	4.96E-02	1.00E+00
retrotransposon nucleocapsid (GO:0000943)	< 0.01	5.29E-02	1.00E+00
endoplasmic reticulum tubular network (GO:0071782)	3.03	5.30E-02	1.00E+00
nucleolus (GO:0005730)	0.47	5.36E-02	1.00E+00

The yeast gene library collection was then screened using the HS1 high affinity sensor. Screening with this sensor allows for the detection of small, yet significant changes in nuclear labile heme. Because the HS1 sensor is poised at 100 % bound in WT yeast, only decreases in heme are detected using this sensor. This screen identified 86 mutants with statistically significantly less nuclear heme relative to WT, whose sensors were less than or equal to 50 % heme bound (Figure 11D). Analyzing using PANTHER did not reveal a particular biological function enriched within the list of 86 mutants (data not shown). This makes sense since only 86 genes were submitted for PANTHER analysis, which is not a substantial amount. 34 of these 86 mutants with low heme were also identified in the HS1-M7A screen having low heme (Figure 12). These 34 genes are listed in Tables 3 and 4. The 34 genes cover a wide range of pathways.

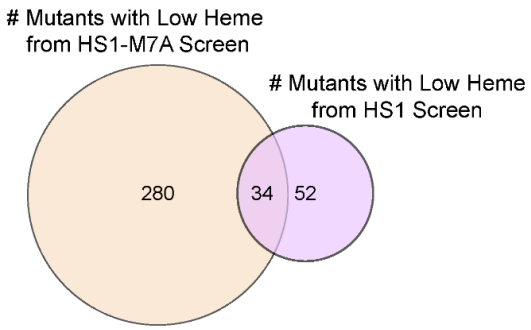

Figure 12 – Venn Diagram of gene deletion mutants with low nuclear heme from HS1 and HS1-M7A screens. Screening with HS1 and HS1-M7A sensors revealed the same 34 gene deletion mutants having low nuclear heme.

Table 3. Common Mutants Identified with Low Nuclear Heme from HS1 and M7A Screens

Gene	ORF	M7A		HS1	
		Ratio	Ratio Stdev	Ratio	Ratio Stdev
LDB7	YBL006C	17.0	2.3	7.6	3.7
YBL053W	YBL053W	30.0	4.6	7.1	1.1
AAC3	YBR085W	44.5	14.2	8.2	2.4
AHK1	YDL073W	22.0	5.6	9.6	2.2
STE7	YDL159W	32.9	6.4	9.1	3.9
MKC7	YDR144C	15.4	2.7	8.3	1.1
RTN1	YDR233C	21.7	2.8	9.3	3.2
SUM1	YDR310C	13.8	1.8	8.4	1.2
MRPL28	YDR462W	27.9	12.7	9.6	2.8
FMP52	YER004W	11.8	2.0	8.0	1.4
UBP9	YER098W	31.6	5.9	7.3	3.7
EMP47	YFL048C	18.2	1.7	8.6	4.6
YFR018C	YFR018C	30.7	5.3	7.0	3.0
RPL1B	YGL135W	23.6	3.9	7.2	0.6
BUD9	YGR041W	23.9	5.6	6.9	1.6
YGR291C	YGR291C	38.6	13.4	5.6	2.8
QDR2	YIL121W	20.7	6.0	9.8	2.4
UBX6	YJL048C	35.8	6.5	12.3	4.6
UBP12	YJL197W	21.1	4.9	5.3	0.8
YKL030W	YKL030W	24.7	5.9	8.8	3.8
YKL066W	YKL066W	20.1	2.8	9.5	2.2
TRP3	YKL211C	43.0	8.1	10.0	5.4
RFX1	YLR176C	12.3	3.1	7.1	4.4
ADY4	YLR227C	20.7	0.9	9.2	3.3
ARV1	YLR242C	33.6	4.8	11.1	4.1
CAR2	YLR438W	32.2	8.6	7.8	2.5
SRV2	YNL138W	33.8	6.4	7.0	2.9
SDD3	YOL098C	24.8	2.4	7.8	2.7
RUP1	YOR138C	26.6	6.7	7.2	4.0
UBP16	YPL072W	23.5	8.1	11.4	6.2
FRK1	YPL141C	17.4	1.9	12.2	3.4
DSS4	YPR017C	22.4	6.1	7.5	1.2
SRO7	YPR032W	20.3	1.9	7.6	2.2

Table 4. Description of Common Mutants Identified with Low Nuclear Heme from HS1 and M7A Screens

Gene	ORF	Description
LDB7	YBL006C	Component of the RSC chromatin remodeling complex
YBL053W	YBL053W	Dubious open reading frame
AAC3	YBR085W	Mitochondrial inner membrane ADP/ATP translocator
AHK1	YDL073W	Scaffold protein in the HKR1 sub-branch of the Hog1p-signaling pathway
STE7	YDL159W	Signal transducing MAP kinase kinase
MKC7	YDR144C	GPI-anchored aspartyl protease
RTN1	YDR233C	Reticulon protein
SUM1	YDR310C	Transcriptional repressor that regulates middle-sporulation genes
MRPL28	YDR462W	Mitochondrial ribosomal protein of the large subunit
FMP52	YER004W	Protein of unknown function
UBP9	YER098W	Ubiquitin-specific protease that cleaves ubiquitin-protein fusions
EMP47	YFL048C	Integral membrane component of ER-derived COPII-coated vesicles
YFR018C	YFR018C	Putative protein of unknown function
RPL1B	YGL135W	Ribosomal 60S subunit protein L1B
BUD9	YGR041W	Protein involved in bud-site selection
YGR291C	YGR291C	Dubious open reading frame
QDR2	YIL121W	Plasma membrane transporter of the major facilitator superfamily
UBX6	YJL048C	UBX (ubiquitin regulatory X) domain-containing protein
UBP12	YJL197W	Ubiquitin-specific protease
YKL030W	YKL030W	Dubious open reading frame
YKL066W	YKL066W	Dubious open reading frame
TRP3	YKL211C	Indole-3-glycerol-phosphate synthase
RFX1	YLR176C	Major transcriptional repressor of DNA-damage-regulated genes
ADY4	YLR227C	Structural component of the meiotic outer plaque
ARV1	YLR242C	Cortical ER protein
CAR2	YLR438W	L-ornithine transaminase (OTAse)
SRV2	YNL138W	CAP (cyclase-associated protein)
SDD3	YOL098C	Putative metalloprotease
RUP1	YOR138C	Protein that regulates ubiquitination of Rsp5p
UBP16	YPL072W	Mitochondrial inner membrane protein with similarity to Mdm31p
FRK1	YPL141C	Deubiquitinating enzyme anchored to the outer mitochondrial membrane

Table 4 Continued

DSS4	YPR017C	Protein kinase of unknown cellular role
SRO7	YPR032W	Guanine nucleotide dissociation stimulator for Sec4p

3.2.3 Comparison of Nuclear and Cytosolic Screen Hits

A similar screen was performed by our lab that identified determinants of cytosolic heme.[113] Gene deletion mutants with altered nuclear heme were compared with gene deletion mutants with altered cytosolic heme. These lists will reveal if heme buffering capacity is restricted to specific organelles or if the mutants affect heme in both cytosolic and nuclear compartments. If a single gene affects both cytosolic and nuclear heme, it could regulate heme similarly in both organelles (causing an increase in both the cytosol and nucleus or causes a decrease in both the cytosol and nucleus) or heme can be regulated oppositely in these organelles (causing a decrease in one organelle and an increase in the other). If there is a dual organelle heme buffering effect, this protein could be localized to both cytosolic and nuclear compartments.

We analyzed gene lists of mutants that had significant increases or decreases in cytosolic heme and nuclear heme and generated the venn diagrams below. 46 gene deletion mutants resulted in significantly lower heme in both cytosolic and nuclear compartments (Figure 13A, Table 5). 10 gene deletion mutants had significantly higher heme in both cytosolic and nuclear organelles (Figure 13B, Table6). 25 mutants had lower cytosolic heme and higher nuclear heme (Figure 13C, Table 7). 11 mutants had higher cytosolic and lower nuclear heme (Figure 13D, Table 8).

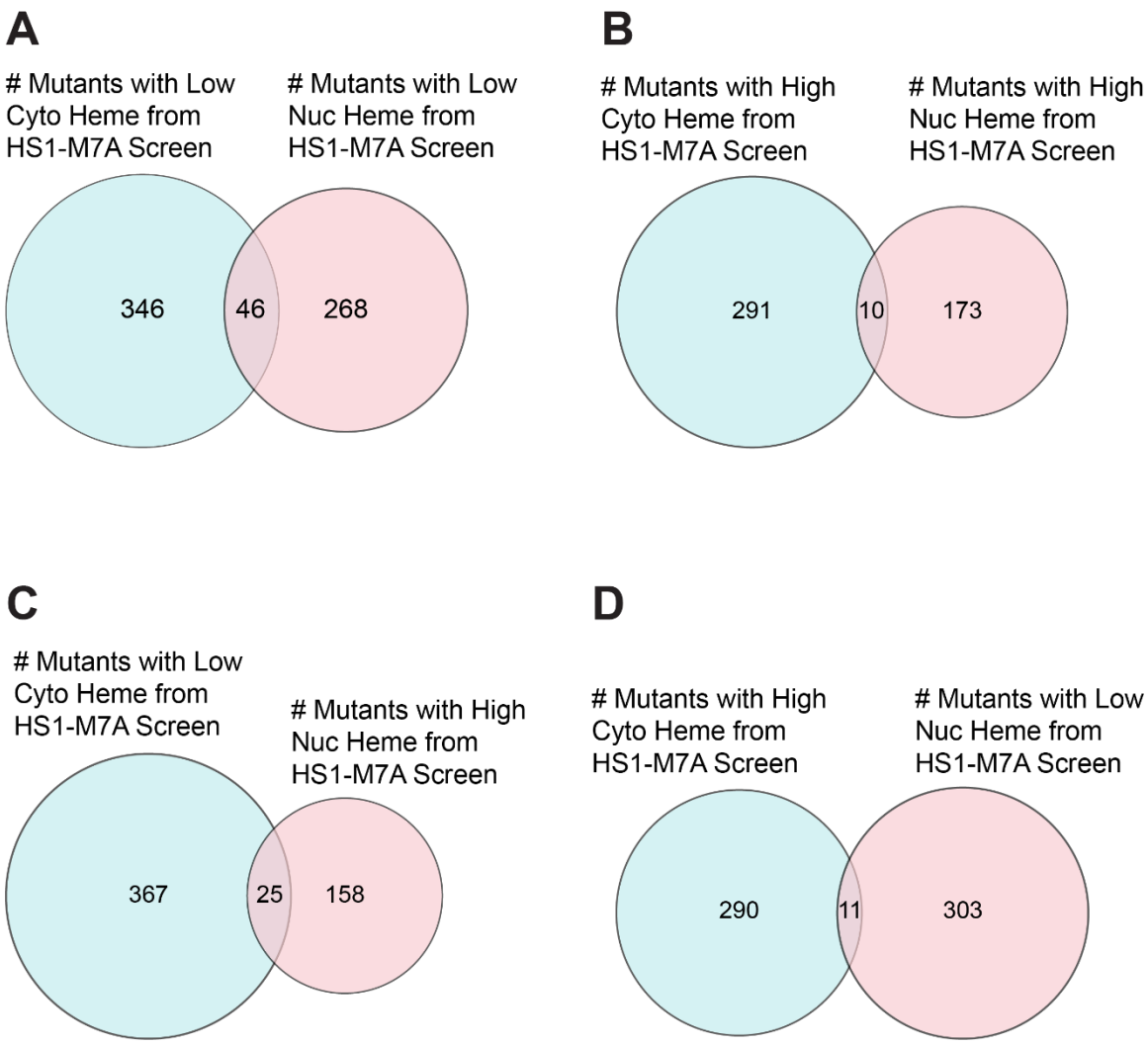

Figure 13 – Venn Diagrams Comparing Lists of Mutants with Altered Cytosolic and Nuclear Heme Levels Relative to WT. Venn diagrams of mutants with lower cytosolic and nuclear heme **(A)**, higher cytosolic and nuclear heme **(B)**, low cytosolic and high nuclear heme **(C)** and vice versa **(D)** as revealed by screening with the HS1-M7A sensors.

Table 5. List of Gene Deletion Mutants with Low Cyto and Nuclear Heme

ORF	Gene	Description
YAL055W	PEX22	Putative peroxisomal membrane protein
YBR133C	HSL7	Protein arginine N-methyltransferase
YBR195C	MSI1	Subunit of chromatin assembly factor I (CAF-1)
YBR227C	MCX1	Non-proteolytic ATPase of the AAA family
YDL073W	AHK1	Scaffold protein in the HKR1 sub-branch of the Hog1p-signaling pathway
YDL119C	HEM25	Mitochondrial glycine transporter
YDR080W	VPS41	Subunit of the HOPS endocytic tethering complex
YDR098C	GRX3	Glutathione-dependent oxidoreductase
YDR101C	ARX1	Nuclear export factor for the ribosomal pre-60S subunit
YDR120C	TRM1	tRNA methyltransferase
YDR265W	PEX10	Peroxisomal membrane E3 ubiquitin ligase
YDR363W-A	SEM1	19S proteasome regulatory particle lid subcomplex component
YDR369C	XRS2	FHA domain-containing component of the Mre11 complex
YDR377W	ATP17	Subunit f of the F0 sector of mitochondrial F1F0 ATP synthase
YEL037C	RAD23	Protein with ubiquitin-like N terminus
YEL057C	SDD1	Protein of unknown function
YER040W	GLN3	Transcriptional activator in nitrogen catabolite repression system
YER048C	CAJ1	Nuclear type II J heat shock protein of the E. coli dnaJ family
YER087W	AIM10	Protein with similarity to tRNA synthetases
YGL033W	HOP2	Meiosis-specific protein that localizes to chromosomes
YGL244W	RTF1	Subunit of RNAPII-associated chromatin remodeling Paf1 complex
YGR291C	YGR291C	Dubious open reading frame
YIL017C	VID28	GID Complex subunit
YJR102C	VPS25	Component of the ESCRT-II complex
YKL040C	NFU1	Protein involved in Fe-S cluster transfer to mitochondrial clients
YKL041W	VPS24	One of four subunits of the ESCRT-III complex
YLL049W	LDB18	Component of the dynactin complex
YLR015W	BRE2	Subunit of COMPASS (Set1C) complex
YLR124W	YLR124W	Dubious open reading frame

Table 5 Continued

YMR036C	MIH1	Protein tyrosine phosphatase involved in cell cycle control and retrograde protein transport
YMR105W-A	YMR105W-A	Putative protein of unknown function
YMR169C	ALD3	Cytoplasmic aldehyde dehydrogenase
YNL021W	HDA1	Putative catalytic subunit of a class II histone deacetylase complex
YNL148C	ALF1	Alpha-tubulin folding protein
YNL319W	YNL319W	Dubious open reading frame
YOL032W	OPI10	Protein with a possible role in phospholipid biosynthesis
YOL044W	PEX15	Tail-anchored type II integral peroxisomal membrane protein
YOR147W	MDM32	Mitochondrial inner membrane protein with similarity to Mdm31p
YPL002C	SNF8	Component of the ESCRT-II complex
YPL023C	MET12	Protein with MTHFR activity in vitro
YPL055C	LGE1	Protein involved in histone H2B ubiquitination
YPL065W	VPS28	Component of the ESCRT-I complex
YPL139C	UME1	Component of both the Rpd3S and Rpd3L histone deacetylase complexes
YPL182C	YPL182C	Dubious open reading frame
YPR066W	UBA3	Protein that activates Rub1p (NEDD8) before neddylation
YPR127W	YPR127W	Putative pyridoxine 4-dehydrogenase

Table 6. List of Gene Deletion Mutants with High Cyto and Nuclear Heme

ORF	Gene	Descr.
YBR189W	RPS9B	Protein component of the small (40S) ribosomal subunit
YEL059W	HHY1	Putative protein of unknown function
YHR034C	PIH1	Component of the conserved R2TP complex (Rvb1-Rvb2-Tah1-Pih1)
YIL103W	DPH1	Protein required for synthesis of diphthamide
YIR005W	IST3	Component of the U2 snRNP
YJL016W	TPH3	Putative protein of unknown function
YJR144W	MGM101	Protein with a role in mitochondrial DNA recombinational repair
YLR315W	NKP2	Central kinetochore protein and subunit of the Ctf19 complex
YLR451W	LEU3	Zinc-knuckle transcription factor
YPL017C	IRC15	Microtubule associated protein

Table 7. List of Gene Deletion Mutants with Low Cyto and High Nuc Heme

ORF	Gene	Descr.
YAL055W	PEX22	Putative peroxisomal membrane protein
YBR133C	HSL7	Protein arginine N-methyltransferase
YBR195C	MSI1	Subunit of chromatin assembly factor I (CAF-1)
YBR227C	MCX1	Non-proteolytic ATPase of the AAA family
YDL073W	AHK1	Scaffold protein in the HKR1 sub-branch of the Hog1p-signaling pathway
YDL119C	HEM25	Mitochondrial glycine transporter
YDR080W	VPS41	Subunit of the HOPS endocytic tethering complex
YDR098C	GRX3	Glutathione-dependent oxidoreductase
YDR101C	ARX1	Nuclear export factor for the ribosomal pre-60S subunit
YDR120C	TRM1	tRNA methyltransferase
YDR265W	PEX10	Peroxisomal membrane E3 ubiquitin ligase
YDR363W-A	SEM1	19S proteasome regulatory particle lid subcomplex component
YDR369C	XRS2	FHA domain-containing component of the Mre11 complex
YDR377W	ATP17	Subunit f of the F0 sector of mitochondrial F1F0 ATP synthase
YEL037C	RAD23	Protein with ubiquitin-like N terminus
YEL057C	SDD1	Protein of unknown function
YER040W	GLN3	Transcriptional activator in nitrogen catabolite repression system
YER048C	CAJ1	Nuclear type II J heat shock protein of the E. coli dnaJ family
YER087W	AIM10	Protein with similarity to tRNA synthetases
YGL033W	HOP2	Meiosis-specific protein that localizes to chromosomes
YGL244W	RTF1	Subunit of RNAPII-associated chromatin remodeling Paf1 complex
YGR291C	YGR291C	Dubious open reading frame
YIL017C	VID28	GID Complex subunit
YJR102C	VPS25	Component of the ESCRT-II complex
YKL040C	NFU1	Protein involved in Fe-S cluster transfer to mitochondrial clients
YKL041W	VPS24	One of four subunits of the ESCRT-III complex
YLL049W	LDB18	Component of the dynactin complex
YLR015W	BRE2	Subunit of COMPASS (Set1C) complex
YLR124W	YLR124W	Dubious open reading frame

Table 7 Continued

YMR036C	MIH1	Protein tyrosine phosphatase involved in cell cycle control and retrograde protein transport
YMR105W-A	YMR105W-A	Putative protein of unknown function
YMR169C	ALD3	Cytoplasmic aldehyde dehydrogenase
YNL021W	HDA1	Putative catalytic subunit of a class II histone deacetylase complex
YNL148C	ALF1	Alpha-tubulin folding protein
YNL319W	YNL319W	Dubious open reading frame
YOL032W	OPI10	Protein with a possible role in phospholipid biosynthesis
YOL044W	PEX15	Tail-anchored type II integral peroxisomal membrane protein
YOR147W	MDM32	Mitochondrial inner membrane protein with similarity to Mdm31p
YPL002C	SNF8	Component of the ESCRT-II complex
YPL023C	MET12	Protein with MTHFR activity in vitro
YPL055C	LGE1	Protein involved in histone H2B ubiquitination
YPL065W	VPS28	Component of the ESCRT-I complex
YPL139C	UME1	Component of both the Rpd3S and Rpd3L histone deacetylase complexes
YPL182C	YPL182C	Dubious open reading frame
YPR066W	UBA3	Protein that activates Rub1p (NEDD8) before neddylation
YPR127W	YPR127W	Putative pyridoxine 4-dehydrogenase

Table 8. List of Gene Deletion Mutants with High Cyto and Nuc Heme

ORF	Gene	Descr.
YCR006C	YCR006C	Putative protein of unknown function
YCR067C	SED4	Integral ER membrane protein that stimulates Sar1p GTPase activity
YDL137W	ARF2	ADP-ribosylation factor
YDR043C	NRG1	Transcriptional repressor
YEL062W	NPR2	Subunit of the Iml1p/SEACIT complex
YIL121W	QDR2	Plasma membrane transporter of the major facilitator superfamily
YJR010W	MET3	ATP sulfurylase
YKL157W	APE2	Aminopeptidase yscII
YOR178C	GAC1	Regulatory subunit for Glc7p type-1 protein phosphatase (PP1)
YOR267C	HRK1	Protein kinase
YPR057W	BRR1	snRNP protein component of spliceosomal snRNPs

3.2.4 Validation of the 86 Mutants with Low Nuclear Heme Identified from the HS1 Screen

The 86 mutants with low nuclear heme identified in the HS1 screen were validated by obtaining single colonies and re-screening the sensor ratios from the three independent clones. Data from 29/86 mutants had re-producible results where at least 2/3 clones for a given mutant had high ratios like in the initial screen (Table 9). The identity of these 29 mutants was confirmed in 13 mutants (highlighted in green in Table 9) via a process called barcoding. In this process, DNA flanking regions of the *KanMX4* deletion cassette in each mutant was amplified by PCR and sequenced. One of the mutants validated was *bud25Δ*. This candidate was removed from further analysis since its ORF overlaps with the heme

synthesis gene, *HEM14*. The protein localization for each gene is from Yeast Protein Localization ^{Plus} (YPL+) Database.[114]

Table 9. Mutants with High Ratios after Secondary Screening

ORF	GENE	LOCALE	DESCR.
AHP1	YLR109W	CYTO	Thiol-specific peroxiredoxin
ARV1	YLR242C	NA	Cortical ER protein
BMH2	YDR099W	CYTO	14-3-3 protein
CBC2	YPL178W	NUC	subunit of the heterodimeric cap binding complex
MUM3	YOR298W	NA	Unknown
PUT3	YKL015W	NUC	Transcriptional activator
RPD3	YNL330C	NA	Histone deacetylase
RPL8A	YHL033C	CYTO, FOCI	Ribosomal 60S subunit protein
YCR101C	YCR101C	NA	Unknown
YKL097C	YKL097C	NA	Unknown
ZDS1	YMR273C	NA	regulating Swe1p-dependent polarized growth
AIM11	YER093C-A	NA	Unknown
LDB7	YBL006C	NA	Component of the RSC chromatin remodeling complex
RSM25	YIL093C	MITO	Mitochondrial ribosomal protein
TRP3	YKL211C	CYTO	Indole-3-glycerol-phosphate synthase
AAC3	YBR085W	MITO	Mitochondrial inner membrane ADP/ATP translocator
AHK1	YDL073W	NA	Hog1p Signaling Pathway
BUD25	YER014C-A	NA	Bud-site selection
COA1	YIL157C	MITO	Mitochondrial inner membrane protein
IMP2	YIL154C	NA	Transcriptional activator
KGD1	YIL125W	MITO	Mitochondrial alpha-ketoglutarate dehydrogenase complex
MDM32	YOR147W	MITO	Mitochondrial inner membrane protein
MRPL28	YDR462W	MITO	Mitochondrial ribosomal protein
QDR2	YIL121W	CELL PERIPH.	Plasma membrane transporter
RPL1B	YGL135W	CYTO	Ribosomal 60S subunit
SRV2	YNL138W	CYTO, FOCI	CAP (cyclase-associated protein)
SUC2	YIL162W	NA	Invertase
YOR366W	YOR366W	NA	Unknown
YPL183W	YPL183W	MITO?..	Unknown

To further validate the observed low heme phenotypes in the remaining 12 candidate mutants, we tested if the phenotype was dependent on growth protocol. Mutant sensor fluorescence ratios grown in 96-well plates (like in the screen) were compared to shaking cultures. Four of these mutants (*ahp1Δ*, *trp3Δ*, *mum3Δ* and *zds3Δ*) did not display the low heme phenotype when grown shaking as they did when grown in the standing 96-well plate. In fact, these mutants have heme sensor ratios like WT when grown shaking (a representative example is shown in Figure 14A). The remaining eight mutants displayed low nuclear heme when grown in shaking cultures (Figure 14B-I). Interestingly, ratio differences between WT and the mutants are diminished when grown shaking compared to growth in standing 96-well plates.

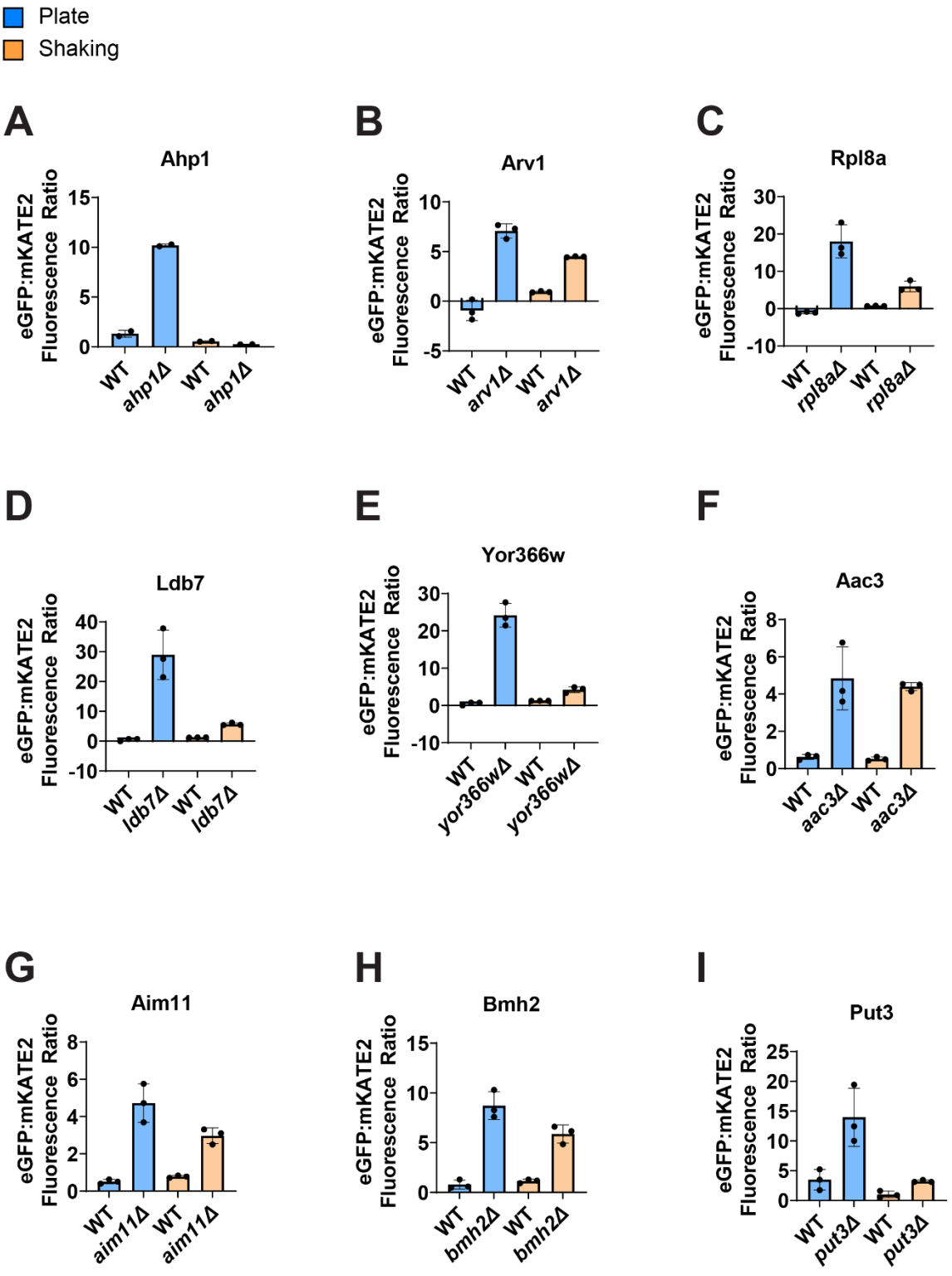

Figure 14 – Nuclear Heme Sensor Ratios of Mutants grown in standing vs. shaking cultures. *ahp1Δ* **(A),** *arv1Δ* **(B)**, *rpl8aΔ* **(C)**, *ldb7Δ* **(D)**, *yor366wΔ* **(E)**, *aac3Δ* **(F)**, *aim11Δ* **(G)**, *bmh2Δ* **(H),** and *put3Δ* **(I)** nuclear heme sensor ratios grown in a 96-well plate (blue) or shaking (orange). Each *dot* represents a biological replicate.

3.2.5 Complementation Experiments of Validated Mutants with Low Nuclear Heme

Lastly, to confirm the heme phenotype observed is due to the identified gene deletion, we performed complementation experiments. Two gene expression plasmids were designed to complement each of the seven gene deletion mutants; one where gene expression is under a strong promoter (GPD) or a weak promoter (TEF). YOR366W gene expression plasmids were not made to due inability to amplify the gene from genomic DNA using PCR. Therefore, only seven mutants were tested for complementation. Expressing either of these gene expression plasmids did not rescue the observed low heme phenotype in any of the identified seven deletion mutants (Figure 15).

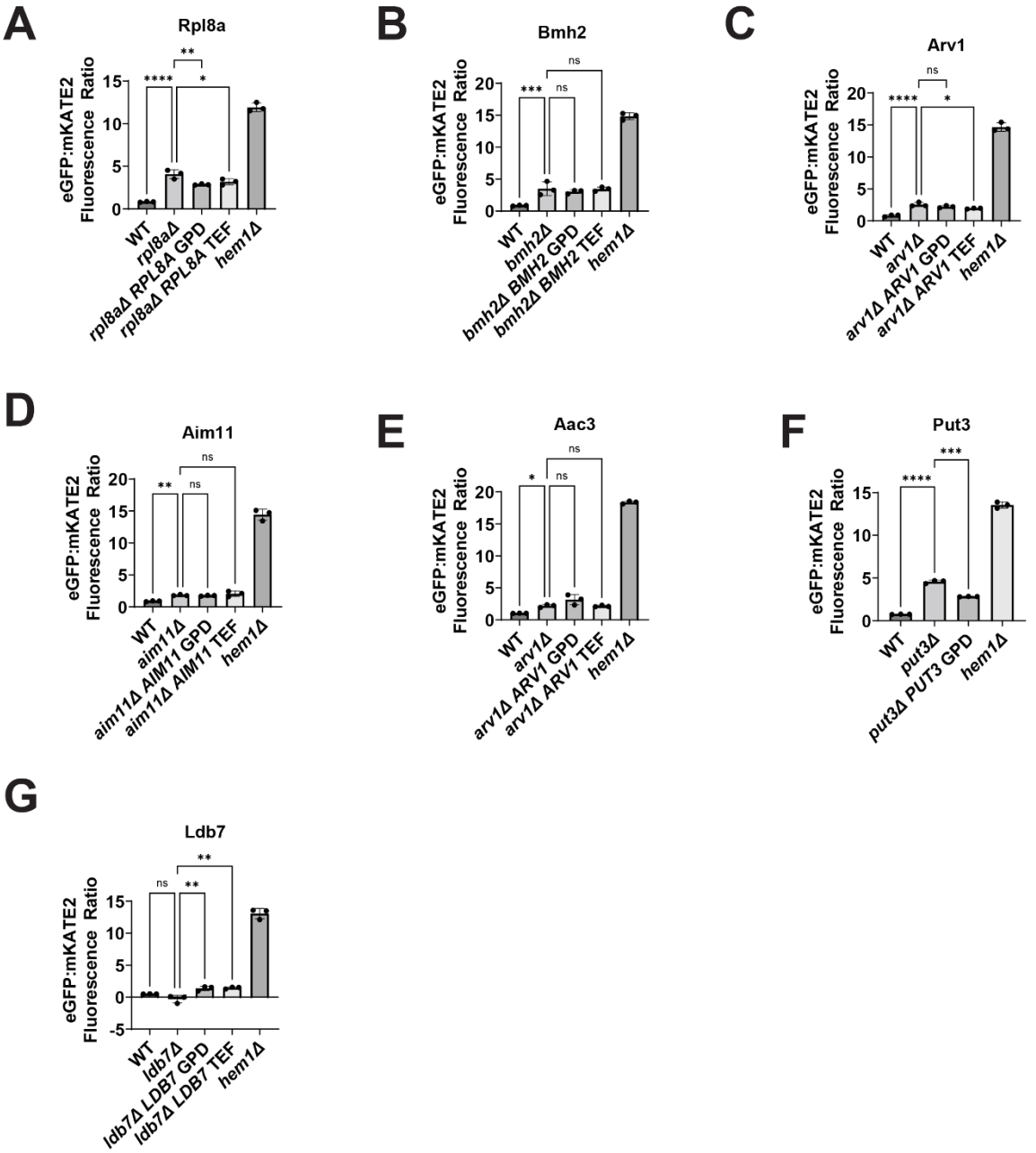

Figure 15 – Nuclear Labile Heme Complementation Experiments. Nuclear heme complementation experiments using strong (GPD) and weak (TEF) gene expression promoter plasmids in rpl8a*Δ* **(A)**, bmh2*Δ* **(B)**, arv1*Δ* **(C)**, aim11*Δ* **(D)**, aac3*Δ* **(E)**, put3*Δ* **(F)**, and *lbd7Δ* **(G)**. Each *dot* represents a biological replicate. The significance is indicated by asterisks using a two-way ANOVA for multiple comparisons with Dunnett's post hoc test: * $p < 0.05$, ** $p < 0.01$, *** $p < 0.001$, **** $p < 0.0001$, ns, not significant.

To validate the gene expression plasmids were being expressed, we tested growth rescue of mutants with known growth deficiencies. BMH2 has been identified as a suppressor of the well-recognized growth deficiency phenotype due to rapamycin.[115, 116] *bm2hΔ* yeast growth is more sensitive on media containing rapamycin.[115]

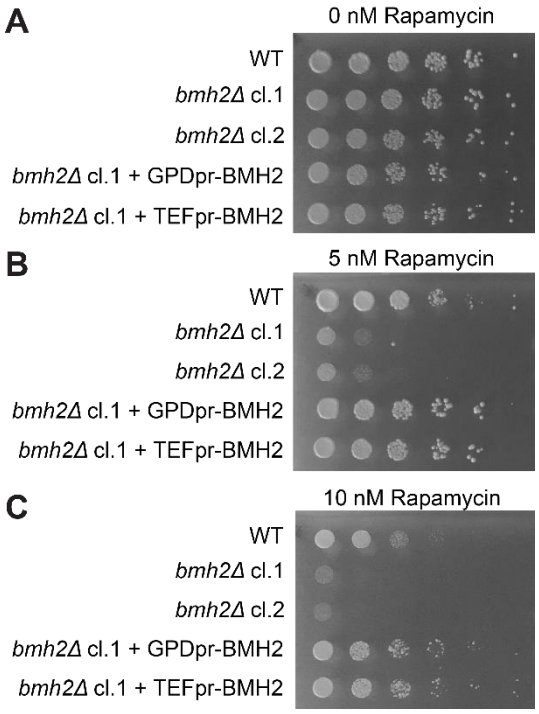

Figure 16 – *bmh2Δ* Growth Complementation. *bmh2Δ* yeast strains with and without GPD- and TEF-driven BMH2 expression plasmids grown on agar plates with or without 5 and 10 nM rapamycin.

In yeast, rapamycin targets members of the PIK-related kinase family, Tor1p and Tor2p proteins.[117, 118] The fidelity of our BMH2 gene expression plasmids by performing spot tests on agar plates with and without 5 and 10 nM rapamycin using WT and *bm2hΔ* yeast transformed with GPD- or TEF-BMH2 gene

expression plasmids or empty vector (EV) plasmids (Figure 16). Two *bm2hΔ* clones were tested and displayed a growth defect on rapamycin plates, as expected. Growth was rescued in Bmh2 deletion yeast containing BMH2 expression plasmids (Figure 16). This experiment shows that these strains phenotypically behave as *bm2hΔ* yeast, and that the BMH2 expression plasmids are being expressed correctly. Despite BMH2 expression, Bmh2 is not able to rescue the low labile heme levels observed.

We conducted a similar analysis with the *arv1Δ* yeast mutants. Arv1 is a gene involved in sterol distribution and uptake. *arv1Δ* yeast exhibit altered intracellular sterol distribution and are defective in sterol uptake. ARV1 mutants are also inviable when grown anaerobically.[119] ARV1 expression plasmids were tested by observing *arv1Δ* anaerobic growth. Spot tests were conducted using WT and two different *arv1Δ* clones transformed with GPD- or TEF-ARV1 gene expression plasmids or empty vector (EV) plasmids and were incubated in the COY chamber. The ARV1 expression plasmids were able to rescue *arv1Δ* growth when grown anaerobically (Figure 17).

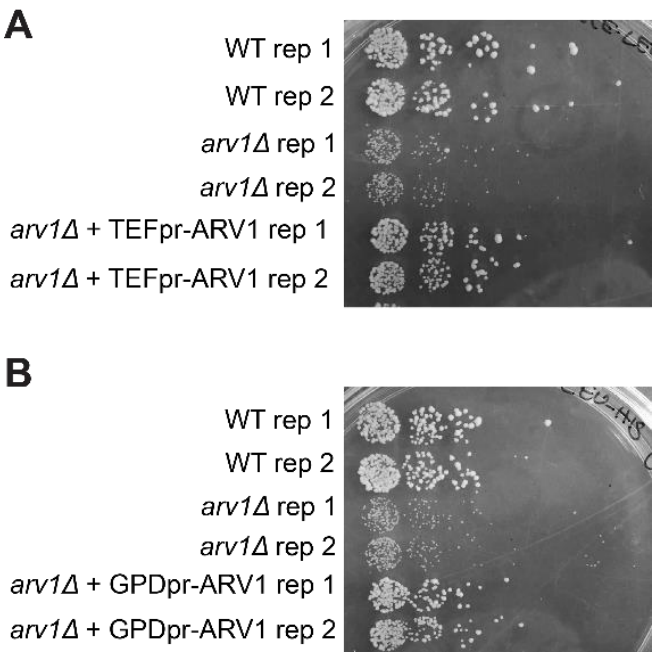

Figure 17 – *arv1Δ* Growth Complementation. *Arv1Δ* yeast strains with and without GPD- and TEF-driven ARV1 expression plasmids grown on agar plates grown anaerobically at 30 ^{O}C.

In conclusion, the expression plasmids rescued growth in the bmh2 and arv1 mutants, but not the low heme phenotypes. Based on these results, we hypothesized the heme phenotype observed may be due to a background mutation in the strain. To investigate this, new *bm2hΔ* yeast were generated using a PCR-based gene disruption strategy to replace the BMH2 open reading frame (ORF) with the *KanMX4* marker. Three different clones of these new *bm2hΔ* strains were validated by PCR and are referred to below as "*bm2hΔ* new." The *bm2hΔ* yeast derived from the gene deletion library are referred to below as "*bm2hΔ* Lib." The total heme in these strains was like WT (Figure 18A). However, the *bm2hΔ* new strains did not exhibit low nuclear heme compared to WT strains, and do not look like the *bm2hΔ* Lib derived strains (Figure 18B). The *bm2hΔ* new strains exhibit growth defects on rapamycin plates which can be rescued by BMH2 expression

plasmids (Figure 18C). Altogether, the new *bm2hΔ* generated yeast strains behave as expected and like the library derived strains by growth, but the labile heme levels in these strains are different.

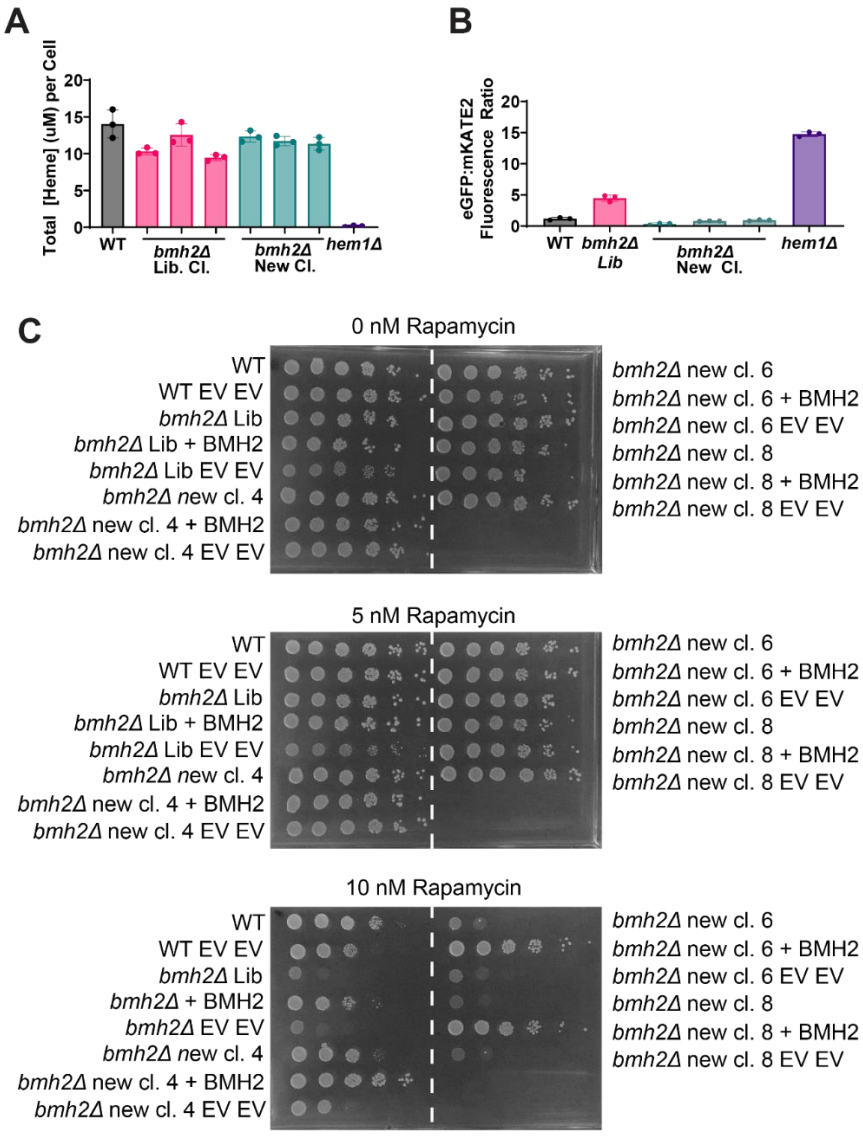

Figure 18 – Labile Heme and Growth Complementation in Library-derived and Newly Generated *bmh2Δ* Strains. Total heme content **(A)** and nuclear sensor ratios **(B)** in WT, *hem1Δ*, library-derived *bmh2Δ* ("Lib"), and newly generated *bmh2Δ* ("new") strains. **(C)** Growth test complementation in *bmh2Δ* Lib and three clones of *bmh2Δ* new strains with and without BMH2 expression plasmids grown with or without 5 or 10 nM rapamycin. Each *dot* represents a biological replicate. Growth test images were taken after 2 days of growth at 30 ^{o}C.

A similar analysis was performed with the *put3Δ* yeast mutants. New Put3 deletion yeast were generated. Total heme among all the strains is similar, however labile heme in the new *put3Δ* strains looks like WT (Figure 19A, B, respectively). Put3 is a zinc finger transcription factor that activates PUT1 and PUT2 genes that are essential in proline utilization and catabolism pathways.[120, 121] Therefore, when yeast is forced to use proline as a nitrogen source, PUT1-3 genes are essential. Spot tests were performed using WT and *put3Δ* Lib and two different clones of the *put3Δ* new yeast (generated the same way as the new *bmh2Δ* yeast described previously) transformed with PUT3 gene expression plasmids or empty vector (EV) plasmids. Strains were spotted on agar plates with different nitrogen sources (0.2 % ammonium sulfate, AS, 0.1 % Proline, or sterile water). Growth of the *put3Δ* strains should not grow on media where proline is the only nitrogen source. As expected, the *put3Δ* Lib and *put3Δ* new yeast did not grow on the 0.1 % Proline plates (Figure 19C). Further, this growth is rescued in strains transformed with PUT3 expression plasmids, except clone 2 of the newly generated *put3Δ* mutant (Figure 19C). Since the total and labile heme levels in the two different *put3Δ* new clones look the same, I believe there was error in spotting the correct *put3Δ* new clone 2 culture on the agar plate. This would explain why growth complementation was not observed for clone number 2.

Taken together, we can confirm the newly generated mutant yeast behave as expected based on the indicated and well-reported growth phenotypes. The gene expression plasmids are being expressed correctly as growth is rescued in strains transformed with the expression plasmids. Differences in labile heme

levels in the library derived mutants compared to the newly generated mutants were revealed. The newly generated mutants have labile heme levels like WT. This suggests there is something fundamentally different between the library and newly derived mutant strains. We suspect there is/are background mutations in the library-derived strains that are responsible for the low nuclear heme phenotype observed.

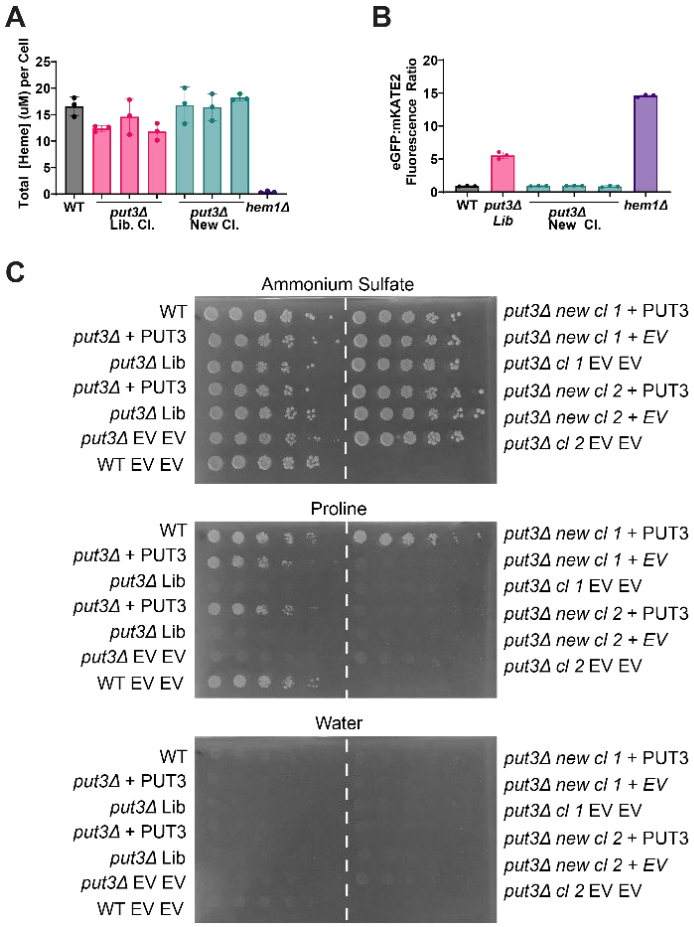

Figure 19 - Labile Heme and Growth Complementation in Library-derived and Newly Generated *put3Δ* Strains. Total heme content **(A)** and nuclear sensor ratios **(B)** in WT, *hem1Δ*, library-derived *put3Δ* ("Lib"), and newly generated *put3Δ* ("new") strains. **(C)** Growth test complementation in *put3Δ* strains with and without PUT3 expression plasmids grown on agar plates with 0.2 % Ammonium Sulfate, 0.1 % Proline or Sterile Water as nitrogen sources. Each *dot* represents a biological replicate. Growth test images were taken after 4 days of growth at 30 ^{o}C.

3.2.6 Whole Genome Sequencing to Uncover Background Mutations

The experiments above support the library and newly made deletion strains have different nuclear heme levels. We hypothesize strains derived from the library contain background mutations that are responsible for the low nuclear heme phenotype. To identify these background mutations relative to our lab's WT strains, our WT, ***bm2hΔ*** Lib, ***bm2hΔ*** new, ***arv1Δ*** Lib, and ***rpl8aΔ*** Lib were submitted for whole genome sequencing (WGS) provided by MigsCenter (Pittsburgh, PA).

Results from WGS show that most of the mutations identified are localized to intergenic regions (Figure 20A-D). Only one coding gene mutation is common among the library-derived mutants and not present in the newly generated Bmh2 deletion strain (Figure 20E). This mutation is in the HXT11 gene. Alternatively, there is one coding gene mutation in the newly generated Bmh2 deletion strain that is not present in the library-derived strains. This mutation is in the CRZ1 gene (Figure 20E). To confirm the mutation in HXT11, we prepared samples for Sanger Sequencing. Interestingly, the results from Sanger Sequencing did not reveal a mutation in the specified region as the WGS analysis did.

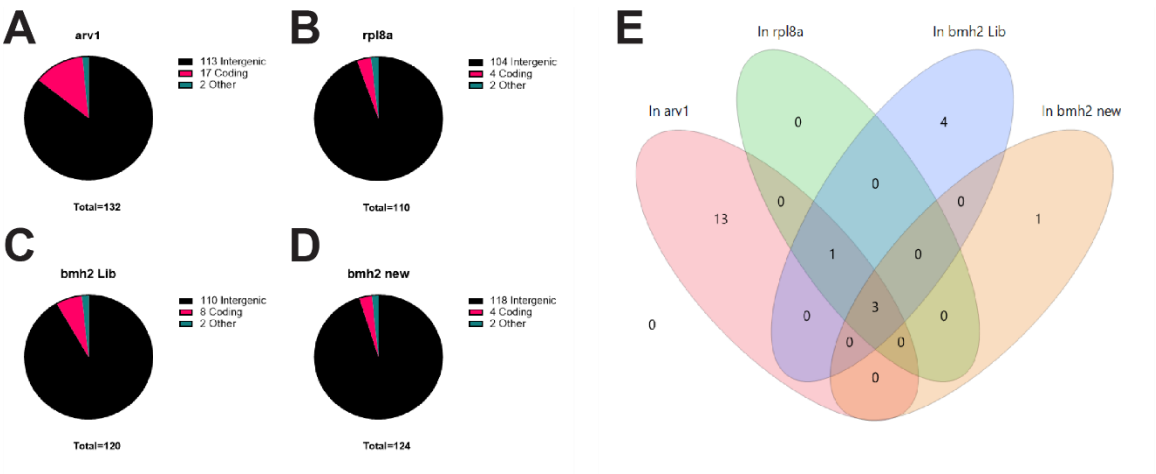

Figure 20 – Pie Charts and Venn Diagrams Representing the Background Mutations Revealed by WGS. Types of mutations identified by WGS in *arv1Δ* **(A)**, r*pl8A Δ* **(B)**, *bmh2Δ-Lib* **(C)**, and *bmh2Δ new* **(D)** mutants relative to WT. **(E)** Venn Diagram displaying unique *bmh2Δ new* and library-derived strain mutations relative to WT.

3.3 Discussion

To identify determinants of nuclear heme availability, high throughput genetic screens were performed. Screening using the HS1-M7A sensor targeted to the nucleus revealed hundreds of yeast mutants with significantly altered heme levels relative to WT strains. This list of mutants was not enriched in a particular pathway, biological function, or cellular compartment. Three explanations can be provided for this: 1) several things function in regulating nuclear heme such that there is not a single pathway or protein contributor involved in nuclear heme homeostasis, 2) essential genes rather than non-essential genes are responsible for regulating nuclear heme, and 3) the HS1-M7A sensor may not be the most appropriate sensor for this screen. To address the first explanation, one would need to disrupt multiple genes and probe the effects on nuclear heme. The second explanation is possible where an essential gene is responsible for regulating

nuclear heme. This would support the importance of heme in the nucleus where its regulation is an essential pathway or protein and is not present in the deletion library we screened. Finally, the nucleus has very little labile heme concentrations (< 2.5 nM).[27] The heme affinity of the HS1-M7A sensor may be too low to detect the small changes in nuclear heme that may be occurring. To overcome this, the library was screened using the high affinity HS1 sensor. The high affinity of the HS1 sensor would allow for the detection of the small, yet significant changes that may be present in the different yeast mutants relative to WT. Screening with the HS1 sensor revealed 86 mutants with significantly less heme compared to WT yeast. Comparing these 86 mutants with the 314 mutants with low heme identified from the HS1-M7A screen identified 34 common mutants. These 34 genes are not enriched in a particular pathway or cellular compartment. Interestingly, several reside in the ER and mitochondria (Tables 3 and 4). This result supports the notion that heme may be trafficked to the nucleus via the ER.[66]

When validating the 86 candidates from the HS1 screen, it became clear that labile heme levels were dependent on how the yeast were grown. Labile heme levels were different when grown in a shallow, standing 96-well plates compared to liquid shaking cultures. Perhaps this is not too surprising since these environments are very different. Growth in the 96-well plates provides a small and shallow space for growth. Further, as yeast grow, they settle to the bottom of plate, and are oxygen and nutrient limited. Whereas, in shaking cultures, the yeast are constantly mixed and interchanging with the media and nutrients. Shaking growth cultures are also more aerated than in a shallow, standing 96-well plate. In the

shaking cultures, there may be a higher demand for heme. Gene deletion yeast mutants that exhibited low heme in 96-well plates are more reliant on heme when grown shaking. In this shaking environment, yeast may be more pressured to adapt. The yeast mutants that do adapt may be doing so by activating other pathways to get heme to the nucleus. It would be interesting to probe protein differential expression or transcription analyses (ex. ChIP-seq) in the gene deletion yeast or WT strains when grown shaking vs standing to identify proteins and transcriptional differences that may be aiding in nuclear heme availability.

Experiments showed that the low nuclear heme phenotypes observed could not be complemented by episomal gene expression under non-native GPD (strong) and TEF (weak) promoters. However, these same expression plasmids were able to rescue well-reported growth phenotypes. There are multiple explanations for this selective complementation. Gene expression may need to be expressed in a different way to see labile heme complementation. For example, integrating the gene into the genome may express better and complement labile heme where episomal expression is not adequate or optimal. Second, expressing the gene under its native promoter could be done to achieve complementation, rather than the GPD- or TEF-driven promoters. Third, the deletion strains from the library collection may have developed background mutations that are resulting in low nuclear heme rather than the deletion of the gene itself.

The yeast gene deletion collection was generated in the 1980s. Over the past 50 years, the strains could have acquired a handful of mutations. In fact, reports have described the rise of genomic changes associated with cancers in

organisms with loss or duplication of chromosome segments.[122] To further investigate this, new deletion strains using our lab's isogenic WT strains were generated and probed for nuclear heme. The newly made deletion mutants had heme levels like WT rather than low heme level, despite both being the same gene deletion mutant. This suggested background mutations were present in the library-derived strains.

To uncover these background mutation(s), strains from the library collection with low nuclear heme, along with a WT strain, and the newly made Bmh2 deletion strains were sent for whole genome sequencing (WGS). We hoped to identify a common mutation among the library-derived strains that is absent in the newly generated Bmh2 deletion strain. One coding gene mutation was revealed by WGS that followed these requirements: *HXT11*. However, Sanger Sequencing did not recognize a mutation in *HXT11* as did WGS. Therefore, the HXT11 mutant identified in WGS was not validated.

Overall, the screens identified mutants with low nuclear heme. However, it is still unclear what is responsible for this phenotype. We hypothesize the changes in nuclear heme observed are due to reasons beyond genetics and possibly epigenetics or post-translational modifications are responsible. To test this, ATAC-seq experiments and mass spectrometry would be useful to investigate these possibilities.

3.4 Materials and Methods

3.4.1 Cell Strains, Transformations, Growth Conditions, and Plasmids

3.4.1.1 Yeast Strains and Growth

S. cerevisiae strains used in this work were derived from BY4741 (*MATa, his3Δ1, leu2Δ0, met15Δ0, ura3Δ0*). Deletion mutant strains were obtained from the yeast gene deletion collection (Thermo Fisher Scientific). We also utilized the previously reported strain DH001b-3 (*hem1::HIS3*).[27] All strains derived from the yeast deletion collection were confirmed by sequencing the unique barcodes flanking the *KanMX4* deletion cassette. All growth cultures were maintained at 30 ^{o}C and grown in either shaking liquid cultures or standing liquid cultures in 96-well plates overnight for 14 – 16 hr.

3.4.1.2 Yeast Transformation

Yeast Transformations were performed by the lithium acetate procedure.[101, 123] Strains were maintained at 30 ^{o}C on either enriched yeast extract (1 %), peptone (2 %) based medium supplemented with 2 % glucose (YPD) and G418 (200 ug/mL) or synthetic complete medium (SC) supplemented with 2 % glucose and the appropriate amino acids to maintain selection.[27] Cells cultured on solid media plates were done so with YPD or SC media supplemented with 2 % agar.[27] Selection for yeast strains containing the *KanMX4* marker was done with YPD agar plates supplemented with G418 (200 ug/mL).[27] Cells for the screen were resuspended in SC media supplemented with 15 mg/mL ergosterol and 0.5 %

Tween-80 (SCE). All liquid cultures were maintained at 30 ^{o}C and grown in either shaking liquid cultures or standing liquid cultures in 96-well plates.

3.4.1.3 Plasmids

Cytosolic, mitochondrial, and nuclear-targeted heme sensors were sub-cloned into pRS415 and driven by GPD promoters as previously described.[27] PCR based mutagenesis was used to generate the affinity variants of HS1 (M7A and M7A-H102A, bisALA).[27] The Hap1 reporter plasmid in which eGFP is driven by the CYC1 promoter was also previously described.[27]

BMH2 Expression Plasmids. The yeast Bmh2p expression plasmid was generated by amplifying BMH2 nucleotides 1-822 from yeast genomic DNA using forward and reverse primers, and sub-cloning into the XbaI/BamHI sites of p413-GPD and p413-TEF to generate plasmids pMW021 and pMW028, respectively.

PUT3 Expression Plasmids. The yeast Put3p expression plasmid was generated by amplifying PUT3 nucleotides 1-2940 from yeast genomic DNA and sub-cloning into the XbaI/XhoI sites of p413-GPD and p413-TEF to generate plasmids pMW024 and pMW031, respectively.

ARV1 Expression Plasmids. The yeast Arv1p expression plasmids were generated by amplifying ARV1 nucleotides 1-966 from yeast genomic DNA with and without a C-term HA tag. PCR amplification products were sub-cloned into the XbaI/BamHI sites of p413-GPD and p413-TEF to generate tagged plasmids

pMW018 and pMW017, respectively, and untagged p413-GPD and p413-TEF plasmids pMW020 and pMW019, respectively.

LDB7 Expression Plasmid. The yeast Ldb7p expression plasmid was generated by amplifying LDB7 nucleotides 1-543 from yeast genomic DNA and sub-cloning into the SpeI/BamHI sites of p413-GPD and p413-TEF to generate plasmids pMW033 and pMW032, respectively.

AAC3 Expression Plasmid. The yeast Aac3p expression plasmid was generated by amplifying AAC3 nucleotides 1-924 from yeast genomic DNA and sub-cloning into the XbaI/BamHI sites of p413-GPD and p413-TEF to generate plasmids pMW026 and pMW027, respectively.

RPL8A Expression Plasmid. The yeast Rpl8a expression plasmid was generated by amplifying RPL8A nucleotides 1-771 from yeast genomic DNA and sub-cloning into the XbaI/BamHI sites of p413-GPD and p413-TEF to generate plasmids pMW023 and pMW030, respectively.

AIM11 Expression Plasmid. The yeast Aim11 expression plasmid was generated by amplifying AIM11 nucleotides 1-489 from yeast genomic DNA and sub-cloning into the XbaI/BamHI sites of p413-GPD and p413-TEF to generate plasmids pMW022 and pMW029, respectively.

3.4.2 Experimental Methods

3.4.2.1 High throughput Transformations

Yeast high throughput transformations were performed in standard clear sterile 96-well plates (Falcon Cat. # 353072 or Corning Cat. # 3595). Yeast mutants from the Gene Deletion Library (Sigma) were precultured in YPD + G418 (200 µg/mL) media by inoculating 10 uL of the thawed freezer stock into 200 uL of YPD + G418 media using the the robotic liquid handling system (BioTek Precision XS) and sterile 96-well plates. The inoculated plates were grown standing in a 30 ^{o}C incubator for 48 hours. The culture volume needed for one OD of cells in 200 uL was transferred to a new sterile 96-well plate using a multi-channel pipette and transformed by using the lithium acetate procedure adapted for 96 well plates.[124] To calculate the volume needed for one OD of cells, the given *A*600 value in a microplate reader was divided by 0.24. This new value is the OD value as if in a 1 cm path length cuvette. Then, the volume of culture needed was calculated to achieve one OD in 200 uL and transferred to a new 96-well plate using a multi-channel pipette. Once transferred, plates were spun at 3000 rpm, the supernatant was discarded and 150 uL of transformation mix was used to resuspend the cells. Transformation reagents for one reaction (one well) consist of: 15 uL of 1 M LiAc, 5 uL of ssDNA (boiled before use) + 15 uL of sterile ultrapure water, 15 uL of sterile ultrapure water containing 500 ng, and 100 uL of 50 % PEG. Transformation reagents were mixed, and cells were resuspended in 150 uL of the transformation mix using a multi-channel pipette. Cells were then incubated with the transformation reagents for six hours at 42 °C sitting in a shallow water bath in

baking dishes. Following the incubation, the 96-well plates were spun at 3000 rpm in a centrifuge, the supernatant was discarded, and cells were resuspended in 200 uL of SC media with the appropriate amino acids to maintain selection.[27] Plates were incubated for 96 hours at 30 ^{o}C. The cells were then diluted into fresh SC media supplemented with the appropriate amino acids to confirm and maintain selection by inoculating 10 uL of culture into 200 uL SC media using the robotic liquid handling system (BioTek Precision XS) or by a multi-channel pipette. Plates were incubated at 30 ^{o}C for an additional 48 hours. Freezer stocks were made by spinning the 96-well plates at 3000 rpm to pellet the cells, the supernatant was discarded, and cells were resuspended in 150 uL of YPD + 20 % glycerol. Stocks were stored at -80 ^{o}C.

3.4.2.2 <u>High Throughput Screens</u>

Nuclear HS1-M7A or HS1 sensor expressing cells were pre-cultured on SC agar plates with appropriate amino acids to maintain selection and supplemented with 200 ug/mL ALA to support any heme defective mutants. To do this, yeast from the thawed frozen stocks were stamped onto agar plates using a Microplate Replicator 96 Pinning tool (Boekel Scientific) and were grown at 30 ^{o}C for 48 hrs. Using the replicator pin (Boekel Scientific), cells were then transferred to a clear sterile 96-well plate containing 200 uL sterile ultrapure water which served as the source/stock plate. Cells were diluted from this stock plate by inoculating 10 uL into 200 uL SCE-LEU and grown standing for 14 – 16 hours at 30 ^{o}C. After culturing, cells were harvested, washed twice with 200 uL ultrapure water and finally suspended in 200 uL of 1x PBS. Fluorescence was monitored on 200 uL

of ~ 4 OD/mL (2 x 10^7 cells/mL) cell suspension using black Grenier Bio-one flat bottom fluorescence plates and a Synergy Mx multi-modal plate reader. eGFP (ex. 488 nm, em. 510) and mKATE2 (ex. 588 nm, em. 620 nm) fluorescence was recorded every 30 seconds for 5 min. Z-score values were calculated by subtracting the sensor fluorescence ratio for a given strain screened from the average sensor fluorescence ratio of all the samples screened within the plate and dividing it by the STDEV of the sensor fluorescence ratio of all the strains screened in the plate (Equation 2).

3.4.2.3 Steady-State Heme Measurements

To measure steady-state labile heme in strains expressing the heme sensors, yeast were cultured in 10 mL SCE-LEU media, with or without 0.5 mM succinylacetone, for ~14–16 hr to mid-exponential phase (*A*600 ≈ 1–2). Cytosolic-, nuclear-, and mitochondrial-targeted sensors were expressed on low copy centromeric plasmids and were driven by the GPD promoter (p415-GPD). After culturing, cells were collected, washed in water, and resuspended in phosphate buffered saline (PBS) solution to a density of 10 *A*600 units per mL. Two-hundred microliters of cell suspension, corresponding to 2 *A*600 units or 4 x 10^7 cells, was used to measure EGFP (excitation 488 nm, emission 510 nm) and mKATE2 (excitation 588, emission 620) HS1-M7A sensor fluorescence. Background autofluorescence of cells not expressing the sensors was recorded and subtracted from the EGFP and mKATE2 sensor fluorescence values. Fluorescence was recorded on a Synergy Mx multi-modal plate reader using black Greiner Bio-one flat bottom fluorescence plates.

3.4.2.4 Growth Spot Tests

BMH2 Spot Tests on Rapamycin. Agar plates were made containing 0, 5, or 10 nM Rapamycin (TCI America). The Rapamycin stock was made by diluting in sterile DMSO and the appropriate volume amount was added to freshly autoclaved agar media before pouring. Overnight cultures of WT and *bmh2Δ* yeast expressing EV or GPD- or TEF-driven BMH2 plasmids were grown in SCE media to mid-exponential phase. Cultures were washed twice in sterile MilliQ water and diluted to 0.2 OD/mL stocks in sterile MilliQ water. 5-fold serial dilutions were made using sterile MilliQ water and 5 uL was spotted onto agar plates containing 0, 5 or 10 nM Rapamycin (TCI America). Images were taken after 4 days of growth at 30 ^{o}C.

PUT3 Spot Tests on Ammonium Sulfate and Proline. Agar plates were made containing YNB without Ammonium Sulfate (MP Biomedical) with or without 0.2 % Ammonium Sulfate (Amresco), or 0.01 % Proline (Amresco). Ammonium sulfate and proline stocks were made by diluting into MillIQ and autoclaving. The appropriate volume amount was added to freshly autoclaved agar media before pouring. Overnight cultures of WT and *put3Δ* yeast expressing p416-EV, p411-EV, and p415-EV plasmids in addition to p413-GPD- or TEF-driven PUT3 plasmids were grown in SCE media to mid-exponential phase. Cultures were washed twice in sterile MilliQ water and diluted to 0.2 OD/mL stocks in sterile MilliQ water. 5-fold serial dilutions were made using sterile MilliQ water and 5 uL was spotted onto agar plates containing 0, 0, 0.2 % Ammonium Sulfate (Alfa Aesar), or 0.01 % Proline (Alfa Aesar). Images were taken after 4 days of growth at 30 ^{o}C.

ARV1 Spot Tests Grown Anaerobically. Overnight cultures of WT and *arv1Δ* yeast expressing EV or p413-GPD- or TEF-driven PUT3 plasmids were grown in SCE media to mid-exponential phase. Cultures were washed twice in sterile MilliQ water and diluted to 0.2 OD/mL stocks in sterile MilliQ water. 5-fold serial dilutions were made using sterile MilliQ water and 3 uL were spotted onto SCE agar plates containing. Images were taken after 4 days of growth at 30 ^{o}C in the COY chamber or in the presence of oxygen.

3.4.2.5 Total Heme Quantification

Measurements of total heme were performed using a fluorometric assay designed to measure the fluorescence of protoporphyrin IX upon the release of iron from heme as previously described.[103] For all total heme measurements, ~ 1 x 10^8 cells were harvested, washed in ultrapure water, and resuspended in 500 uL 20 mM oxalic acid and stored in a closed box at 4 ^{o}C overnight (16 – 18 hours). An equal volume (500 uL) of 2 M oxalic acid was added to the cell suspensions in 20 mM oxalic acid. The samples were split, where half of the cell suspension was transferred to a heat block set at 95 ^{o}C and heated for 30 minutes, and the other sample half was kept in a closed box at room temperature (~ 25 ^{o}C) for 30 minutes. All suspensions were then centrifuged for two minutes on a table-top microfuge at 21000 x g and the porphyrin fluorescence (ex. 400 nm, em. 608 nm) or 200 uL of each sample was measured using a Synergy mx multi-modal plate reader in black Grenier Bio-one flat bottom fluorescence plates. Heme concentrations were calculated from a standard curve prepared by diluting 500 – 1500 uM hemin chloride stock solutions in 0.1 M NaOH into ultrapure MilliQ water and from there

prepared the same as the cell samples as described above. To calculate heme concentrations, the fluorescence of the un-boiled sample (representing background levels of protoporphyrin IX) was subtracted from the fluorescence of the boiled sample (representing the free base porphyrin generated upon heme iron release). The cellular concentration of heme was determined by dividing the moles of heme determined in this fluorescence assay by the number of cells analyzed, to give moles of heme per cell. To convert this to a cellular concentration the moles of heme per cell were divided by the volume of a yeast cell (given to be 50 fL).

CHAPTER 4. EXPLORING THE RELATIONSHIP BETWEEN HEME UTILIZATON AND HEME BIOAVAILABILITY

4.1 Preface

The work discussed in this chapter is un-published. The manuscript for this work is in preparation.

4.2 Introduction

Heme is an essential iron-containing molecule, essential for all aerobic life. Heme enables the execution of several diverse critical functions; including, catalysis, electron transfer, gas transport and signaling.[3, 4] Heme is synthesized via a conserved eight-step pathway, culminating in the mitochondria matrix, and is found in virtually every subcellular compartment. This necessitates the need for heme mobilization and bioavailability throughout the cell. Heme's unique redox and hydrophobic properties make it a versatile molecule; unfortunately, these same characteristics render it potentially cytotoxic. These attributes allow heme to promote membrane and protein disruption, as well as catalyze deleterious redox reactions.[4, 7] Heme homeostasis defects have been associated with disorders; including, cancer, cardiovascular, and neurological diseases.[5, 82, 125, 126] Consequently, there is an urgent need to decipher the mechanisms and associated molecules that mediate heme trafficking and availability.

Recent reports demonstrate distinct parallel pathways that transport heme to various cellular locations.[66] One proposed route for heme distribution is through

membrane contact sites.[66, 127] Trafficking in this manner is less deleterious as it would limit heme exposure to the diffuse aqueous environment and interactions with off-target proteins and destinations. Specifically, mobilization via ER-Mitochondria organelle contact sites have been reported as a more direct route to the nucleus.[66] Similarly, heme trafficking regulation through metabolon complexes has been described.[12, 128] Protein interactions with terminal heme biosynthetic enzyme, ferrochelatase (FECH), have been identified and shown to facilitate mitochondrial export directly following synthesis. This regulation would also limit heme off-target interactions by directly funneling heme to chaperones and/or trafficking proteins following synthesis. For example, PGRMC1 interacts with FECH and aids in heme transfer in murine erythroleukemia cells (MEL).[12]

More broadly, heme dynamics is most likely regulated by exchange labile and inert heme interactions. Exchange inert heme is tightly bound to proteins and is kinetically inaccessible, while labile heme is kinetically accessible and dissociable. To mobilize heme, it must be either released from exchange inert heme-bound molecules or exchanged between various buffering factors, transporters, trafficking factors, or apo-hemoproteins.[11] Each of these mechanisms requires dynamic and specific interactions between heme and interacting proteins. The cell balances its direct needs for heme by incorporating heme into apo-hemoproteins and the bioavailable heme pool. To meet this demand, the current paradigm is one in which the cell limits the amount of bioavailable heme by synthesizing enough heme to meet utilization requirements. To directly probe this, we investigated the effects of heme utilization on heme

bioavailability. To alter heme utilization and the cell's need for heme, Hap1p mutant yeast strains defective in transcription activity were used. Hap1p is a transcription factor regulating the expression of ~ 50 % of the currently identified hemoproteins in yeast.

Hap1p is a heme-dependent transcription factor primarily localized to the nucleus with a small fraction present in mitochondria. Hap1p transcriptional activation has been well studied and is regulated by intracellular heme concentration.[14, 129-134] This activation involves a two-tier regulatory mechanism; namely, inactivation in the absence of heme and activation in the presence of heme.[14, 130, 135] In the absence of heme, Hap1 forms a higher-order molecular complex, containing Hsp82 and Ydj1 among others.[131] Heme disrupts this complex and exposes the Hap1 dimer DNA binding domains, allowing for DNA binding and subsequent transcription.[131, 136]

Most notably, Hap1p has been extensively studied in the context of oxygen sensing by heme.[137, 138] Cells sense changes in oxygen through oxygen-dependent pathways, including heme synthesis.[137] Heme is an essential molecule for sensing oxygen levels.[138] One way that cells respond to rising oxygen levels using heme is by its ability to regulate oxygen-mediated transcription through heme's ability to bind and activate Hap1p. In turn, heme controls transcription of aerobic genes (half of which are hemoproteins) via Hap1p.[14, 139-141] Therefore, mutant Hap1p yeast strains defective in transcription were used to alter hemoprotein expression and the cell's need for heme. In these strains, labile heme can be probed using our heme sensors, allowing for further insight in regard to the

relationship between heme utilization and bioavailable heme. Hap1p's transcriptional regulation by heme and its ability to elicit hemoprotein (and potentially heme buffer protein) expression make it a unique target to directly probe its role in heme homeostatic regulation, and the unique balance between heme utilization and bioavailability.

Here, genetically encoded fluorescent heme sensors were used to investigate heme availability and dynamics in WT and mutant Hap1p yeast strains to explore the relationship between heme utilization and bioavailability. Our experiments describe heme utilization and bioavailability are inversely related, where Hap1p mutants have increased labile heme and similar total heme levels despite having lower heme utilization requirements compared to WT yeast. Our work describes that Hap1p buffers labile heme in the cytosol, mitochondria, and nucleus through its ability to activate transcription, and facilitates cytosolic heme trafficking dynamics. Hap1p mutants unable to elicit transcription are observed to have more labile heme in the cytosol, mitochondria, and nucleus, while total heme levels are minimally affected. Further, the increased labile heme observed in Hap1p mutants is partially rescued by sequestration of the excess labile heme by cytochrome b_{562} overexpression. In addition, Hap1p mutants with high labile heme are hypersensitivity to hydrogen peroxide. This is not surprising as Hap1p regulates the expression and activity of the enzyme responsible for removing hydrogen peroxide, catalase. Interestingly, decreasing the amount of labile heme in Hap1p mutants by sequestration by cytochrome b_{562} expression is more detrimental to hydrogen peroxide-treated cells rather than less. In this context, we

hypothesize heme acts as a peroxidase to remove the hydrogen peroxide in the absence of catalase, thereby protecting the cells. For the first time, we observe that excess labile heme, and in the absence of catalase, seems to play a protective role against hydrogen peroxide. Based on our observations, we have proposed a model in which 1) heme utilization is inversely related to heme bioavailability, 2) bioavailable heme is regulated by hemoproteins under Hap1p transcription, and 3) excess labile heme plays a protective role against hydrogen peroxide toxicity in the absence of catalase.

4.3 Results

4.3.1 Hap1p Regulates Expression of Several Hemoproteins

As an oxygen sensor, Hap1p is known to regulate expression of genes involved in oxygen-related activities, like respiration, including catalase, and cytochromes.[3, 4] To alter heme utilization in cells, we wanted to expand our knowledge and ask what hemoproteins are regulated by Hap1p transcription. By cross-referencing a list of known hemoproteins in yeast (Table 10, columns A and B) against a list of genes previously reported having promoters occupied by Hap1p vis ChIP-seq experiments (Table 10, column D) and the *Yeastract* list of genes having promoter sequences recognized by Hap1p (Table 10, column E), we found 50 % of the known hemoproteins yeast, including the most abundant hemoproteins, contain Hap1p promoter DNA sequences (Table 10, column E) or have promoters occupied by Hap1p in ChIP-seq experiments (Table. 10, column D).[142-144]

Table 10. Yeast Hemoproteins Regulated by Hap1p

A Systematic Name	B Standard Name	C Mean molecules per cell	D Hap1 Regulated? (Y/N) (From Hickman)	E Hap1-Recognized Promoter Sequence (Y/N) (From Yeastract)
YGR234W	YHB1	62331	Y	Y
YHR007C	ERG11	21584	Y	Y
YJR048W	CYC1	11829	Y	Y
YJR137C	MET5	11812	N	N
YML054C	CYB2	10577	Y	Y
YGL055W	OLE1	9820	Y	Y
YKR066C	CCP1	9350	N	N
YMR015C	ERG5	9136	Y	Y
YPL170W	DAP1	8687	Y	Y
YNL111C	CYB5	7894	Y	Y
YOR065W	CYT1	7559	Y	Y
YGR088W	CTT1	6811	Y	Y
YLR205C	HMX1	6086	Y	Y
YMR272C	SCS7	4610	Y	Y
YKL141W	SDH3	4105	N	N
YDR178W	SDH4	3404	N	N
YEL039C	CYC7	3253	Y	Y
YLR214W	FRE1	3006	Y	Y
YMR073C	IRC21	2572	NA	Y
YAL039C	CYC3	2561	Y	Y
Q0045	COX1	2325	NA	N
YOR384W	FRE5	2212	N	N
YLL051C	FRE6	2117	N	Y
YKL087C	CYT2	1521	N	N
YDR256C	CTA1	1495	Y	Y
YLR256W	HAP1	1375	Y	Y
YNR060W	FRE4	1141	Y	Y
YGL160W	AIM14	1109	NA	Y
YNL234W	YNL234W	1075	N	N
YJR078W	BNA2	1060	Y	Y
Q0055	AI2	287	NA	N
YOL152W	FRE7	120	N	N
Q0105	COB	NA	NA	N
YLR164W	SHH4	NA	NA	N
YDR402C	DIT2	NA	N	N
YMR118C	SHH3	NA	NA	N
YKL220C	FRE2	NA	N	N
YOR381W	FRE3	NA	N	N

To alter hemoprotein expression (heme utilization), Hap1p mutant yeast strains previously reported by Hickman, et al. were used, and are described here.[142] In this work, S288C BY4741 strains bearing a transposon yeast (ty1) insertion at the carboxy-terminal of *HAP1* gene (hereafter referred to as *ty1 hap1*), and strains where the *ty1 hap1* mutant gene is replaced with wild-type *HAP1* derived from Sigma1278b (hereafter referred to as HAP1) or a complete deletion of *HAP1* (*hap1Δ*).[142] Hap1p transcription activity in these strains was measured by using a transcriptional reporter that activates GFP expression driven by the CYC1 promoter, a Hap1p target gene. Interestingly, *ty1 hap1* strains maintain some Hap1p activity compared to *hap1Δ* strains, while HAP1 strains have significantly higher transcription activity (Figure 21A).

Additionally, Hap1p activity was measured using a reporter that activates mKATE2 expression. Using this reporter, mKATE2 expression is under the HMG2 promoter which is negatively regulated by Hap1p. As expected, HAP1 and *hap1Δ* yeast have low and high activity, respectively (Figure 21B). Based on these results, we can infer strains with lower Hap1p transcription activity (*ty1 hap1* and *hap1Δ*) express less hemoproteins resulting in a decreased need for heme and utilization.

Experiments to analyze total heme levels were performed. To measure total heme levels, a porphyrin fluorescence assay was used.[103] In this assay, protoporphyrin IX's inherent fluorescence is measured. After lysing the yeast cells, samples are split where one set is treated with excessive heat to remove the iron

from heme to produce the fluorescent protoporphyrin IX molecule, and the other set is left at room temperature. The samples at room temperature serve as a control representing the background protoporphyrin levels in the cells. The fluorescent spectra fingerprint for protoporphyrin is unique having two distinct emission peaks at ~ 608 and 665 nm wavelengths. The fluorescence intensity at 608 nm was recorded, and a standard heme curve is used to calculate the total heme concentration per yeast cell. Despite lacking most hemoproteins, total heme in *ty1 hap1* and *hap1Δ* strains is only minimally decreased compared to strains with WT HAP1 (Figure 21C).

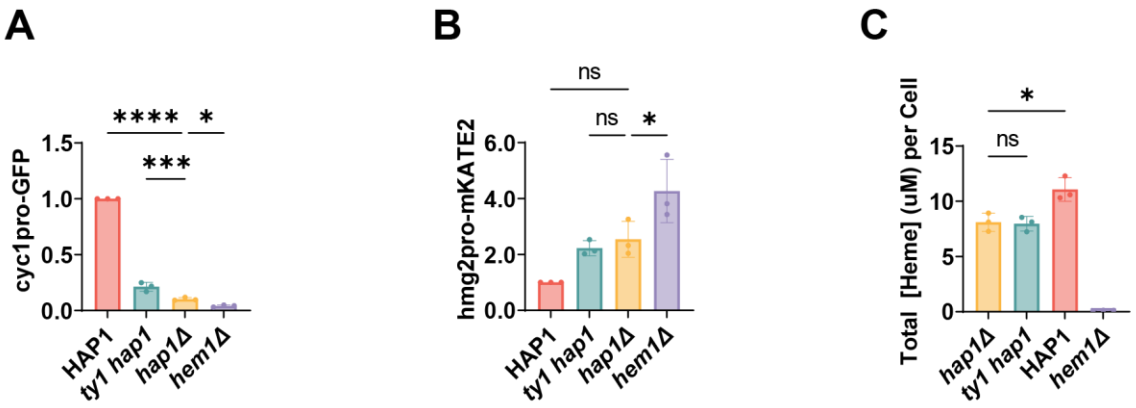

Figure 21 – Transcription Activity and Total Heme in Hap1p Mutant Strains. Hap1p transcription activity as assessed by fluorescence of cyc1pro-GFP reporters **(A)** and hmg2pro-mKATE2 reporters **(B)** in yeast. Total heme was measured by using a porphyrin fluorescence assay **(C)**.

4.3.2 Hap1p Regulates Bioavailable Heme

The experiments above establish that Hap1p transcription and hemoprotein expression and utilization are decreased in *ty1 hap1* and *hap1Δ* yeast. Labile heme in the cytosol, mitochondria matrix, and nucleus was then probed to observe the effects of altered heme utilization in these strains. WT HAP1 strains have lower

labile heme levels in the cytosolic, nuclear, and mitochondria compartments, indicated by higher eGFP/mKATE2 sensor fluorescence ratios relative to that of *hap1Δ* strains (Figure 22A, B, C, respectively). The mitochondrial matrix has very little free heme, below the limit of detection of the HS1-M7A sensor. The ratio of this sensor matches that of a strain with zero heme (*hem1Δ*). Therefore, the HS1 sensor must be used for accurate mitochondrial matrix labile heme measurements. Hap1p has minimal effect on the mitochondrial labile heme pool, indicated by the HS1 sensor (Figure 22C).

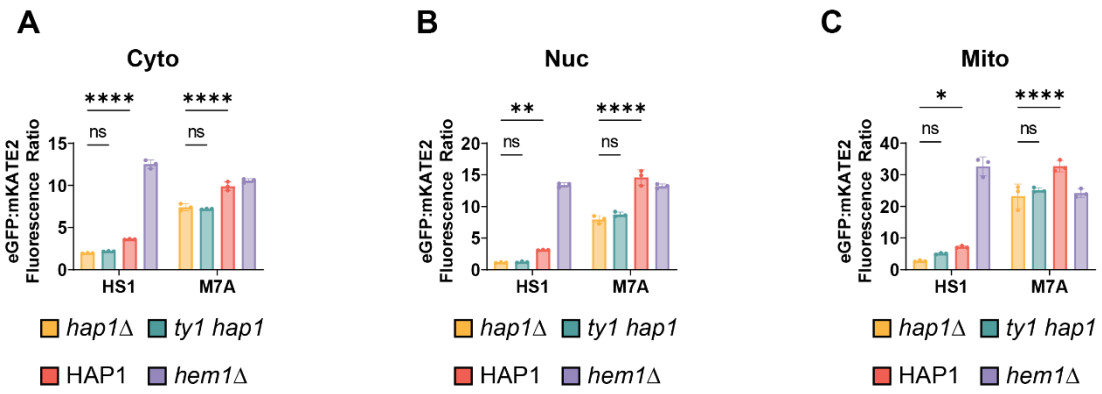

Figure 22 – Labile Heme Distribution in Different Hap1p Mutants. Steady State cytosolic **(A)**, nuclear **(B)**, and mitochondrial matrix **(C)** labile heme was measured in strains with fully functional Hap1 or mutant Hap1. Each *dot* represents a biological replicate. The significance is indicated by asterisks using two-way ANOVA for multiple comparisons with Dunnett's post hoc test: * $p < 0.05$, ** $p < 0.01$, **** $p < 0.0001$, ns, not significant.

Even though *ty1 hap1* strains have slightly more transcription activity compared to *hap1Δ* strains (Figure 21A), both strains phenocopy each other in terms of heme sensor measurements (Figure 22). Altogether, mutant Hap1 strains have less transcriptional activity, more labile heme compared to WT Hap1 yeast, while only minimally affecting total heme. This suggests heme utilization and bioavailable heme levels are inversely related in these strains. Removing the need

for heme does not result in a comparative or synergistic decrease bioavailable heme.

4.3.3 Hap1p Facilitates Cytosolic Heme Trafficking Dynamics

Heme transport rates in the different yeast Hap1p mutants was investigated by monitoring inter-compartmental trafficking kinetics. This SA pulse-chase experiment is described in Martinez-Guzman, et al.[66] Briefly, heme synthesis is blocked using succinylacetone, an inhibitor of the heme synthetic enzyme, PBGS (also known as ALAD).[66] Heme synthesis is then re-initiated by removing the inhibitor from the media, and heme loading into HS1 in nuclear, mitochondria matrix, and cytosolic compartments is monitored over time. This experiment displayed labile heme trafficking to the cytosol is significantly delayed in *hap1Δ* strains (Figure 23A). Conversely, trafficking rates to the nucleus and mitochondrial matrix are unaffected by Hap1 (Figure 23B, C, respectively). The delay in cytosolic heme trafficking rates is not due to defects in heme synthesis rates (Figure 24). These results show Hap1p facilitates cytosolic heme trafficking dynamics.

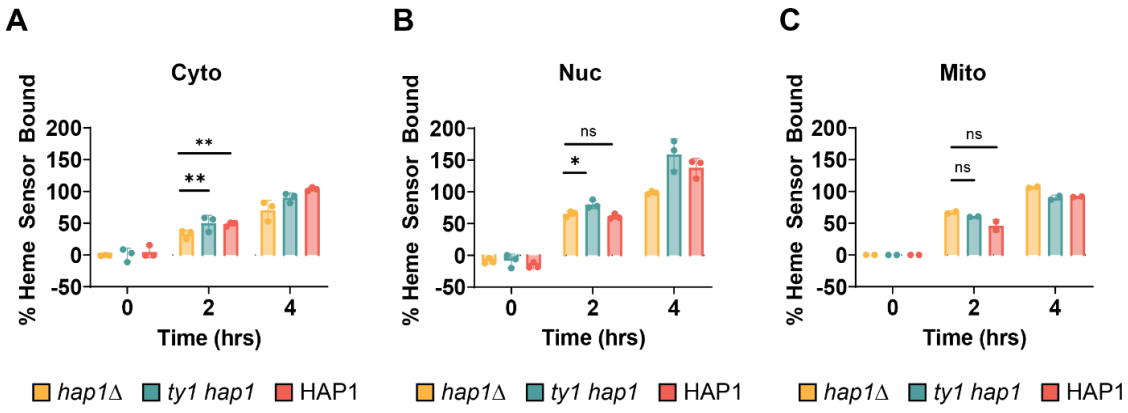

Figure 23. Inter-compartmental Heme Trafficking Dynamics Measured by the HS1 Heme Sensors. Heme trafficking kinetics were monitored using the SA pulse-chase assay in WT HAP1 and Hap1 mutant strains expressing HS1 in the cytosol **(A)**, nucleus **(B)**, and mitochondria matrix **(C)**. Each *dot* represents a biological replicate. The significance is indicated by asterisks using one-way ANOVA with Dunnett's post hoc test: * $p < 0.05$, ** $p < 0.01$, ns, not significant.

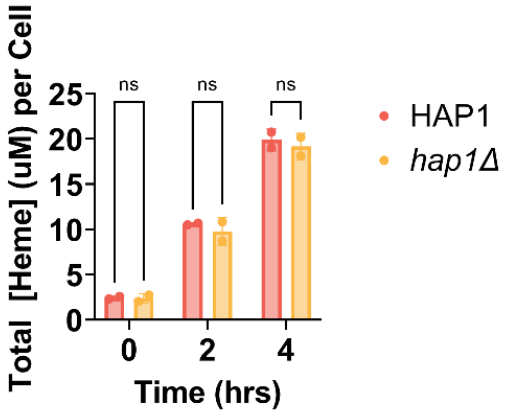

Figure 24 – Heme Synthesis Kinetics in *hap1Δ* yeast. Following an overnight period of heme synthesis inhibition using 500 uM SA, heme synthesis was re-initiated. During this period, time points were taken at 0, 2, and 4 hours of HAP1 and *hap1Δ* cultures, and total heme was measured using a porphyrin fluorescence assay.

4.3.4 Hap1p Transcription Activity is Indispensable for Buffering Labile Heme

Hap1p has several regulatory domains that could be responsible for regulating labile heme. The following experiments probe whether this regulation

is dependent on Hap1p-heme interactions or transcription activation. Expressing the WT HAP1 gene episomally in the background of *ty1 hap1* or ***hap1Δ*** yeast will rescue transcription activity (Figure 25A). A *hap1* mutant with a Serine to Arginine mutation at amino acid residue 63 (*hap1-18*) rendering it unable to bind DNA does not display transcription activity, as expected (Figure 25A). Further, the high heme phenotypes and the cytosolic trafficking defect are also rescued by episomal WT HAP1 expression, but not by the *hap1-18* mutant (Figure 25B, C).

Apart from Hap1p's transcription activity, this transcription factor has several regulatory domains: Zn cluster motif, dimerization element, three repression modules (RPMs), seven heme-responsive motifs (HRMs), and the activation domain (Figure 25D). To determine if these other domains affect heme homeostasis, nuclear labile heme in ***hap1Δ*** strains expressing various *HAP1* gene truncations was investigated (Figure 25D). ***hap1Δ*** strains episomally expressing mutant Hap1 gene constructs absent of RPMs or HRM domains (***ΔHeme, H7-d2***), resulted in higher sensor fluorescence ratios relative to ***hap1Δ*** strains, indicative of low labile heme (Figure 25E). This suggests that the HRMS and RPMs of Hap1p are not important for regulating heme homeostasis as they phenocopy WT strains. It is important to note that despite missing HRM and RPM domains, these mutants maintain transcription activity (Figure 25D).[145] On the other hand, *HAP1* mutants lacking the C-terminal activation domain (*HB, HG, HK*) are unable to activate transcription, and phenocopy ***hap1Δ*** nuclear labile heme (Figure 25E). Altogether, Hap1p's ability to buffer labile heme to low levels is dependent on transcription activity, not heme binding.

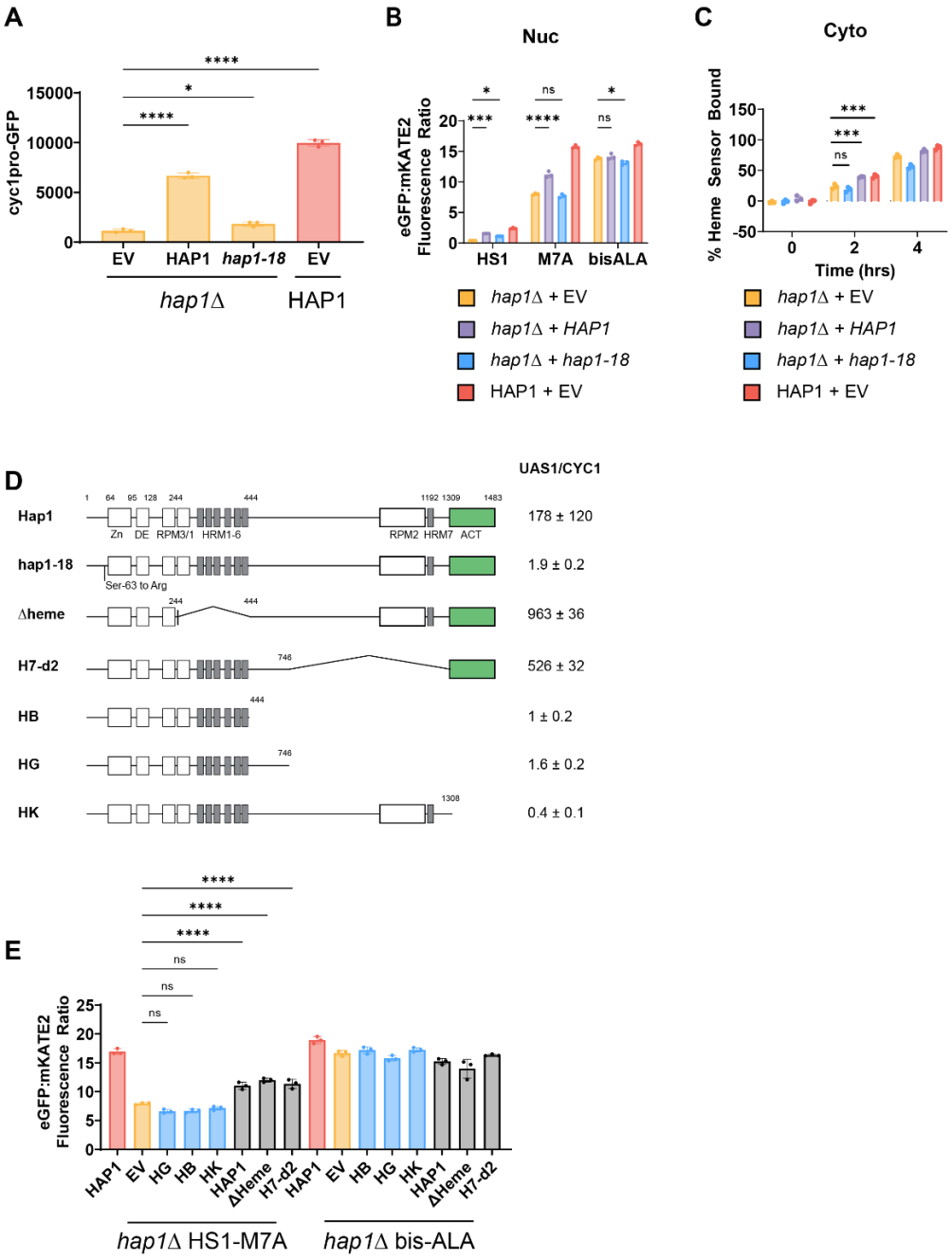

Figure 25. Phenotype Complementation is Dependent on Hap1 Transcription Activity. (A) Hap1p transcription reporter activity assessed by fluorescence in Hap1 mutant yeast with and without episomal WT *HAP1* and *hap1-18* mutant expression. **(B)** Steady State nuclear heme measured using HS1, HS1-M7A and HS1-M7A-H012A sensors in Hap1 mutants with and without episomal WT *HAP1* and *hap1-18* mutant expression. **(C)** Cytosolic heme trafficking in Hap1 mutant yeast with and without episomal WT *HAP1* and *hap1-18* mutant expression. **(D)** Map of Hap1 truncation mutants and their associated UAS1/CYC1 transcription activity. **(E)** Steady State nuclear heme in *hap1Δ* strains episomally expressing WT *HAP1* or Hap1 truncation mutants. Each *dot* represents a biological replicate. The significance is indicated by asterisks using one-way ANOVA (**A, C, E**) and two-way (**B**) ANOVA with Dunnett's post hoc test: * $p < 0.05$, ** $p < 0.01$, *** $p < 0.001$, **** $p < 0.0001$, ns, not significant.

4.3.5 Hap1p Targets Buffers Labile Heme

Hap1 mutant strains lacking transcriptional activity have increased labile heme compared to WT. We hypothesize Hap1p regulates expression of proteins that function in buffering the labile heme pool. Referring to the list Hap1p-regulated hemoproteins, several were tested for their role as a heme buffer.

Hmx1 expression is regulated by Hap1p and is the enzyme responsible for degrading heme is Hmx1p. Heme sensor ratios in BY4741 yeast expressing WT HAP1 are the same regardless of HMX1 expression (Figure 26A). This result validates the decrease in labile heme observed in HAP1 strains are not due to heme degradation. The Hap1-regulated hemoprotein candidate with the highest intracellular abundance is yeast flavohemoglobin (Yhb1p). Yhb1p reversibly binds oxygen and contains heme- and flavin-binding domains.[146] It is described as a nitric oxide oxidoreductase that plays a role in oxidative and nitrosative stress responses, protecting nitration of cellular targets.[147, 148] Nuclear labile heme in BY4741 *yhb1Δ* strains with and without *HAP1* was measured. Regardless of Yhb1p, *HAP1* expression resulted in lower labile heme, therefore, Yhb1p is not the downstream product of Hap1p that is regulating labile heme (Figure 26B).

Next, catalase expression and activity in *ty1 hap1*, *hap1Δ*, HAP1, *ctt1Δ*, and *hem1Δ* strains was tested. *ctt1Δ* yeast do not express catalase and therefore do not possess catalase activity, as expected (Figure 26C). Similarly, *hem1Δ* strains lack heme and therefore do not express the heme-dependent enzyme catalase, as shown in (Figure 26C). HAP1 strains have greater catalase expression and

activity compared to *ty1 hap1* and *hap1Δ* strains (Figure 26C). While *ty1 hap1* and *hap1Δ* have significantly less catalase expression, activity is still present. This suggests an additional regulator of catalase other than Hap1p. Further, *HAP1* expression in BY4741 *ctt1Δ* was not able to decrease nuclear labile heme levels, suggesting catalase plays a role in heme regulation (Figure 26D).

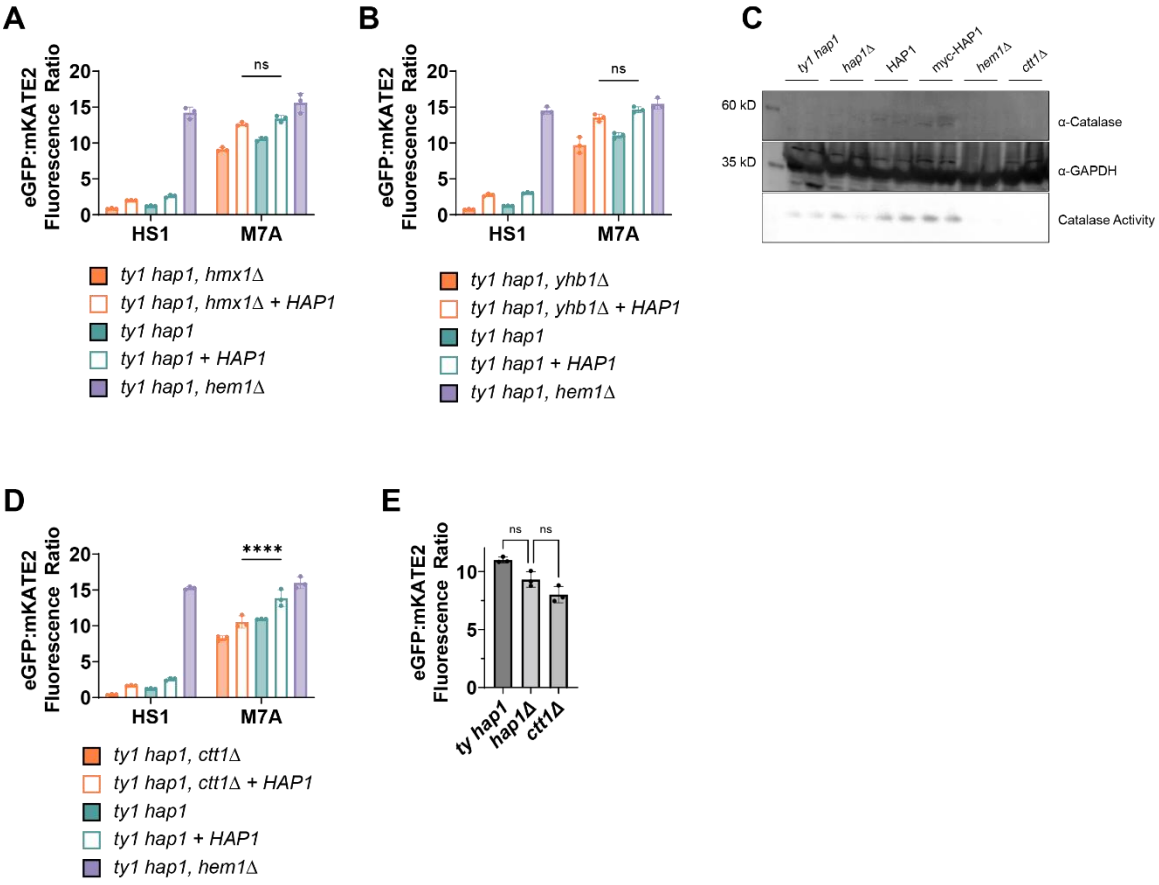

Figure 26. **Identifying Hap1 Targets that Buffer Heme.** Steady state nuclear heme measured in BY4741 strains with and without episomal WT HAP1 and with and without HMX1 **(A)**, YHB1 **(B)**, and CTT1 **(D)**. **(C)** Western blot probing for catalase and GAPDH expression in different Hap1 strains and catalase activity. **(E)** Steady state nuclear heme in *ty hap1*, *hap1Δ*, and *ctt1Δ* strains. Each *dot* represents a biological replicate. The significance is indicated by asterisks using two-way ANOVA for multiple comparisons with Dunnett's post hoc test (B, E): * $p < 0.05$, ** $p < 0.01$, *** $p < 0.001$, **** $p < 0.0001$, ns, not significant.

4.3.6 Cytochrome b_{562} Expression Rescues hap1Δ Labile Heme

Finally, to see if expression of any other hemoprotein could complement *hap1Δ* labile heme levels, the hemoprotein, cytochrome b_{562}, was episomally over-expressed in *hap1Δ* strains under a galactose inducible promoter. HAP1 and *hap1Δ* strains containing cytochrome b_{562} expression or EV plasmids were precultured in 2 % raffinose-containing media and grown to mid-exponential phase. The next day cultures were washed and maintained in 2 % raffinose media treated with or without 1 % galactose. Cytochrome b_{562} expression in *hap1Δ* strains (indicated as "CC" in Figure 27A) raised the cytosolic and nuclear eGFP/mKATE2 sensor fluorescence ratios, indicating less labile heme, compared to strains carrying an EV plasmid or untreated with galactose (Figure 27A). After determining Hap1p as a regulator of free heme, we sought to investigate the biological consequence of having increased labile heme levels. Heme is a pro-oxidant and has the potential to catalyze the production of deleterious reactive oxygen species.[4, 40] Therefore, we expect cells with high labile heme to be hypersensitive to hydrogen peroxide treatment. Indeed, exposing *hap1Δ* and HAP1 yeast to hydrogen peroxide resulted in an observable and severe growth delay in hydrogen peroxide-treated *hap1Δ* yeast (Figure 27B). This observation could be due to the lack of catalase in these strains and not necessarily the excess of free heme itself.

Lastly, complementation experiments were performed to see if the hydrogen peroxide growth sensitivity in *hap1Δ* cells could be rescued by limiting the amount of free heme. To do so, the galactose-inducible cytochrome b_{562}

expression strains were used to sequester the labile heme and were treated with and without hydrogen peroxide. Opposite of what was expected, *hap1Δ* treated with hydrogen peroxide and expressing the cytochrome experienced an enhanced growth delay than hydrogen peroxide-treated *hap1Δ* strains lacking cytochrome. (Figure 27C). This suggests the excess labile heme in *hap1Δ* strains serve a protective role against hydrogen peroxide toxicity.

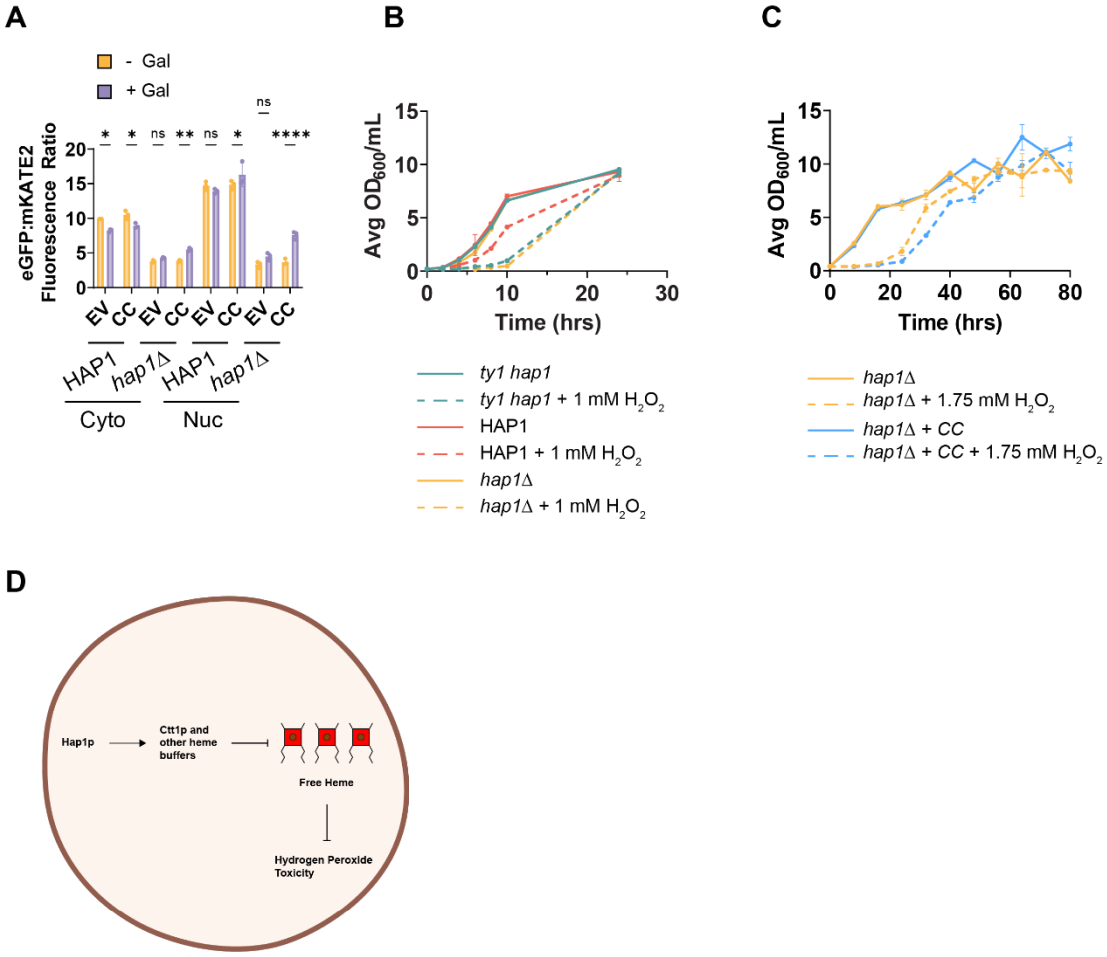

Figure 27. The Effects of Cytochrome b_{562} Expression on Labile Heme and Growth. (A) Steady state nuclear heme in HAP1 and *hap1Δ* strains expressing cytochrome b_{562} ("CC") or EV under a galactose-inducible promoter treated with or without 1 % galactose. **(B)** Growth curve of WT HAP1 and *hap1Δ* yeast treated with or without 1 mM hydrogen peroxide. OD, optical density at 600 nm. n = 2 biological replicates. **(C)** Growth curve of WT HAP1 and *hap1Δ* yeast with and without cytochrome b_{562} expression plasmids treated with and without1 % galactose. **(D)** Model for Hap1p heme regulation. Each *dot* represents a biological replicate. The significance is indicated

by asterisks using two-way ANOVA for multiple comparisons with Dunnett's post hoc test (**A**): * $p < 0.05$, ** $p < 0.01$, **** $p < 0.0001$, ns, not significant.

4.3.7 Hydrogen Peroxide Stimulates Nuclear Heme Availability

The above work describes how yeast catalase affects nuclear heme availability. Compartmental heme effects were then probed in catalase deletion yeast. Cytosolic, mitochondrial, and nuclear heme were analyzed using the heme sensors in catalase deletion and WT yeast (Figure 28A, B, C). Only nuclear heme is significantly perturbed in cells without catalase (Figure 28 C).

The yeast GAPDH isoform, Tdh3, has been previously identified as a cytosolic heme buffer.[27, 30] Interestingly, yeast Tdh3 also buffers heme in the nuclear and mitochondrial compartments (Figure 28D, and E). To investigate if Tdh3 and Ctt1 function in the same pathway to buffer nuclear heme, double deletion yeast mutants were generated. If Tdh3 and Ctt1 act in the same pathway, when both genes are deleted, there should not be an additive effect. On the contrary, there is increased nuclear heme in the *tdh3Δ ctt1Δ* double deletion yeast mutant compared to the single *tdh3Δ* or *ctt1Δ* mutants (Figure 28 F).

Tdh3 has been reported to be in the cytosol and the nucleus.[149-151] However, yeast catalase, Ctt1, is cytosolic. How then is catalase affecting nuclear heme availability? Catalase functions to remove hydrogen peroxide in the cell. The high levels of hydrogen peroxide in yeast lacking catalase could be the reason for increased nuclear heme. In this case, catalase is not acting as a nuclear heme buffer, but heme is performing a signaling role as a result of the presence of hydrogen peroxide. To directly test this, WT yeast were pre-cultured overnight.

The next day, cells were exposed to varying concentrations of hydrogen peroxide for about 90 minutes. After the exposure, cells were washed, and the heme sensor fluorescence was read. Lower heme sensor ratios were observed in yeast exposed to high concentration of hydrogen peroxide (500 uM – 2 mM) (Figure 28 G). The low ratios observed were like that of catalase deletion yeast (Figure 28 G).

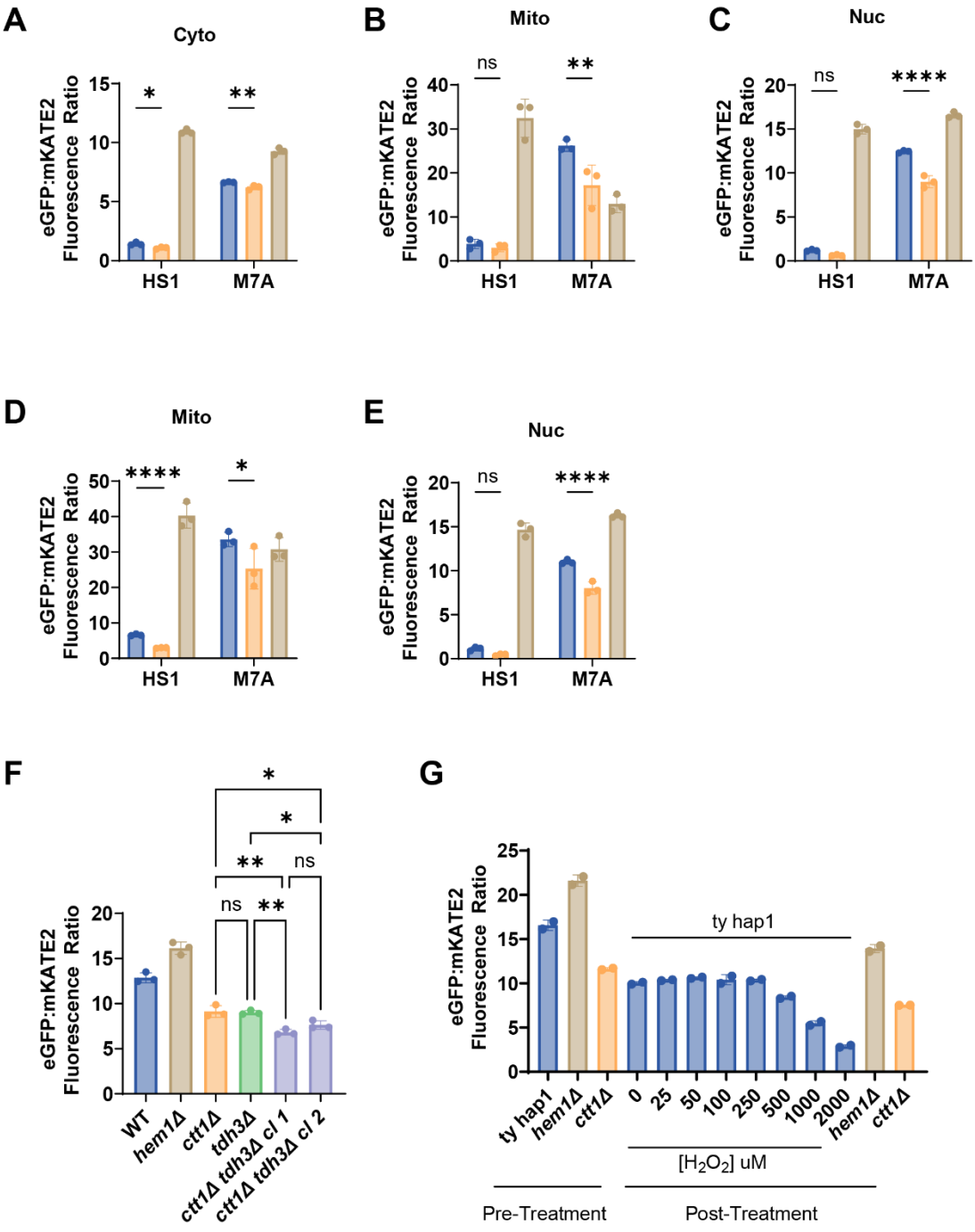

Figure 28. Catalase and GAPDH Affect Nuclear Heme Availability. WT and *ctt1Δ* cellular heme distribution in Cytosolic **(A)**, Mitochondrial **(B)**, and Nuclear **(C)** compartments. WT and *tdh3Δ* cellular heme distribution in Mitochondrial **(D)**, and Nuclear **(E)** compartments. **(F)** Nuclear heme in single *tdh3Δ* and *ctt1Δ* mutant yeast and *tdh3Δ ctt1Δ* double deletion mutants. Nuclear heme in cells exposed to hydrogen peroxide **(G)**. Each *dot* represents a biological replicate. The significance is indicated by asterisks using two-way ANOVA for multiple comparisons with Dunnett's post hoc test: * $p < 0.05$, ** $p < 0.01$, **** $p < 0.0001$, ns, not significant.

4.3.8 Yeast Strains Have Different Heme Levels

Strains derived from S288C, including BY4741, carry the natural Ty1 insertion in the *HAP1* gene, while other yeast strains such as W303 and Sigma1278b do not.[147] In BY4741 yeast, HS1 sensors have a high affinity for ferrous heme, such that this sensor is poised at 100 % heme bound (Figure 29A).[27] The weaker affinity HS1-M7A sensor is 20 % - 80 % heme bound and is more appropriate to use to detect changes in labile heme (Figure 29A). In contrast, HS1 and HS1-M7A sensors in W303 yeast are ~ 70 % and ~ 5 % heme bound, respectively (Figure 28B). The low labile heme levels in W303 yeast phenocopy yeast with WT HAP1. Indeed, W303 and Sigma1278b yeast have WT HAP1 while BY4741 yeast have mutant HAP1 (Figure 29C).[152]

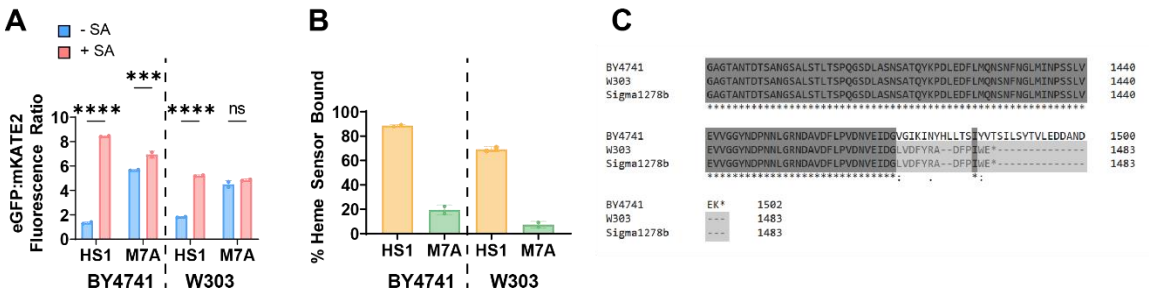

Figure 29 - BY4741 yeast have more labile heme than W303 yeast. HS1 and M7A cytosolic sensor ratio values in BY4741 and W303 yeast treated with and without 500 uM succinylacetone (SA) **(A)** and corresponding % Heme Sensor Bound values **(B)**. **(C)** Sequence alignment of the C-terminal regions of Hap1p in BY4741, W303, and Sigma1278b yeast strains.

4.4 Discussion

Here we identified heme utilization is inversely related to heme bioavailability. To alter heme utilization, hemoprotein expression was altered by

using yeast strains lacking Hap1p, the transcription factor responsible for regulating ~ 50 % all the known hemoproteins in yeast. Hap1p is a heme regulator, where it controls the expression of heme buffering proteins, including catalase, that limit the amount of free heme, where higher free heme levels seem protect against hydrogen peroxide toxicity in the absence of catalase (Figure 26D). Hap1p has been extensively studied in the context of oxygen sensing through heme but has never been directly implicated in heme homeostasis.[135, 138, 145] Here, this work describes for the first time, 1) the inverse relationship between heme utilization and bioavailability, 2) Hap1p as a regulator of the labile heme pool in yeast, and 3) increased free heme serves a protective role against hydrogen peroxide.

Hap1p regulates labile heme in cytosolic, nuclear, and mitochondrial compartments. This regulation is dependent on Hap1p transcription activity inferring that Hap1p controls the expression of proteins that act to buffer the labile heme (heme buffering proteins). Without Hap1p transcription activity, these proteins are not expressed, resulting in an increase in the labile heme pool. This increase in labile heme is not due to defects in heme degradation, as the heme degradation enzyme, Hmx1p did not have an effect on labile heme levels.

Strains lacking Hap1p have delayed heme trafficking rates to the cytosol, while rates to the nucleus and mitochondria matrix are unaffected. Based on this result, it is presumed that a protein under Hap1p regulation is responsible for cytosolic heme trafficking. Further, this selective heme trafficking defect to a single compartment suggests other Hap1p-independent pathways exist for nuclear and mitochondrial heme mobilization. Interestingly, Hap1p does not affect nuclear

heme trafficking, despite heme binding to Hap1p takes place in this organelle. This suggests an additional protein or chaperone for nuclear heme trafficking exists that ultimately may affect heme-Hap1p regulation.

Specific Hap1p targets were tested to identify which ones were responsible for regulating steady-state heme. Our work identified Cttp1, catalase, as a determinant of labile heme. Ctt1p is a cytosolic hemoprotein responsible for removing hydrogen peroxide. Despite having WT HAP1, strains without CTT1, have high labile heme with levels comparable to *ty1 hap1* strains. Interestingly *ctt1Δ* have more labile heme than *ty1 hap1* mutants. One explanation for this is that *ty1 hap1* mutants maintain minimal Hap1p transcription and catalase activity. This residual activity is enough to result in less labile heme in *ty1 hap1* strains compared to true *ctt1Δ.* Indeed, *hap1Δ* and *ctt1Δ* have the same nuclear heme levels and are not statistically different (Figure 26E). Since *hap1Δ* strains maintain some catalase activity, yet nuclear heme phenocopies *ctt1Δ*, it can be hypothesized that an additional downstream target of Hap1p is involved in regulating heme.

Yhb1p was also explored as a potential heme buffer. Although being the most abundant hemoprotein in the cell, it does not exhibit a role in heme homeostasis. One explanation for this is Yhb1p may have a heme affinity that is too low. On the contrary, catalase abundance is not as high as Yhb1p, yet catalase may have a higher heme affinity, allowing it to function as a heme buffer to regulate heme.

Cytochrome b_{562} expression was able to complement *hap1Δ* labile heme, but not rescue the hydrogen peroxide growth defect as we first hypothesized. In fact, cytochrome expression had an opposite effect, where growth was further delayed in the presence of hydrogen peroxide compared to strains lacking cytochrome. This suggests that the excess free heme in *hap1Δ* cells play a protective role against hydrogen peroxide. Heme can have peroxidase activity, which would remove hydrogen peroxide and associated detrimental effects. Cytochrome b_{562} has a high reduction potential and would not act as a reducing agent to remove hydrogen peroxide. Therefore, heme is the only reagent that could function to remove hydrogen peroxide.

Further, it is possible that the *hap1Δ* hydrogen peroxide growth defect (Figure 27B) is not singularly due to increased labile heme per se, but the perhaps the absence of hemoproteins that function in hydrogen peroxide signaling or detoxification, including catalase. Hap1p transcription mutants are defective in the expression of several proteins, including catalase, and potentially others involved in hydrogen peroxide signaling. Therefore, the effects of hydrogen peroxide treatment in *hap1Δ* strains may not be singularly heme-related but may be due to the lack of other hydrogen peroxide defense mechanisms that could be regulated by Hap1p. For example, if lowering labile heme in *hap1Δ* strains would not rescue associated hydrogen peroxide growth defects, catalase expression probably would.

In addition, yeast catalase only affects nuclear labile heme (Figure 28), while the yeast GAPDH isoform tdh3 affects heme in the cytosol, nucleus, and

mitochondria (Figure 28).[27] Catalase and tdh3 function in separate pathways to regulate nuclear heme as the effect is additive when both genes are deleted compared to when they are individually deleted (Figure 28 F). Since catalase localization has not been reported in the nucleus, we hypothesized that catalase is not acting as a heme buffer. Rather the resulting hydrogen peroxide levels present in yeast without catalase stimulate nuclear heme accumulation. In fact, decreasing heme sensor ratios were observed with increasing hydrogen peroxide concentration (Figure 28 F). This suggests hydrogen peroxide triggers heme mobilization to the nucleus, possibly for a role in signaling. A similar result has been published. Katherisan, et al. reported that hydrogen peroxide triggers heme transfer between proteins.[153] Specifically, heme is released from Ccp1p and is transferred to apo-Cta1p.[153]

In conclusion, heme utilization and bioavailability are inversely related. When heme utilization requirements are decreased such as in *hap1Δ* yeast, heme bioavailability is increased while total heme levels are moderately perturbed relative to WT. Hap1p transcription activity is indispensable in regulating labile heme to low levels. We provide a model where Hap1p regulates the expression of downstream targets that function to limit or buffer the labile heme pool. Without these heme buffering proteins, there is an increase in labile heme and added protection against hydrogen peroxide in the absence of catalase.

4.5 Materials and Methods

4.5.1 Yeast Strains, Yeast Growth, and Plasmids

4.5.1.1 Yeast Strains and Growth Conditions

S. cerevisiae strains used in this study were derived from BY4741 (MATa, *his3*Δ1, *leu2*Δ0, *met15*Δ0, *ura3*Δ0), *ctt1Δ::KanMX4*, *hmx1Δ::KanMX4*, *yhb1Δ::KanMX4* strains were obtained from the yeast gene deletion collection (Thermo Fisher Scientific) and confirmed by sequencing the barcodes flanking the KanMX4 deletion cassette. We also used the previously reported strain DH001b-3 (*hem1Δ::HIS3*).[27] FY2607, FY2609, FY2611, and FY2613 strains were kindly provided by Fred Winston (Harvard Medical School, Boston, USA) and used for these experiments.[142]

Yeast Transformations were performed by the lithium acetate procedure.[101] Strains were maintained at 30 °C on either enriched yeast extract (1 %) and peptone (2 %) based medium supplemented with 2 % glucose (YPD), or synthetic complete medium (SC; Sunrise Science Products) supplemented with 2 % glucose and the appropriate amino acids to maintain selection.[27] Cells cultured on solid medium plates were done so with YPD or SC media supplemented with 2 % agar.[27] Selection for yeast strains containing the KanMX4 marker was done on YPD agar plates supplemented with G418 (200 µg/ml).[27] WT cells treated with the heme synthesis inhibitor, SA, and *hem1Δ* cells were cultured in YPD or SC media supplemented with 50 µg/ml of 5-aminolevulinic acid (ALA) or 15 mg/ml of

ergosterol and 0.5% TWEEN 80 (YPDE or SCE, respectively).[27, 102] All liquid cultures were maintained at 30°C and shaken at 220 rpm.

4.5.1.2 Plasmids

Hap1p activity reporter plasmid. The Hap1p activity reporter plasmid in which GFP is driven by the *CYC1* promoter was generated by PCR amplifying the upstream (-369 to -1) sequence relative to the *CYC1* translational start site, introducing 5' SpeI and 3' BamHI restriction sites. The PCR product was digested and ligated into pRS415, generating pMW002. The GFP gene was PCR amplified from pRH003-1 using primers prRC004 and prRC007, containing 5' BamHI and 3' HindII sites, respectively. The PCR product was digested with enzymes and ligated into pMW002, resulting in pMW003.

Hmg2 activity reporter plasmid. The Hmg2 reporter plasmid in which mKATE2 is driven by the *HMG2* promoter was generated by PCR amplifying the upstream (-614 to -1) sequence relative to the *HMG2* translational start site, introducing 5' EagI and 3' XbaI restriction sites. The PCR product was digested and ligated into pRS316, generating pMW050. The mKATE2 gene was PCR amplified from pDH013 using prID067 and prMW071 containing 5' XbaI and 3' BamHI sites, respectively. The PCR product was digested and ligated into pMW050, generating pMK001. The HMG2 terminator was generated by PCR amplifying the downstream (+6 to +328) sequence relative to the translational stop codon, introducing 5' BamHI and 3' EcoRI restriction sites. The PCR product was digested and ligated into pMK001, generating pMK002.

Cytochrome b_{562} expression plasmid. The cytochrome b_{562} expression plasmid under a galactose inducible promoter (p316-GAL) was generated by PCR amplifying an allele of the high-affinity hemoprotein cytochrome b_{562}. The amplified gene was sub-cloned into the XbaI/BamHI sites of p316-GAL to generate plasmid pDH039.[49]

HAP1 expression plasmids. The Hap1 expression plasmids were a generous gift from Professor Li Zhang and are described in Hon, et al.[145] Briefly, all expression plasmids are under the native Hap1 promoter and were subcloned into the pYES2 plasmid backbone containing URA markers. The *hap1-18* mutant plasmid contains a single amino acid residue change. The Serine at position 63 is changed to an Arginine. *ΔHeme* plasmid is missing amino acid residues 244 – 444. *H7-d2* is missing amino acids residues 746 – 1309. *HB* is missing amino acids 444 – 1483. *HG* is missing amino acids 746 – 1483. *HK* is missing amino acids 1308 – 1483.

4.5.2 Experimental Methods

4.5.2.1 Trafficking Dynamics Measurements

Inter-compartmental heme trafficking rates were monitored as described in Martinez-Guzman, et al.[66] HS1-expressing cells were cultured with or without 500 μM succinylacetone (SA, Sigma-Aldrich) in SCE-LEU medium. Triplicate 5-mL cultures were seeded at an initial density of 0.01-0.03 *A*600 units per ml (2–6 x 10^5 cells per ml) and grown for 14 - 16 h at 30 °C, with or without 500 μM succinylacetone (Sigma-Aldrich) in SCE-LEU medium, shaking at 220 rpm until

cells reached a final density with *A*600 approximately 1.0 (2 x 10^7 cells per mL). After culturing, 1 absorbance unit (~2 x 10^7 cells) of cells were collected, washed twice with 1 mL sterile ultrapure water, and resuspended in 1 mL fresh SC-LEU medium. The cells that were pre-cultured without succinylacetone provided reference values for EGFP/mKATE2 fluorescence ratios associated with maximal heme loading of HS1 (R_{max} values). The succinylacetone-conditioned cells were split into two 500 µL fractions. One fraction was treated with 500 µM succinylacetone to give EGFP/mKATE2 fluorescence ratios associated with minimal heme loading of HS1 (R_{min} values). The other fraction was not treated with succinylacetone so that heme synthesis could be re-initiated to give compartment-specific heme trafficking rates. HS1 fluorescence was monitored using 200 µL of 1 *A*600 unit per ml (2 x 10^7 cells per ml) cell suspension in black Greiner Bio-one flat bottom fluorescence plates with a Synergy Mx multi-modal plate reader. EGFP (excitation 488 nm, emission 510 nm) and mKATE2 (excitation 588 nm, emission 620 nm) fluorescence was recorded every 5 min for 4 h, with the plate being shaken at medium strength for 30 s prior to each read. Background fluorescence of cells not expressing the heme sensors was recorded and subtracted from the EGFP and mKATE2 fluorescence values. The fractional heme saturation of the sensor was determined using the following equation: sensor bound (%) = (R – R_{min})/(R_{max} – R_{min}).

4.5.2.2 Total Heme Quantification

Measurements of total heme were performed using a fluorometric assay designed to measure the fluorescence of protoporphyrin IX upon the release of

iron from heme as previously described.[103] For all total heme measurements, ~ 1 x 10^8 cells were harvested, washed in ultrapure water, and resuspended in 500 uL 20 mM oxalic acid and stored in a closed box at 4 ^oC overnight (16 – 18 hours). An equal volume (500 uL) of 2 M oxalic acid was added to the cell suspensions in 20 mM oxalic acid. The samples were split, where half of the cell suspension was transferred to a heat block set at 95 ^oC and heated for 30 minutes, and the other sample half was kept in a closed box at room temperature (~ 25 ^oC) for 30 minutes. All suspensions were then centrifuged for two minutes on a table-top microfuge at 21000 x g and the porphyrin fluorescence (ex. 400 nm, em. 608 nm) or 200 uL of each sample was measured using a Synergy mx multi-modal plate reader in black Grenier Bio-one flat bottom fluorescence plates. Heme concentrations were calculated from a standard curve prepared by diluting 500 – 1500 uM hemin chloride stock solutions in 0.1 M NaOH into ultrapure MilliQ water and from there prepared the same as the cell samples as described above. To calculate heme concentrations, the fluorescence of the un-boiled sample (representing background levels of protoporphyrin IX) was subtracted from the fluorescence of the boiled sample (representing the free base porphyrin generated upon heme iron release). The cellular concentration of heme was determined by dividing the moles of heme determined in this fluorescence assay by the number of cells analyzed, to give moles of heme per cell. To convert this to a cellular concentration the moles of heme per cell were divided by the volume of a yeast cell (given to be 50 fL).

4.5.2.3 Hap1p Transcriptional Reporter Assay

Wild-type HAP1, *hap1*Δ, *ty hap1*, and *hem1Δ* yeast strains expressing p415–CYC1–EGFP or p415-HMG2-MKATE2 were cultured in 10 mL SCE-LEU media for ~14–16 h to a density of 1–2 *A*600 units per mL. Cells were resuspended in 1x PBS to a concentration of 10 *A*600 units per ml and 200 µL (2 *A*600 units or 4 x 10^7 cells) was used to measure EGFP fluorescence (excitation 488 nm, emission 510 nm). Background autofluorescence of cells not expressing EGFP was recorded and subtracted from the EGFP-expressing strains.

4.5.2.4 Catalase Activity Measurements in Yeast

The activity of yeast catalase were measured using methods described previously.[104, 105] Yeast cells were cultured in 10 mL SCE media for 14–16 h to mid-exponential phase. Cells were lysed using zirconium oxide beads in a Bullet Blender (Next Advance).[27] Protein concentrations were determined by the Bradford method (Bio-Rad). To detect the catalase activity, 15 µg protein lysates were analyzed by native PAGE on a 10% Tris-glycine gel (Invitrogen). The native gel ran in Tris-Glycine buffer at 4 ^{o}C overnight (16 – 18 hrs) at 5 mAmps/20 Volts. After electrophoresis, an in-gel activity stain was utilized to measure catalase activity.[105] While the gel is washing in ultrapure water (rocking at room temperature) the staining solution was made. In brief, the catalase staining solution was prepared by mixing 1 part dopamine (20 mg/mL) and 1 part para-phenylenediamine (3.5 mg/mL) in 0.2 M potassium phosphate buffer, pH 8, 1 part 15% H_2O_2 (JT Baker), and 2 parts DMSO in the order listed. The staining solution

was added directly to the gel and allowed to stain for 2 min while gently rocking by hand, followed by imaging on an Amersham Imager. There is not a de-staining or washing step before imaging.

4.5.2.5 Immunoblotting

The expression of yeast catalase was measured using methods described previously.[104, 105] Yeast cells were cultured in 10 mL SCE media for 14–16 h to mid-exponential phase. Cells were lysed using zirconium oxide beads in a Bullet Blender (Next Advance).[27] Protein concentrations were determined by the Bradford method (Bio-Rad). To detect catalase expression, 50 – 100 ug protein lysates were analyzed by SDS-PAGE. After preparing the samples, samples were boiled at 100 ^{o}C for five minutes, and briefly centrifuged. Proteins in individual samples were resolved on 14 % SDS–PAGE gels (Invitrogen), run in Tris-Glycine SDS buffer at room temperature at a constant 20 mAmps. After resolving, proteins were transferred onto nitrocellulose membranes overnight at 4 ^{o}C at 20 mAmps/100 Volts for 16 – 18 hrs. Following the overnight transfer, the Revert^{TM} 700 Total protein stain kit for protein normalization was used (LiCOR). Following the total protein analysis, the membranes were then blocked for 1 hr, rocking at room temperature in LiCOR. The blot was incubated with the anti-Ctt1 (Reddi Lab) primary antibody diluted 1:1000 in LiCOR. Primary antibody incubation was performed for overnight (16 – 18 hr), rocking at 4 ^{o}C. Two, eight-minute washes were performed using 1X-TBS-T, rocking at room temperature. Both blots were then incubated with the secondary antibody, Goat anti-Rb (Biotium Cat. # 20067) diluted 1:5000 in LiCOR. This incubation was performed for 1 hr, rocking at room

temperature. Two, eight-minute washes were performed in 1X-TBS-T rocking at room temperature before imaging on a LiCOR Odyssey Infrared imager.

4.5.2.6 Steady-State Heme Measurements

To measure steady-state labile heme, wild-type, *hem1*Δ, and *tango2*Δ cells expressing the HS1-M7A heme sensors were cultured in 10 mL SCE-LEU media, with or without 0.5 mM succinylacetone, for ~14–16 hr to mid-exponential phase (*A*600 ≈ 1–2). Cytosolic and mitochondrial-targeted sensors were expressed on low copy centromeric plasmids and were driven by the GPD promoter (p415-GPD). After culturing, cells were collected, washed in water, and resuspended in phosphate buffered saline (PBS) solution to a density of 10 *A*600 units per mL. Two-hundred microliters of the cell suspension, corresponding to 2 *A*600 units or 6 x 10^7 cells, was used to measure EGFP (excitation 488 nm, emission 510 nm) and mKATE2 (excitation 588, emission 620) HS1-M7A sensor fluorescence. Background autofluorescence of cells not expressing the sensors was recorded and subtracted from the EGFP and mKATE2 sensor fluorescence values. Fluorescence was recorded on a Synergy Mx multi-modal plate reader using black Greiner Bio-one flat bottom fluorescence plates.

4.5.2.7 Yeast Growth Tests

Growth tests of wild-type HAP1, *ty1 hap1*, and *hap1Δ* cells were performed by growing 10-mL cultures for 14-16 hr to mid-exponential phase. Cultures were then diluted to 0.2 *A*600 units per mL in 10-mL cultures in SC media supplemented with or without 1 mM hydrogen peroxide (Millipore Sigma). Cultures were grown

for 24 hrs and OD_{600} readings were taken every two hours using a Cary 60 UV/vis spectrophotometer (Agilent).

Growth tests with strains expressing cytochrome b_{562} were performed similarly. Strains were pre-cultured in media containing 2 % raffinose and 1 % galactose for 14-16 hr to mid-exponential phase, and then diluted to 0.4 *A*600 units per mL in 10-mL cultures in SC media supplemented with 2 % raffinose, 1 % galactose, with or without 1.75 mM hydrogen peroxide.

4.5.2.8 Hydrogen Peroxide Exposure Stimulates Nuclear Heme Availability

WT and *ctt1Δ* yeast expressing HS1-M7A nuclear sensors were pre-cultured overnight shaking in flasks at 30 ^{o}C for 14 – 16 hr to mid-exponential phase. Cultures were pelleted at 4000 rpm, washed twice using sterile ultrapure water, and diluted into 10 mL SC-LEU cultures seeded at 0.8 OD/mL. Cultures were treated with varying hydrogen peroxide (Sigma Cat. # 386790) concentrations and incubated shaking at 30 ^{o}C for about 90 minutes. After the 90 minutes, 6 OD of cells were collected, washed in ultrapure water, and resuspended in 1x phosphate buffered saline (PBS) solution to a density of 6 *A*600 units per mL. Two-hundred microliters of the cell suspension, corresponding to ~ 1 *A*600 units or 3 x 10^7 cells, was used to measure EGFP (excitation 488 nm, emission 510 nm) and mKATE2 (excitation 588, emission 620) HS1-M7A sensor fluorescence. Background autofluorescence of cells not expressing the sensors was recorded and subtracted from the EGFP and mKATE2 sensor fluorescence values.

Fluorescence was recorded on a Synergy Mx multi-modal plate reader using black Greiner Bio-one flat bottom fluorescence plates.

CHAPTER 5. CONCLUSIONS AND FUTURE DIRECTIONS

Work from our lab has supported the existence of a labile heme pool by displaying the dynamic movement of heme in different yeast mutants and upon different stressors using our fluorescent heme sensors.[27] Our labs' work, in addition to work done by others, has refuted the canonical view of heme existing only as a tightly bound cofactor. In addition, this thesis work further supports that the here-to-fore belief that heme is synthesized only when needed, and degraded when not utilized is not completely accurate. Further, the concept of a labile heme pool has posed questions regarding both heme management and regulation. The work described in this thesis contributes to a more accurate understanding of heme homeostasis and more fully identifies factors that regulate mitochondrial heme export, steady-state nuclear heme availability, and the relationship between heme utilization and bioavailability (Table 11 and Figure 30).

This thesis describes and establishes yeast systems that can be used in the future to identify and further understand heme trafficking factors and pathways and related diseases. I found that human PGRMC1 aids in nuclear heme trafficking in yeast and can rescue the nuclear heme trafficking defect observed in Dap1 (PGRMC1 homolog) deletion yeast. This result and established yeast system can be used in future studies to elucidate the PGRMC1-dependent nuclear heme trafficking pathways in yeast, a pathway that is to date unclear.

Similarly, WT TANGO2 and/or human TANGO2 genes should be tested to see if either can rescue the mitochondrial heme accumulation observed in

Tango2 deletion yeast. If the human TANGO2 gene is capable of rescuing mitochondrial heme levels yeast tango2 mutants, this will allow for the study of human Tango2 disease-causing mutations in yeast. Specifically, yeast could be a great system to study Tango2p and related diseases, and its implications in heme homeostasis, a connection that has not be studied thus far.

Further, complementation experiments should be tried to rescue the low nuclear heme phenotypes in the mutants identified by the high throughput screen. Specifically, instead of re-expressing the gene episomally, as described in this thesis, the gene should be integrated into the genome and tested. Integrating the gene may allow it to be expressed better and may result in a more obvious rescue phenotype. In addition, adapting the high throughput screen described here and by Martinez-Guzman to probe regulators of nuclear heme dynamics (or mitochondrial-nuclear heme trafficking) rather than at steady state would be extremely valuable.[113] This thesis work shows there are several proteins and pathways that facilitate heme getting to the nucleus. Further, heme trafficking kinetics assays performed by Martinez-Guzman, et al, reveal heme trafficking rates to the nucleus occur faster.[66] It would be worthwhile to identify other proteins that aid in mitochondrial-nuclear heme trafficking kinetics.

Lastly, this research identified that hemoproteins under the regulation of the transcription factor, Hap1p, function in buffering the labile heme to low levels in the cytosol, mitochondria, and nuclear compartments, namely, catalase. Yeast with transcriptionally inactive Hap1p or lacking catalase have increased labile heme. This yeast system can be used to probe the effects of having increased

labile heme on other cellular functions. In other words, this system will aid in research to understand the consequences of having increased amounts of labile heme more fully. Proteomics could also be performed on WT and mutant Hap1 strains to identify proteins that are differentially expressed and are acting as heme buffers. GAPDH has also been identified as a cytosolic heme buffer in yeast. Yeast without the GAPDH isoform, Tdh3, have increased cytosolic labile heme.

Overall, this thesis research in elucidating factors regulating mitochondrial heme export, nuclear heme trafficking, and heme buffering, will act as a foundation in providing enhanced understanding beyond our current knowledge of heme-related diseases. Enhanced understanding of the specific heme trafficking and buffering mechanisms will also allow scientists to develop and improve upon targeted therapeutic treatments.

Table 11. Summary of Proteins and Themes Studied, and Their Effects on Heme Homeostasis

Protein or Subject Studied	Outcomes
Tango2	• Facilitates Mitochondrial Heme Export and Nuclear Heme Trafficking in Yeast
DAP1/PGRMC1	• Facilitates Nuclear Heme Trafficking in Yeast
Mic60 (MICOS)	• Needed for Optimal Heme Biosynthesis
Mito-Nuc Tethers	• Ybr063c (Cnm1), Yet3 and Ysc3 do not affect nuclear heme trafficking • Yet3 overexpression yeast have altered steady state mitochondrial and nuclear heme levels
Genome-Wide Determinants of Steady State Nuclear Heme Bioavailability	• Several distinct genes regulate nuclear heme availability • The low nuclear heme observed in mutants from the gene deletion library is not rescued by complementation experiments
Heme Utilization and Bioavailability	• Heme utilization does not govern heme bioavailability • Free Heme prevents hydrogen peroxide toxicity • Hap1 regulates expression of hemoproteins that act as buffers to limit the amount of free heme

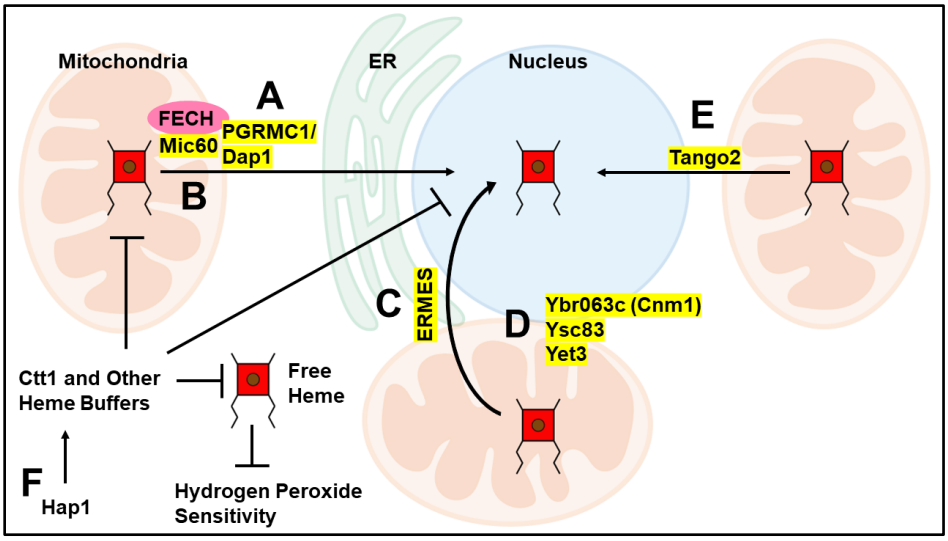

Figure 30 – Comprehensive model of studied heme trafficking pathways and proteins discussed in this thesis. Heme metabolon interacting proteins Dap1 **(A)** and Mic60 **(B)** affect nuclear heme trafficking and are complemented by mammalian homologs and heme synthesis, respectively. Membrane contact sites between the mitochondria and ER (ERMES, **C**) facilitated nuclear heme trafficking. **(D)** Ybr063c, Ysc83, and Yet3 mitochondria-nuclear tether proteins do not affect heme trafficking. **(E)** Tango2 facilitates mitochondria heme export and nuclear heme trafficking. **(F)** Hap1 regulates cell-wide labile heme through its ability to control gene expression of heme buffering proteins, including catalase. **(G)** Without these heme buffers, there is an increase in the amount of labile heme which serves a protective role against hydrogen peroxide toxicity.

APPENDIX A. SUPPLEMENTAL METHODS, TABLES AND FIGURES

A.1 Chapter 2

A.1.1 Yeast Strains used in Chapter 2

Table A1. List of *Saccharomyces cerevisiae* strains and plasmids used in Chapter 2

Strain	Cell Type	Plasmid Names	Plasmid Construction
DH018	BY4741 WT	pDH013	p415-GPD-HS1
DH106	BY4741 WT	NA	P415-GPD-HS1-M7A-NLS
DH071	BY4741 WT	pDH046	p415-GPD-HS1-NLS
DH072	BY4741 *hem1::HIS3*	pDH046	p415-GPD-HS1-NLS
RH021	BY4741 WT	pRH021	p415-GPD-HS1-M7A
RH027	BY4741 *hem1::HIS3*	pRH021	p415-GPD-HS1-M7A
DH013	BY4741 *hem1::HIS3*	pDH013	p415-GPD-HS1
OM168	BY4741 WT	pAR1046	p415-GPD-MITO-HS1
OM169	BY4741 hem1::HIS3	pAR1046	p415-GPD-MITO-HS1
WT EV	BY4741 WT	p415-GPD	EV
MW018	BY4741 *mic60::KanMX4*	pDH013	p415-GPD-HS1
MW019	BY4741 *mic60::KanMX4*	pAR1046	p415-GPD-MITO-HS1
MW020	BY4741 *mic60::KanMX4*	pDH046	p415-GPD-HS1-NLS
MW021	BY4741 *mic60::KanMX4*	pRH021	p415-GPD-HS1-M7A
MW022	BY4741 *mic60::KanMX4*	pCM016-4	p415-GPD-MITO-HS1-M7A
MW023	BY4741 *mic60::KanMX4*	NA	p415-GPD-HS1-M7A-NLS
MW034	W303 WT	pRS425; p413-GPD	EV; EV
MW035	W303 *mic60::URA*	NA; pMW006	pRS425-Hem15pr-HEM15; p413-GPD-MITO-HS1
MW036	W303 WT	NA; pMW006	pRS425-Hem15pr-HEM15; p413-GPD-MITO-HS1

Table A1 Continued

MW037	W303 *mic60::URA*	pRS425; pMW006	EV; p413-GPD-MITO-HS1
MW038	W303 WT	pRS425; pMW006	EV; p413-GPD-MITO-HS1
MW039	W303 *mic60::URA*	pRS425; p413-GPD	EV; EV
MW040	W303 *mic60::URA*	NA; pMW004	pRS425-Hem15pr-HEM15; p413-GPD-HS1
MW042	W303 WT	NA; pMW004	pRS425-Hem15pr-HEM15; p413-GPD-HS1
MW044	W303 *mic60::URA*	pRS425; pMW004	EV; p413-GPD-HS1
MW046	W303 WT	pRS425; pMW004	EV; p413-GPD-HS1
mic60Δ	BY4741 *mic60::KanMX4*	None	
WT	BY4741 WT	None	
MW164	BY4741 WT	pDH013; pMW011-2	p415-GPD-HS1; p413-GPD-HA-DAP1
MW166	BY4741 WT	pDH046; pMW011-2	p415-GPD-HS1-NLS; p413-GPD-HA-DAP1
MW167	BY4741 *dap1::KanMX4* clone 1	pDH013; pMW011-2	p415-GPD-HS1; p413-GPD-HA-DAP1
MW168	BY4741 *dap1::KanMX4* clone 1	pDH046; pMW011-2	p415-GPD-HS1-NLS; p413-GPD-HA-DAP1
MW170	BY4741 WT	pDH013; pMW010-2	p415-GPD-HS1; p413-GPD-HA-PGRMC1
MW172	BY4741 WT	pDH046; pMW010-2	p415-GPD-HS1-NLS; p413-GPD-HA-PGRMC1
MW173	BY4741 *dap1::KanMX4* clone 1	pDH013; pMW010-2	p415-GPD-HS1; p413-GPD-HA-PGRMC1
MW174	BY4741 *dap1::KanMX4* clone 1	pDH046; pMW010-2	p415-GPD-HS1-NLS; p413-GPD-HA-PGRMC1
MW613	BY4741 *dap1::KanMX4* clone 1	pMW016-2	p415-GPD-MITO-HS1
MW616	BY4741 *dap1::KanMX4* clone 1	p415-GPD	EV

Table A1 Continued

MW617	BY4741 *dap1::KanMX4* clone 2	pMW016-2	p415-GPD-MITO-HS1
MW620	BY4741 *dap1::KanMX4* clone 2	p415-GPD	EV
DH001b-3	BY4741 *hem1::HIS3*	None	
MW077-1a	BY4741 ybr063c*::NAT*	pDH013	p415-GPD-HS1
MW078-1A	BY4741 ybr063c*::NAT*	pRH021	p415-GPD-HS1-M7A
MW079-1a	BY4741 ybr063c*::NAT*	pAR1046	p415-GPD-MITO-HS1
MW080-1a	BY4741 ybr063c*::NAT*	pCM016-4	p415-GPD-MITO-HS1-M7A
MW081-1a	BY4741 ybr063c*::NAT*	pDH046	p415-GPD-HS1-NLS
MW082-1a	BY4741 ybr063c*::NAT*	NA	p415-GPD-HS1-M7A-NLS
MW083-1a	BY4741 ybr063c *OE*	pDH013	p415-GPD-HS1
MW083-1a	BY4741 ybr063c *OE*	pRH021	p415-GPD-HS1-M7A
MW085-1a	BY4741 ybr063c *OE*	pAR1046	p415-GPD-MITO-HS1
MW086-1a	BY4741 ybr063c *OE*	pCM016-4	p415-GPD-MITO-HS1-M7A
MW087-1a	BY4741 ybr063c *OE*	pDH046	p415-GPD-HS1-NLS
MW088-1a	BY4741 ybr063c *OE*	NA	p415-GPD-HS1-M7A-NLS
MW089-1a	BY4741 WT from Maya Schuldiner	pDH013	p415-GPD-HS1
MW090-1a	BY4741 WT from Maya Schuldiner	pRH021	p415-GPD-HS1-M7A
MW091-1a	BY4741 WT from Maya Schuldiner	pAR1046	p415-GPD-MITO-HS1
MW092-1a	BY4741 WT from Maya Schuldiner	pCM016-4	p415-GPD-MITO-HS1-M7A
MW093-1a	BY4741 WT from Maya Schuldiner	pDH046	p415-GPD-HS1-NLS
MW094-1a	BY4741 WT from Maya Schuldiner	NA	p415-GPD-HS1-M7A-NLS

Table A1 Continued

MW095-1	BY4741 WT from Maya Schuldiner	p415-GPD	EV
MW100-1a	BY4741 yet3*::NAT*	pDH013	p415-GPD-HS1
MW101-1a	BY4741 yet3*::NAT*	pRH021	p415-GPD-HS1-M7A
MW102-1a	BY4741 yet3*::NAT*	pAR1046	p415-GPD-MITO-HS1
MW103-1a	BY4741 yet3*::NAT*	pCM016-4	p415-GPD-MITO-HS1-M7A
MW104-1a	BY4741 yet3*::NAT*	pDH046	p415-GPD-HS1-NLS
MW105-1a	BY4741 yet3*::NAT*	NA	p415-GPD-HS1-M7A-NLS
MW106-1a	BY4741 yet3 *OE*	pDH013	p415-GPD-HS1
MW107-1a	BY4741 yet3 *OE*	pRH021	p415-GPD-HS1-M7A
MW108-1a	BY4741 yet3 *OE*	pAR1046	p415-GPD-MITO-HS1
MW109-1a	BY4741 yet3 *OE*	pCM016-4	p415-GPD-MITO-HS1-M7A
MW110-1a	BY4741 yet3 *OE*	pDH046	p415-GPD-HS1-NLS
MW111-1a	BY4741 yet3 *OE*	NA	p415-GPD-HS1-M7A-NLS
MW112-1a	BY4741 ysc833*::NAT*	pDH013	p415-GPD-HS1
MW113-1a	BY4741 ysc833*::NAT*	pRH021	p415-GPD-HS1-M7A
MW114-1a	BY4741 ysc833*::NAT*	pAR1046	p415-GPD-MITO-HS1
MW115-1a	BY4741 ysc833*::NAT*	pCM016-4	p415-GPD-MITO-HS1-M7A
MW116-1a	BY4741 ysc833*::NAT*	pDH046	p415-GPD-HS1-NLS
MW117-1a	BY4741 ysc833*::NAT*	NA	p415-GPD-HS1-M7A-NLS
MW118-1a	BY4741 ysc833 *OE*	pDH013	p415-GPD-HS1
MW119-1a	BY4741 ysc833 *OE*	pRH021	p415-GPD-HS1-M7A
MW120-1a	BY4741 ysc833 *OE*	pAR1046	p415-GPD-MITO-HS1
MW121-1a	BY4741 ysc833 *OE*	pCM016-4	p415-GPD-MITO-HS1-M7A
MW122-1a	BY4741 ysc833 *OE*	pDH046	p415-GPD-HS1-NLS
MW123-1a	BY4741 ysc833 *OE*	NA	p415-GPD-HS1-M7A-NLS
MW005-1	BY4741 *tango2::KanMX4*	pOM003	p415-CYC1-eGFP
MW006-1	BY4741 *tango2::KanMX4*	pDH013	p415-GPD-HS1
MW007-1	BY4741 *tango2::KanMX4*	pDH046	p415-GPD-HS1-NLS

Table A1 Continued

MW008-1	BY4741 *tango2::KanMX4*	pAR1046	p415-GPD-MITO-HS1
MW009-1a	BY4741 *tango2::KanMX4*	pRH021	p415-GPD-HS1-M7A
MW010-1a	BY4741 *tango2::KanMX4*	pCM016-4	p415-GPD-MITO-HS1-M7A
MW011-1a	BY4741 *tango2::KanMX4*	NA	p415-GPD-HS1-M7A-NLS
tango2Δ	BY4741 *tango2::KanMX4*	None	
mic60 Δ	BY4741 *mic60::KanMX4*	None	

A.2 Chapter 3

A.2.1 Yeast Strains used in Chapter 3

Table A2. List of *Saccharomyces cerevisiae* strains and plasmids used in Chapter 3

Strain	Cell Type	Plasmid Names	Plasmid Construction
DH018	BY4741 WT	pDH013	p415-GPD-HS1
DH106	BY4741 WT	NA	P415-GPD-HS1-M7A-NLS
DH071	BY4741 WT	pDH046	p415-GPD-HS1-NLS
DH072	BY4741 *hem1::HIS3*	pDH046	p415-GPD-HS1-NLS
RH021	BY4741 WT	pRH021	p415-GPD-HS1-M7A
RH027	BY4741 *hem1::HIS3*	pRH021	p415-GPD-HS1-M7A
DH013	BY4741 *hem1::HIS3*	pDH013	p415-GPD-HS1
OM168	BY4741 WT	pAR1046	p415-GPD-MITO-HS1
OM169	BY4741 *hem1::HIS3*	pAR1046	p415-GPD-MITO-HS1
WT EV	BY4741 WT	p415-GPD	EV
WT	BY4741 WT	None	
DH001b-3	BY4741 *hem1::HIS3*	None	
MW530	BY4741 *rpl8a::KanMX4*	p415-GPD	EV

Table A2. Continued

MW534	BY4741 *rpl8a::KanMX4*	p415-GPD; 413-GPD	EV; EV
MW231	BY4741 *rpl8a::KanMX4*	pDH046; pMW023	p415-GPD-HS1-NLS; p413-GPD-RPL8A
MW232	BY4741 *rpl8a::KanMX4*	pDH046; p413-GPD	p415-GPD-HS1-NLS; EV
MW250	BY4741 *rpl8a::KanMX4*	pDH046; pMW023	p415-GPD-HS1-NLS; p413-TEF-RPL8A
MW313	BY4741 *bmh2::KanMX4*	p415-GPD	EV
MW405	BY4741 *bmh2::KanMX4*	pDH046; pMW042	p415-GPD-HS1-NLS; p413-TEF-BMH2-HA
MW408	BY4741 *bmh2::KanMX4*	pDH046; pMW043	p415-GPD-HS1-NLS; p413-GPD-BMH2-HA
MW446	BY4741 *bmh2::KanMX4*	p415-GPD; 413-GPD	EV; EV
WT BKOC-4	BY4741 *bmh2::KanMX4*, NEW	None	
WT BKOC-6	BY4741 *bmh2::KanMX4*, NEW	None	
WT BKOC-8	BY4741 *bmh2::KanMX4*, NEW	None	
MW514	BY4741 *bmh2::KanMX4*, NEW, cl. 4	pDH046	p415-GPD-HS1-NLS
MW515	BY4741 *bmh2::KanMX4*, NEW, cl. 4	p415-GPD	EV
MW516	BY4741 *bmh2::KanMX4*, NEW, cl. 6	pDH046	p415-GPD-HS1-NLS
MW518	BY4741 *bmh2::KanMX4*, NEW, cl. 6	p415-GPD	EV
MW519	BY4741 *bmh2::KanMX4*, NEW, cl. 8	pDH046	p415-GPD-HS1-NLS
MW521	BY4741 *bmh2::KanMX4*, NEW, cl. 8	p415-GPD	EV
MW529	BY4741 *arv1::KanMX4*	p415-GPD	EV

Table A2. Continued

MW533	BY4741 *arv1::KanMX4*	p415-GPD; 413-GPD	EV; EV
MW192	BY4741 *arv1::KanMX4*	pDH046; pMW014	p415-GPD-HS1-NLS; p413-GPD-ARV1-HA
MW195	BY4741 *arv1::KanMX4*	pDH046; pMW015	p415-GPD-HS1-NLS; p413-TEF-ARV1-HA
MW227	BY4741 *aim11::KanMX4*	pDH046; pMW022	p415-GPD-HS1-NLS; p413-GPD-AIM11
MW228	BY4741 *aim11::KanMX4*	pDH046; p413-GPD-EV	p415-GPD-HS1-NLS; EV
MW248	BY4741 *aim11::KanMX4*	pDH046; pMW029	p415-GPD-HS1-NLS; p413-TEF-AIM11
MW532	BY4741 *aim11::KanMX4*	p415-GPD; 413-GPD	EV; EV
MW222	BY4741 *bmh2::KanMX4*	pDH046; p413-GPD-EV	p415-GPD-HS1-NLS; EV
MW253	BY4741 *aac3::KanMX4*	pDH046; pMW026	p415-GPD-HS1-NLS; p413-GPD-AAC3
MW256	BY4741 *aac3::KanMX4*	pDH046; p413-GPD-EV	p415-GPD-HS1-NLS; EV
MW259	BY4741 *aac3::KanMX4*	pDH046; pMW027	p415-GPD-HS1-NLS; p413-TEF-AAC3
MW508	BY4741 *put3::KanMX4*	p415-GPD	EV
MW510	BY4741 *put3::KanMX4*	p415-GPD; 413-GPD	EV; EV
MW703	BY4741 *put3::KanMX4*, NEW, cl. 1	pDH046	p415-GPD-HS1-NLS
MW704	BY4741 *put3::KanMX4*, NEW, cl. 2	pDH046	p415-GPD-HS1-NLS
MW705	BY4741 *put3::KanMX4*, NEW, cl. 3	pDH046	p415-GPD-HS1-NLS
MW706	BY4741 *put3::KanMX4*, NEW, cl. 1	p415-GPD	EV
MW707	BY4741 *put3::KanMX4*, NEW, cl. 2	p415-GPD	EV
MW708	BY4741 *put3::KanMX4*, NEW, cl. 3	p415-GPD	EV

MW237	BY4741 *put3::KanMX4*	pDH046; pMW024	p415-GPD-HS1-NLS; p413-GPD-PUT3
MW238	BY4741 *put3::KanMX4*	pDH046; p413-GPD-EV	p415-GPD-HS1-NLS; EV
MW262	BY4741 *put3::KanMX4*	pDH046; pMW031	p415-GPD-HS1-NLS; p413-TEF-PUT3
MW696	BY4741 WT	pDH046; p413-GPD-EV; p416-GPD-EV; pRS411-EV	p415-GPD-HS1-NLS; EV; EV; EV
MW697	BY4741 *put3::KanMX4*, cl. 1	pDH046; pMW024; p416-GPD-EV; pRS411-EV	pDH046; p415-GPD-PUT3; EV; EV
MW698	BY4741 *put3::KanMX4*, cl. 1	pDH046; p413-GPD-EV; p416-GPD-EV; pRS411-EV	p415-GPD-HS1-NLS; EV; EV; EV
MW699	BY4741 *put3::KanMX4*, cl. 2	pDH046; pMW024; p416-GPD-EV; pRS411-EV	pDH046; pMW024; EV; EV
MW700	BY4741 *put3::KanMX4*, cl. 2	pDH046; p413-GPD-EV; p416-GPD-EV; pRS411-EV	p415-GPD-HS1-NLS; EV; EV; EV
MW694	BY4741 *put3::KanMX4*, cl. 1	p415-GPD-EV; p413-GPD-EV; p416-GPD-EV; pRS411-EV	EV; EV; EV; EV
MW695	BY4741 WT	p415-GPD-EV; p413-GPD-EV; p416-GPD-EV; pRS411-EV	EV; EV; EV; EV
MW736	BY4741 *put3::KanMX4*, NEW, cl. 1	pDH046; pMW024; p416-GPD-EV; pRS411-EV	pDH046; p415-GPD-PUT3; EV; EV
MW737	BY4741 *put3::KanMX4*, NEW, cl. 1	pDH046; p413-GPD-EV; p416-GPD-EV; pRS411-EV	p415-GPD-HS1-NLS; EV; EV; EV
MW738	BY4741 *put3::KanMX4*, NEW, cl. 1	p415-GPD-EV; p413-GPD-EV; p416-GPD-EV; pRS411-EV	EV; EV; EV; EV

Table A2. Continued

MW739	BY4741 *put3::KanMX4*, cl. 2	pDH046; pMW024; p416-GPD-EV; pRS411-EV	pDH046; p415-GPD-PUT3; EV; EV
MW740	BY4741 *put3::KanMX4*, cl. 2	pDH046; p413-GPD-EV; p416-GPD-EV; pRS411-EV	p415-GPD-HS1-NLS; EV; EV; EV
MW741	BY4741 *put3::KanMX4*, cl. 2	p415-GPD-EV; p413-GPD-EV; p416-GPD-EV; pRS411-EV	
MW296	BY4741 *ldb7::KanMX4*	pDH046; pMW032	p415-GPD-HS1-NLS; p413-TEF-LDB7
MW299	BY4741 *ldb7::KanMX4*	pDH046; pMW033	p415-GPD-HS1-NLS; p413-GPD-LDB7
MW302	BY4741 *ldb7::KanMX4*	pDH046; p413-GPD-EV	p415-GPD-HS1-NLS; EV
MW507	BY4741 *ldb7::KanMX4*	p415-GPD-EV	EV
MW509	BY4741 *ldb7::KanMX4*	p415-GPD-EV; p413-GPD-EV	EV; EV

A.3 Chapter 4

A.3.1 Yeast Strains used in Chapter 4

Table A3. List of *Saccharomyces cerevisiae* strains and plasmids used in Chapter 4

Strain	Cell Type	Plasmid Names	Plasmid Construction
DH018	BY4741 WT	pDH013	p415-GPD-HS1
DH106	BY4741 WT	NA	P415-GPD-HS1-M7A-NLS
DH071	BY4741 WT	pDH046	p415-GPD-HS1-NLS
DH072	BY4741 *hem1::HIS3*	pDH046	p415-GPD-HS1-NLS
RH021	BY4741 WT	pRH021	p415-GPD-HS1-M7A
RH027	BY4741 *hem1::HIS3*	pRH021	p415-GPD-HS1-M7A
DH013	BY4741 *hem1::HIS3*	pDH013	p415-GPD-HS1
JA110	BY4741 WT	pJA010	p415-GPD-HS1-M7A-H102A

Table A3. Continued

JA210	BY4741 *hem1::HIS3*	pJA010	p415-GPD-HS1-M7A-H102A
CM023	BY4741 WT	pCM009	p415-GPD-HS1-M7A-H102A-NLS
CM034	BY4741 *hem1::HIS3*	pCM009	p415-GPD-HS1-M7A-H102A-NLS
MW306	BY4741 WT	pAF001-3	p415-GPD-HS1-M7A-H102A-MITO
MW307	BY4741 WT	pAF003-4	p415-GPD-HS1-M7A-H102A-MITO
MW239	BY4741 *hem1::HIS3*	pAF001-3	p415-GPD-HS1-M7A-H102A-MITO
MW240	BY4741 *hem1::HIS3*	pAF003-4	p415-GPD-HS1-M7A-H102A-MITO
WT EV	BY4741 WT	p415-GPD	EV
WT	BY4741 WT	None	
FY2607	BY4741 *ty hap1*	None	
FY2609	BY4741 HAP1	None	
FY2611	BY4741 *hap1::KanMX4*	None	
FY2613	BY4741 *MYC-HAP1*	None	
MW488	BY4741 *ty hap1*	pDH013	p415-GPD-HS1
MW490	BY4741 *ty hap1*	p415-GPD-EV	EV
MW742	BY4741 *ty hap1*	pMW003-1	p415-CYC1-UAS1-UAS2-EGFP
MW746	BY4741 *ty hap1*	pDH046	p415-GPD-HS1-NLS
MW747	BY4741 *ty hap1*	NA	p415-GPD-HS1-M7A-NLS
MW748	BY4741 *ty hap1*	pCM009	p415-GPD-HS1-M7A-H102A-NLS (bisALA)
MW758	BY4741 *ty hap1*	pRH021	p415-GPD-HS1-M7A
MW759-2	BY4741 *ty hap1*	pJA010	p415-GPD-HS1-M7A-H102A (bisALA)
MW760	BY4741 *ty hap1*	pMW016-2	p415-GPD-MITO-HS1
MW771	BY4741 *hem1::HIS3*	pMW003-1; pMK002-1	p415-CYC1-UAS1-UAS2-EGFP; pRS316-hmr2pro-MKATE2-hmg2term
MW773	BY4741 *ty hap1*	pMW003-1; pMK002-1	p415-CYC1-UAS1-UAS2-EGFP; pRS316-hmr2pro-MKATE2-hmg2term
MW777	BY4741 *ty hap1*	p415-GPD-EV; pRS16-EV	EV; EV
MW778	BY4741 *ty hap1*	pAF001-3	p415-GPD-MITO-HS1-M7A

Table A3. Continued

MW779	BY4741 *ty hap1*	pAF003-4	p415-GPD-MITO-HS1-M7A-H102A (bisALA)
MW962	BY4741 HAP1	pRH021; pDH039	p415-GPD-HS1-M7A; p316-GALpro-Cytochrome b562
MW961	BY4741 HAP1	pRH021; p316-GALpro-EV	p415-GPD-HS1-M7A; EV
MW963	BY4741 *hap1::KanMX4*	pRH021; p316-GALpro-EV	p415-GPD-HS1-M7A; EV
MW964	BY4741 *hap1::KanMX4*	pRH021; pDH039	p415-GPD-HS1-M7A; p316-GALpro-Cytochrome b562
MW965	BY4741 HAP1	NA; p316-GALpro-EV	p415-GPD-HS1-M7A-NLS
MW966	BY4741 HAP1	NA; pDH039	p415-GPD-HS1-M7A-NLS; p316-GALpro-Cytochrome b562
MW967	BY4741 *hap1::KanMX4*	NA; p316-GALpro-EV	p415-GPD-HS1-M7A-NLS; EV
MW968	BY4741 *hap1::KanMX4*	NA; pDH039	p415-GPD-HS1-M7A-NLS; p316-GALpro-Cytochrome b562
MW491	BY4741 HAP1	pDH013	p415-GPD-HS1
MW493	BY4741 HAP1	p415-GPD-EV	EV
MW749	BY4741 HAP1	pDH046	p415-GPD-HS1-NLS
MW750	BY4741 HAP1	NA	p415-GPD-HS1-M7A-NLS
MW751	BY4741 HAP1	pCM009	p415-GPD-HS1-M7A-H102A-NLS (bisALA)
MW761	BY4741 HAP1	pRH021	p415-GPD-HS1-M7A
MW762	BY4741 HAP1	pJA010	p415-GPD-HS1-M7A-H102A (bisALA)
MW763	BY4741 HAP1	pMW016-2	p415-GPD-MITO-HS1
MW774	BY4741 HAP1	pMW003-1; pMK002-1	p415-CYC1-UAS1-UAS2-EGFP; pRS316-hmr2pro-MKATE2-hmg2term
MW780	BY4741 HAP1	pAF001-3	p415-GPD-MITO-HS1-M7A
MW781	BY4741 HAP1	pAF003-4	p415-GPD-MITO-HS1-M7A-H102A (bisALA)
MW961	BY4741 HAP1	pRH021; p316-GALpro-EV	p415-GPD-HS1-M7A; EV

Table A3. Continued

MW962	BY4741 HAP1	pRH021; pDH039	p415-GPD-HS1-M7A; p316-GALpro-Cytochromeb562
MW965	BY4741 HAP1	NA; p316-GALpro-EV	p415-GPD-HS1-M7A-NLS
MW966	BY4741 HAP1	NA; pDH039	p415-GPD-HS1-M7A-NLS; p316-GALpro-Cytochrome b562
MW969	BY4741 HAP1	p415-GPD-EV; p316-GALpro-EV	EV; EV
MW494	BY4741 *hap1::KanMX4*	pDH013	p415-GPD-HS1
MW446	BY4741 *hap1::KanMX4*	p415-GPD-EV	EV
MW744	BY4741 *hap1::KanMX4*	pMW003-1	p415-CYC1-UAS1-UAS2-EGFP
MW743	BY4741 HAP1	pMW003-1	p415-CYC1-UAS1-UAS2-EGFP
MW752	BY4741 *hap1::KanMX4*	pDH046	p415-GPD-HS1-NLS
MW753	BY4741 *hap1::KanMX4*	NA	p415-GPD-HS1-M7A-NLS
MW754	BY4741 *hap1::KanMX4*	pCM009	p415-GPD-HS1-M7A-H102A-NLS (bisALA)
MW764	BY4741 *hap1::KanMX4*	pRH021	p415-GPD-HS1-M7A
MW765	BY4741 *hap1::KanMX4*	pJA010	p415-GPD-HS1-M7A-H102A (bisALA)
MW766	BY4741 *hap1::KanMX4*	pMW016-2	p415-GPD-MITO-HS1
MW775-2	BY4741 *hap1::KanMX4*	pMW003-1; pMK002-1	p415-CYC1-UAS1-UAS2-EGFP; pRS316-hmr2pro-MKATE2-hmg2term
MW782-2	BY4741 *hap1::KanMX4*	pAF001-3	p415-GPD-MITO-HS1-M7A
MW783	BY4741 *hap1::KanMX4*	pAF003-4	p415-GPD-MITO-HS1-M7A-H102A (bisALA)
MW963	BY4741 *hap1::KanMX4*	pRH021; p316-GALpro-EV	p415-GPD-HS1-M7A; EV
MW964	BY4741 *hap1::KanMX4*	pRH021; pDH039	p415-GPD-HS1-M7A; p316-GALpro-Cytochrome b562

Table A3. Continued

MW967	BY4741 *hap1::KanMX4*	NA; p316-GALpro-EV	p415-GPD-HS1-M7A-NLS; EV
MW968	BY4741 *hap1::KanMX4*	NA; pDH039	p415-GPD-HS1-M7A-NLS; p316-GALpro-Cytochrome b562
MW970	BY4741 *hap1::KanMX4*	p415-GPD-EV; p316-GALpro-EV	EV; EV
MW873	BY4741 *hap1::KanMX4*	pYes2-(URA)-EV	EV
MW874	BY4741 *hap1::KanMX4*	pHAP1 (URA)	pYes2-Hap1pro-HAP1
MW875	BY4741 *hap1::KanMX4*	pHap1-18 (URA)	pYes2-Hap1pro-hap1-18
MW876	BY4741 *hap1::KanMX4*	pKpnF	pYes2-Hap1-pro-Hap1-1-1308
MW904	BY4741 *hap1::KanMX4*	pDH046; pYes2-(URA)-EV	p415-GPD-HS1-NLS; EV
MW905	BY4741 *hap1::KanMX4*	pDH046; pHAP1 (URA)	p415-GPD-HS1-NLS; pYes2-Hap1pro-HAP1
MW906	BY4741 *hap1::KanMX4*	pDH046; pHap1-18 (URA)	p415-GPD-HS1-NLS; pYes2-Hap1pro-hap1-18
MW907	BY4741 *hap1::KanMX4*	NA; pYes2-(URA)-EV	p415-GPD-HS1-M7A-NLS; EV
MW908	BY4741 *hap1::KanMX4*	NA; pHAP1 (URA)	p415-GPD-HS1-M7A-NLS; pYes2-Hap1pro-HAP1
MW909	BY4741 *hap1::KanMX*4	NA; pHap1-18 (URA)	p415-GPD-HS1-M7A-NLS; pYes2-Hap1pro-hap1-18
MW910	BY4741 *hap1::KanMX4*	pCM009; pYes2-(URA)-EV	p415-GPD-HS1-M7A-H102A-NLS (bisALA); EV
MW911	BY4741 *hap1::KanMX4*	pCM009; pHAP1 (URA)	p415-GPD-HS1-M7A-H102A-NLS (bisALA); pYes2-Hap1pro-HAP1
MW912	BY4741 *hap1::KanMX4*	pCM009; pHap1-18 (URA)	p415-GPD-HS1-M7A-H102A-NLS (bisALA); pYes2-Hap1pro-hap1-18
MW929	BY4741 *hap1::KanMX4*	NA; pKpnF	p415-GPD-HS1-M7A-NLS; pYes2-Hap1-pro-Hap1-1-1308

Table A3. Continued

MW930	BY4741 *hap1::KanMX4*	pCM009; pKpnF	p415-GPD-HS1-M7A-H102A-NLS (bisALA); pYes2-Hap1-pro-Hap1-1-1308
MW943	BY4741 *hap1::KanMX4*	NA; ΔBeBam	p415-GPD-HS1-M7A-NLS; pYes2-Hap1-pro-Hap1 excluding 244-444
MW944	BY4741 *hap1::KanMX4*	NA; ΔBeBam	p415-GPD-HS1-M7A-H102A-NLS (bisALA); pYes2-Hap1-pro-Hap1 excluding 244-444
MW945	BY4741 *hap1::KanMX4*	NA; Bam-KpnF	p415-GPD-HS1-M7A-NLS; pYes2-Hap1-pro-Hap1 excluding 444-1308
MW946	BY4741 *hap1::KanMX4*	NA; Bam-KpnF	p415-GPD-HS1-M7A-H102A-NLS (bisALA); pYes2-Hap1-pro-Hap1 excluding 444-1308
MW947	BY4741 *hap1::KanMX4*	NA; Bam	p415-GPD-HS1-M7A-NLS; pYes2-Hap1-pro-Hap-1-444
MW948	BY4741 *hap1::KanMX4*	NA; Bam	p415-GPD-HS1-M7A-H102A-NLS (bisALA); pYes2-Hap1-pro-Hap1-1-444
MW949	BY4741 *hap1::KanMX4*	NA; BglF	p415-GPD-HS1-M7A-NLS; pYes2-Hap1-pro-Hap-1-746
MW950	BY4741 *hap1::KanMX4*	NA; BglF	p415-GPD-HS1-M7A-H102A-NLS (bisALA); pYes2-Hap1-pro-Hap1-1-746
MW902	BY4741 HAP1	NA; pYes2-(URA)-EV	p415-GPD-HS1-M7A-NLS; EV
MW903	BY4741 HAP1	pCM009; pYes2-(URA)-EV	p415-GPD-HS1-M7A-H102A-NLS (bisALA); EV
MW951	BY4741 *hmx1::KanMX4*	pDH046; pYes2-(URA)-EV	p415-GPD-HS1-NLS; EV
MW952	BY4741 *hmx1::KanMX4*	NA; pYes2-(URA)-EV	p415-GPD-HS1-M7A-NLS; EV
MW953	BY4741 *hmx1::KanMX4*	pCM009; pYes2-(URA)-EV	p415-GPD-HS1-M7A-H102A-NLS (bisALA); EV

Table A3. Continued

MW954	BY4741 *hmx1::KanMX4*	pDH046; pHAP1 (URA)	p415-GPD-HS1-NLS; pYes2-Hap1pro-HAP1
MW955	BY4741 *hmx1::KanMX4*	NA; pHAP1 (URA)	p415-GPD-HS1-M7A-NLS; pYes2-Hap1pro-HAP1
MW956	BY4741 *hmx1::KanMX4*	pCM009; pHAP1 (URA)	p415-GPD-HS1-M7A-H102A-NLS (bisALA); pYes2-Hap1pro-HAP1
MW960	BY4741 *hmx1::KanMX4*	p415-GPD-EV; pYes2-(URA)-EV	EV; EV
MW971	BY4741 *ctt1::KanMX4*	pDH046; pYes2-(URA)-EV	p415-GPD-HS1-NLS; EV
MW972	BY4741 *ctt1::KanMX4*	NA; pYes2-(URA)-EV	p415-GPD-HS1-M7A-NLS; EV
MW973	BY4741 *ctt1::KanMX4*	pCM009; pYes2-(URA)-EV	p415-GPD-HS1-M7A-H102A-NLS (bisALA); EV
MW974	BY4741 *ctt1::KanMX4*	pDH046; pHAP1 (URA)	p415-GPD-HS1-NLS; pYes2-Hap1pro-HAP1
MW975	BY4741 *ctt1::KanMX4*	NA; pHAP1 (URA)	p415-GPD-HS1-M7A-NLS; pYes2-Hap1pro-HAP1
MW976	BY4741 *ctt1::KanMX4*	pCM009; pHAP1 (URA)	p415-GPD-HS1-M7A-H102A-NLS (bisALA); pYes2-Hap1pro-HAP1
MW980	BY4741 *ctt1::KanMX4*	p415-GPD-EV; pYes2-(URA)-EV	EV; EV
MW981	BY4741 *ctt1::KanMX4*	pDH046	p415-GPD-HS1-NLS
MW982	BY4741 *ctt1::KanMX4*	NA	p415-GPD-HS1-M7A-NLS
MW983	BY4741*ctt1::KanMX4*	pCM009	p415-GPD-HS1-M7A-H102A-NLS (bisALA)
MW984	BY4741 *ctt1::KanMX4*	p415-GPD-EV	EV
MW832	BY4741 *yhb1::KanMX4*	p415-GPD-EV	EV
MW913	BY4741 *yhb1::KanMX4*	pDH046; pYes2-(URA)-EV	p415-GPD-HS1-NLS; EV

Table A3. Continued

MW914-1	BY4741 *yhb1:: KanMX4*	NA; pYes2-(URA)-EV	p415-GPD-HS1-M7A-NLS; EV
MW915-1	BY4741 *yhb1:: KanMX4*	pCM009; pYes2-(URA)-EV	p415-GPD-HS1-M7A-H102A-NLS (bisALA); EV
MW916-1	BY4741 *yhb1:: KanMX4*	pDH046; pHAP1 (URA)	p415-GPD-HS1-NLS; pYes2-Hap1pro-HAP1
MW917-1	BY4741 *yhb1:: KanMX4*	NA; pHAP1 (URA)	p415-GPD-HS1-M7A-NLS; pYes2-Hap1pro-HAP1
MW918-1	BY4741 *yhb1:: KanMX4*	pCM009; pHAP1 (URA)	p415-GPD-HS1-M7A-H102A-NLS (bisALA); pYes2-Hap1pro-HAP1
MW919-1	BY4741 WT	pDH046; pYes2-(URA)-EV	p415-GPD-HS1-NLS; EV
MW920-1	BY4741 WT	NA; pYes2-(URA)-EV	p415-GPD-HS1-M7A-NLS; EV
MW921-2	BY4741 WT	pCM009; pYes2-(URA)-EV	p415-GPD-HS1-M7A-H102A-NLS (bisALA); EV
MW922-1	BY4741 WT	pDH046; pHAP1 (URA)	p415-GPD-HS1-NLS; pYes2-Hap1pro-HAP1
MW923-1	BY4741 WT	NA; pHAP1 (URA)	p415-GPD-HS1-M7A-NLS; pYes2-Hap1pro-HAP1
MW923-2	BY4741 WT	pCM009; pHAP1 (URA)	p415-GPD-HS1-M7A-H102A-NLS (bisALA); pYes2-Hap1pro-HAP1
MW925-1	BY4741 *hem1::HIS3*	pDH046; pYes2-(URA)-EV	p415-GPD-HS1-NLS; EV
MW926-1	BY4741 *hem1::HIS3*	NA; pYes2-(URA)-EV	p415-GPD-HS1-M7A-NLS; EV
MW926-2	BY4741 *hem1::HIS3*	pCM009; pYes2-(URA)-EV	p415-GPD-HS1-M7A-H102A-NLS (bisALA); EV
MW989	BY4741 *tdh3::KanMX4*	NA	p415-GPD-HS1-M7A-NLS
MW991	BY4741 *tdh3::KanMX4*	p415-GPD-EV	EV
MW1006	BY4741 *ctt1::KanMX4*	pDH013	p415-GPD-HS1

Table A3. Continued

MW1007	BY4741 *ctt1::KanMX4*	pRH021	p415-GPD-HS1-M7A
MW1009	BY4741 *ctt1::KanMX4*	pMW016-2	p415-GPD-MITO-HS1
MW1010	BY4741 *ctt1::KanMX4*	pAF001-3	p415-GPD-MITO-HS1-M7A
MW1012	BY4741 *tdh3::KanMX4*	pAF001-3	p415-GPD-MITO-HS1-M7A
MW1022	BY4741 *tdh3::KanMX4*	pMW016-2	p415-GPD-MITO-HS1
MW1015-1	BY4741 *ctt1::KanMX4*	NA; pOM005-1	p415-GPD-HS1-M7A-NLS; Tdh3 deletion plasmid (HIS)
MW1015-4	BY4741 *ctt1::KanMX4*	NA; pOM005-1	p415-GPD-HS1-M7A-NLS; Tdh3 deletion plasmid (HIS)
MW1021-1	BY4741 *ctt1::KanMX4*	p415-GPD-EV; pOM005-1	EV; Tdh3 deletion plasmid (HIS)
MW1021-2	BY4741 *ctt1::KanMX4*	p415-GPD-EV; pOM005-1	EV; Tdh3 deletion plasmid (HIS)
OM040	BY4741 *tdh3::KanMX4*	pDH046	p415-GPD-HS1-NLS

A.4 Journal Publication Rights and Permissions

A.4.1 This thesis Figure 5B, 5C, 5D.

Hanna, D. A.; Harvey, R. M.; Martinez-Guzman, O.; Yuan, X.; Chandrasekharan, B.; Raju, G.; Outten, F. W.; Hamza, I.; Reddi, A. R. Heme dynamics and trafficking factors revealed by genetically encoded fluorescent heme sensors. *Proceedings of the National Academy of Sciences* **2016**, *113* (27), 7539-7544. DOI: 10.1073/pnas.1523802113.

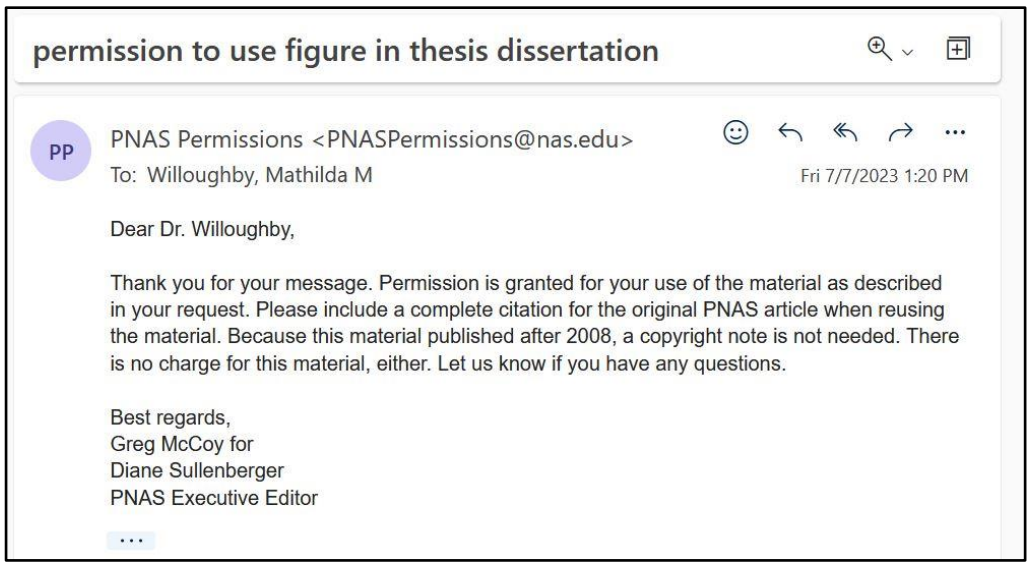

Figure 30 – Permission Correspondence with PNAS. Permission to use figure from Hanna, D., et al., PNAS, 2016 in this thesis.

A.4.2 This thesis Figure 6A, 6B, 6C, 6D, 6E.

Dietz, J. V.; Willoughby, M. M.; Piel, R. B.; Ross, T. A.; Bohovych, I.; Addis, H. G.; Fox, J. L.; Lanzilotta, W. N.; Dailey, H. A.; Wohlschlegel, J. A.; et al. Mitochondrial contact site and cristae organizing system (MICOS) machinery supports heme biosynthesis by enabling optimal performance of ferrochelatase. *Redox Biology* **2021**, *46*, 102125. DOI: https://doi.org/10.1016/j.redox.2021.102125

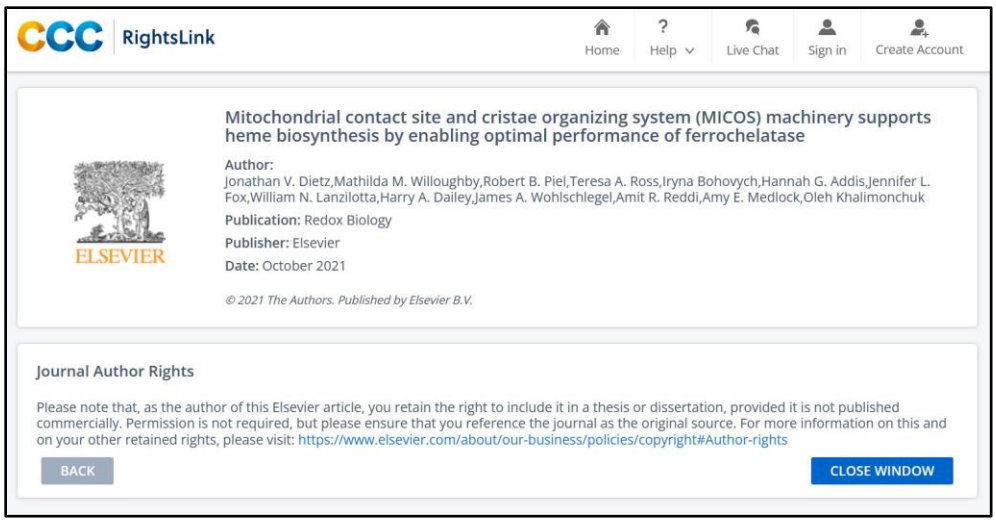

Figure 31 – Permission Correspondence with Elsevier. Permission to use figure from Dietz, J., et al., *Redox Biology*, 2021 in this thesis.

A.4.3 This thesis Figure 10A – G.

Sun, F.; Zhao, Z.; Willoughby, M. M.; Shen, S.; Zhou, Y.; Shao, Y.; Kang, J.; Chen, Y.; Chen, M.; Yuan, X.; et al. HRG-9 homologues regulate haem trafficking from haem-enriched compartments. *Nature* **2022**, *610* (7933), 768-774. DOI: 10.1038/s41586-022-05347-z.

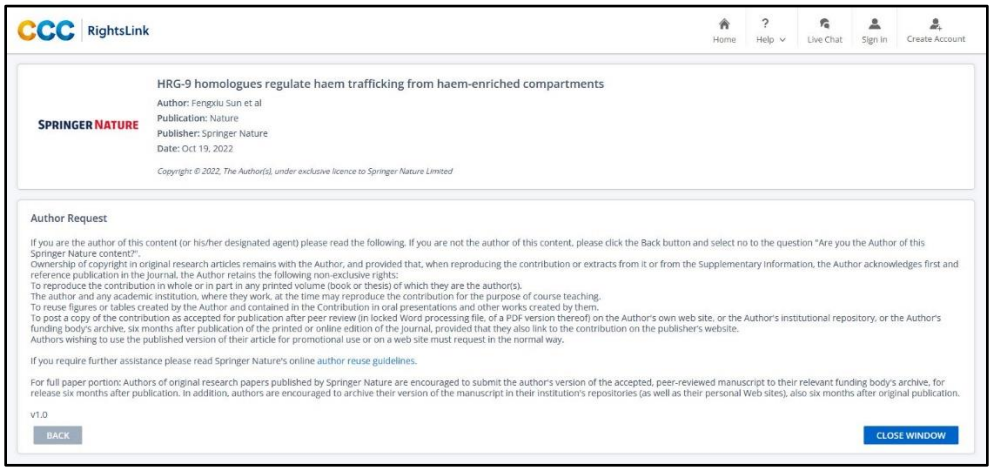

Figure 32 – Permission Correspondence with *Nature*. Permission to use figure from Sun, F., et al., *Nature*, 2022 in this thesis.

REFERENCES

(1) Chiabrando, D.; Vinchi, F.; Fiorito, V.; Mercurio, S.; Tolosano, E. Heme in pathophysiology: a matter of scavenging, metabolism and trafficking across cell membranes. *Frontiers in Pharmacology* 2014, *5*, Review.

(2) Severance, S.; Hamza, I. Trafficking of Heme and Porphyrins in Metazoa. *Chemical Reviews* 2009, *109* (10), 4596-4616. DOI: 10.1021/cr9001116.

(3) Normant, V.; Mourer, T.; Labbé, S. The major facilitator transporter Str3 is required for low-affinity heme acquisition in Schizosaccharomyces pombe. *Journal of Biological Chemistry* 2018, *293* (17), 6349-6362. DOI: https://doi.org/10.1074/jbc.RA118.002132.

(4) Sassa, S. Why Heme Needs to Be Degraded to Iron, Biliverdin IXα, and Carbon Monoxide? *Antioxidants & Redox Signaling* 2004, *6* (5), 819-824. DOI: 10.1089/ars.2004.6.819.

(5) Atamna, H.; Frey, W. H. A role for heme in Alzheimer's disease: Heme binds amyloid β and has altered metabolism. *Proceedings of the National Academy of Sciences* 2004, *101* (30), 11153-11158. DOI: 10.1073/pnas.0404349101.

(6) Atamna, H.; Boyle, K. Amyloid-β peptide binds with heme to form a peroxidase: Relationship to the cytopathologies of Alzheimer's disease. *Proceedings of the National Academy of Sciences* 2006, *103* (9), 3381-3386. DOI: 10.1073/pnas.0600134103.

(7) Kumar, S.; Bandyopadhyay, U. Free heme toxicity and its detoxification systems in human. *Toxicology Letters* 2005, *157* (3), 175-188. DOI: https://doi.org/10.1016/j.toxlet.2005.03.004.

(8) Heinemann, I. U.; Jahn, M.; Jahn, D. The biochemistry of heme biosynthesis. *Archives of Biochemistry and Biophysics* 2008,

474 (2), 238-251. DOI: https://doi.org/10.1016/j.abb.2008.02.015.

(9) Stocker, R.; Perrella, M. A. Heme Oxygenase-1. *Circulation* 2006, *114* (20), 2178-2189. DOI: 10.1161/CIRCULATIONAHA.105.598698.

(10) Reddi, A. R.; Hamza, I. Heme Mobilization in Animals: A Metallolipid's Journey. *Accounts of Chemical Research* 2016, *49* (6), 1104-1110. DOI: 10.1021/acs.accounts.5b00553.

(11) Donegan, R. K.; Moore, C. M.; Hanna, D. A.; Reddi, A. R. Handling heme: The mechanisms underlying the movement of heme within and between cells. *Free Radical Biology and Medicine* 2019, *133*, 88-100. DOI: https://doi.org/10.1016/j.freeradbiomed.2018.08.005.

(12) Piel, R. B., III; Shiferaw, M. T.; Vashisht, A. A.; Marcero, J. R.; Praissman, J. L.; Phillips, J. D.; Wohlschlegel, J. A.; Medlock, A. E. A Novel Role for Progesterone Receptor Membrane Component 1 (PGRMC1): A Partner and Regulator of Ferrochelatase. *Biochemistry* 2016, *55* (37), 5204-5217. DOI: 10.1021/acs.biochem.6b00756.

(13) Scorrano, L.; De Matteis, M. A.; Emr, S.; Giordano, F.; Hajnóczky, G.; Kornmann, B.; Lackner, L. L.; Levine, T. P.; Pellegrini, L.; Reinisch, K.; et al. Coming together to define membrane contact sites. *Nature Communications* 2019, *10* (1), 1287. DOI: 10.1038/s41467-019-09253-3.

(14) Zhang, L.; Hach, A. Molecular mechanism of heme signaling in yeast: the transcriptional activator Hap1 serves as the key mediator. *Cellular and Molecular Life Sciences CMLS* 1999, *56* (5), 415-426. DOI: 10.1007/s000180050442.

(15) Zenke-Kawasaki, Y.; Dohi, Y.; Katoh, Y.; Ikura, T.; Ikura, M.; Asahara, T.; Tokunaga, F.; Iwai, K.; Igarashi, K. Heme Induces Ubiquitination and Degradation of the Transcription Factor Bach1. *Molecular and Cellular Biology* 2007, *27* (19), 6962-6971. DOI: 10.1128/MCB.02415-06.

(16) Carter, E. L.; Gupta, N.; Ragsdale, S. W. High Affinity Heme Binding to a Heme Regulatory Motif on the Nuclear Receptor Rev-erbβ Leads to Its Degradation and Indirectly Regulates Its Interaction with Nuclear Receptor Corepressor*. *Journal of Biological Chemistry* 2016, *291* (5), 2196-2222. DOI: https://doi.org/10.1074/jbc.M115.670281.

(17) Shen, J.; Sheng, X.; Chang, Z.; Wu, Q.; Wang, S.; Xuan, Z.; Li, D.; Wu, Y.; Shang, Y.; Kong, X.; et al. Iron Metabolism Regulates p53 Signaling through Direct Heme-p53 Interaction and Modulation of p53 Localization, Stability, and Function. *Cell Reports* 2014, *7* (1), 180-193. DOI: https://doi.org/10.1016/j.celrep.2014.02.042.

(18) Khan, A. A.; Quigley, J. G. Heme and FLVCR-related transporter families SLC48 and SLC49. *Molecular Aspects of Medicine* 2013, *34* (2), 669-682. DOI: https://doi.org/10.1016/j.mam.2012.07.013.

(19) Rajagopal, A.; Rao, A. U.; Amigo, J.; Tian, M.; Upadhyay, S. K.; Hall, C.; Uhm, S.; Mathew, M. K.; Fleming, M. D.; Paw, B. H.; et al. Haem homeostasis is regulated by the conserved and concerted functions of HRG-1 proteins. *Nature* 2008, *453* (7198), 1127-1131. DOI: 10.1038/nature06934.

(20) Korolnek, T.; Hamza, I. Like iron in the blood of the people: the requirement for heme trafficking in iron metabolism. *Frontiers in Pharmacology* 2014, *5*, Review.

(21) Quigley, J. G.; Burns, C. C.; Anderson, M. M.; Lynch, E. D.; Sabo, K. M.; Overbaugh, J.; Abkowitz, J. L. Cloning of the cellular receptor for feline leukemia virus subgroup C (FeLV-C), a retrovirus that induces red cell aplasia. *Blood* 2000, *95* (3), 1093-1099. DOI: https://doi.org/10.1182/blood.V95.3.1093.003k01_1093_1099.

(22) Chiabrando, D.; Marro, S.; Mercurio, S.; Giorgi, C.; Petrillo, S.; Vinchi, F.; Fiorito, V.; Fagoonee, S.; Camporeale, A.; Turco, E.;

et al. The mitochondrial heme exporter FLVCR1b mediates erythroid differentiation. *The Journal of Clinical Investigation* 2012, *122* (12), 4569-4579. DOI: 10.1172/JCI62422.

(23) White, C.; Yuan, X.; Schmidt, Paul J.; Bresciani, E.; Samuel, Tamika K.; Campagna, D.; Hall, C.; Bishop, K.; Calicchio, Monica L.; Lapierre, A.; et al. HRG1 Is Essential for Heme Transport from the Phagolysosome of Macrophages during Erythrophagocytosis. *Cell Metabolism* 2013, *17* (2), 261-270. DOI: https://doi.org/10.1016/j.cmet.2013.01.005.

(24) Atamna, H.; Ginsburg, H. Heme Degradation in the Presence of Glutathione: A PROPOSED MECHANISM TO ACCOUNT FOR THE HIGH LEVELS OF NON-HEME IRON FOUND IN THE MEMBRANES OF HEMOGLOBINOPATHIC RED BLOOD CELLS (∗). *Journal of Biological Chemistry* 1995, *270* (42), 24876-24883. DOI: https://doi.org/10.1074/jbc.270.42.24876.

(25) Contreras, H.; Chim, N.; Credali, A.; Goulding, C. W. Heme uptake in bacterial pathogens. *Current Opinion in Chemical Biology* 2014, *19*, 34-41. DOI: https://doi.org/10.1016/j.cbpa.2013.12.014.

(26) Piel, R. B.; Dailey, H. A.; Medlock, A. E. The mitochondrial heme metabolon: Insights into the complex(ity) of heme synthesis and distribution. *Molecular Genetics and Metabolism* 2019, *128* (3), 198-203. DOI: https://doi.org/10.1016/j.ymgme.2019.01.006.

(27) Hanna, D. A.; Harvey, R. M.; Martinez-Guzman, O.; Yuan, X.; Chandrasekharan, B.; Raju, G.; Outten, F. W.; Hamza, I.; Reddi, A. R. Heme dynamics and trafficking factors revealed by genetically encoded fluorescent heme sensors. *Proceedings of the National Academy of Sciences* 2016, *113* (27), 7539-7544. DOI: 10.1073/pnas.1523802113.

(28) Taketani, S.; Adachi, Y.; Kohno, H.; Ikehara, S.; Tokunaga, R.; Ishii, T. Molecular Characterization of a Newly Identified Heme-binding Protein Induced during Differentiation of urine

Erythroleukemia Cells*. *Journal of Biological Chemistry* 1998, *273* (47), 31388-31394. DOI: https://doi.org/10.1074/jbc.273.47.31388.

(29) Immenschuh, S.; Iwahara, S.-i.; Satoh, H.; Nell, C.; Katz, N.; Muller-Eberhard, U. Expression of the mRNA of Heme-Binding Protein 23 Is Coordinated with That of Heme Oxygenase-1 by Heme and Heavy Metals in Primary Rat Hepatocytes and Hepatoma Cells. *Biochemistry* 1995, *34* (41), 13407-13411. DOI: 10.1021/bi00041a018.

(30) Sweeny, E. A.; Singh, A. B.; Chakravarti, R.; Martinez-Guzman, O.; Saini, A.; Haque, M. M.; Garee, G.; Dans, P. D.; Hannibal, L.; Reddi, A. R.; et al. Glyceraldehyde-3-phosphate dehydrogenase is a chaperone that allocates labile heme in cells. *Journal of Biological Chemistry* 2018, *293* (37), 14557-14568. DOI: https://doi.org/10.1074/jbc.RA118.004169.

(31) Kamisaka, K.; Habig, W. H.; Ketley, J. N.; Arias, I. M.; Jakoby, W. B. Multiple Forms of Human Glutathione S-Transferase and Their Affinity for Bilirubin. *European Journal of Biochemistry* 1975, *60* (1), 153-161, https://doi.org/10.1111/j.1432-1033.1975.tb20987.x. DOI: https://doi.org/10.1111/j.1432-1033.1975.tb20987.x.

(32) Vincent, S. H.; Muller-Eberhard, U. A protein of the Z class of liver cytosolic proteins in the rat that preferentially binds heme. *Journal of Biological Chemistry* 1985, *260* (27), 14521-14528. DOI: https://doi.org/10.1016/S0021-9258(17)38600-3.

(33) Hanna, D. A.; Moore, C. M.; Liu, L.; Yuan, X.; Dominic, I. M.; Fleischhacker, A. S.; Hamza, I.; Ragsdale, S. W.; Reddi, A. R. Heme oxygenase-2 (HO-2) binds and buffers labile ferric heme in human embryonic kidney cells. *Journal of Biological Chemistry* 2022, *298* (2). DOI: 10.1016/j.jbc.2021.101549.

(34) Chakravarti, R.; Aulak, K. S.; Fox, P. L.; Stuehr, D. J. GAPDH regulates cellular heme insertion into inducible nitric oxide

synthase. *Proceedings of the National Academy of Sciences* 2010, *107* (42), 18004-18009. DOI: 10.1073/pnas.1008133107.

(35) Shi, H.; Bencze, K. Z.; Stemmler, T. L.; Philpott, C. C. A Cytosolic Iron Chaperone That Delivers Iron to Ferritin. *Science* 2008, *320* (5880), 1207-1210. DOI: 10.1126/science.1157643.

(36) Kirby, K.; Jensen, L. T.; Binnington, J.; Hilliker, A. J.; Ulloa, J.; Culotta, V. C.; Phillips, J. P. Instability of Superoxide Dismutase 1 of Drosophila in Mutants Deficient for Its Cognate Copper Chaperone*. *Journal of Biological Chemistry* 2008, *283* (51), 35393-35401. DOI: https://doi.org/10.1074/jbc.M807131200.

(37) Rae, T. D.; Schmidt, P. J.; Pufahl, R. A.; Culotta, V. C.; V. O'Halloran, T. Undetectable Intracellular Free Copper: The Requirement of a Copper Chaperone for Superoxide Dismutase. *Science* 1999, *284* (5415), 805-808. DOI: 10.1126/science.284.5415.805.

(38) Galmozzi, A.; Kok, B. P.; Kim, A. S.; Montenegro-Burke, J. R.; Lee, J. Y.; Spreafico, R.; Mosure, S.; Albert, V.; Cintron-Colon, R.; Godio, C.; et al. PGRMC2 is an intracellular haem chaperone critical for adipocyte function. *Nature* 2019, *576* (7785), 138-142. DOI: 10.1038/s41586-019-1774-2.

(39) Wagener, F. A. D. T. G.; Abraham, N. G.; van Kooyk, Y.; de Witte, T.; Figdor, C. G. Heme-induced cell adhesion in the pathogenesis of sickle-cell disease and inflammation. *Trends in Pharmacological Sciences* 2001, *22* (2), 52-54. DOI: https://doi.org/10.1016/S0165-6147(00)01609-6.

(40) Lesko, S. A.; Lorentzen, R. J.; Ts'o, P. O. P. Role of superoxide in deoxyribonucleic acid strand scission. *Biochemistry* 1980, *19* (13), 3023-3028. DOI: 10.1021/bi00554a029.

(41) Pamplona, A.; Ferreira, A.; Balla, J.; Jeney, V.; Balla, G.; Epiphanio, S.; Chora, Â.; Rodrigues, C. D.; Gregoire, I. P.; Cunha-Rodrigues, M.; et al. Heme oxygenase-1 and carbon monoxide suppress the pathogenesis of experimental cerebral

malaria. *Nature Medicine* 2007, *13* (6), 703-710. DOI: 10.1038/nm1586.

(42) Larsen, R.; Gozzelino, R.; Jeney, V.; Tokaji, L.; Bozza, F. A.; Japiassú, A. M.; Bonaparte, D.; Cavalcante, M. M.; Chora, Â.; Ferreira, A.; et al. A Central Role for Free Heme in the Pathogenesis of Severe Sepsis. *Science Translational Medicine* 2010, *2* (51), 51ra71-51ra71. DOI: 10.1126/scitranslmed.3001118.

(43) Comer, J. M.; Zhang, L. Experimental Methods for Studying Cellular Heme Signaling. In *Cells*, 2018; Vol. 7.

(44) Li, X.; Wang, X.; Zhao, K.; Zhou, Z.; Zhao, C.; Yan, R.; Lin, L.; Lei, T.; Yin, J.; Wang, R.; et al. A Novel Approach for Identifying the Heme-Binding Proteins from Mouse Tissues. *Genomics, Proteomics & Bioinformatics* 2003, *1* (1), 78-86. DOI: https://doi.org/10.1016/S1672-0229(03)01011-8.

(45) Yuan, X.; Rietzschel, N.; Kwon, H.; Walter Nuno, A. B.; Hanna, D. A.; Phillips, J. D.; Raven, E. L.; Reddi, A. R.; Hamza, I. Regulation of intracellular heme trafficking revealed by subcellular reporters. *Proceedings of the National Academy of Sciences* 2016, *113* (35), E5144-E5152. DOI: 10.1073/pnas.1609865113.

(46) Kawai, K.; Hirayama, T.; Imai, H.; Murakami, T.; Inden, M.; Hozumi, I.; Nagasawa, H. Molecular Imaging of Labile Heme in Living Cells Using a Small Molecule Fluorescent Probe. *Journal of the American Chemical Society* 2022, *144* (9), 3793-3803. DOI: 10.1021/jacs.1c08485.

(47) Abshire, J. R.; Rowlands, C. J.; Ganesan, S. M.; So, P. T. C.; Niles, J. C. Quantification of labile heme in live malaria parasites using a genetically encoded biosensor. *Proceedings of the National Academy of Sciences* 2017, *114* (11), E2068-E2076. DOI: 10.1073/pnas.1615195114.

(48) Song, Y.; Yang, M.; Wegner, S. V.; Zhao, J.; Zhu, R.; Wu, Y.; He, C.; Chen, P. R. A Genetically Encoded FRET Sensor for

Intracellular Heme. *ACS Chemical Biology* 2015, *10* (7), 1610-1615. DOI: 10.1021/cb5009734.

(49) Hanna, D. A.; Hu, R.; Kim, H.; Martinez-Guzman, O.; Torres, M. P.; Reddi, A. R. Heme bioavailability and signaling in response to stress in yeast cells. *Journal of Biological Chemistry* 2018, *293* (32), 12378-12393. DOI: https://doi.org/10.1074/jbc.RA118.002125.

(50) Coronado, L. M.; Nadovich, C. T.; Spadafora, C. Malarial hemozoin: From target to tool. *Biochimica et Biophysica Acta (BBA) - General Subjects* 2014, *1840* (6), 2032-2041. DOI: https://doi.org/10.1016/j.bbagen.2014.02.009.

(51) Sun, F.; Zhao, Z.; Willoughby, M. M.; Shen, S.; Zhou, Y.; Shao, Y.; Kang, J.; Chen, Y.; Chen, M.; Yuan, X.; et al. HRG-9 homologues regulate haem trafficking from haem-enriched compartments. *Nature* 2022, *610* (7933), 768-774. DOI: 10.1038/s41586-022-05347-z.

(52) Dietz, J. V.; Willoughby, M. M.; Piel, R. B.; Ross, T. A.; Bohovych, I.; Addis, H. G.; Fox, J. L.; Lanzilotta, W. N.; Dailey, H. A.; Wohlschlegel, J. A.; et al. Mitochondrial contact site and cristae organizing system (MICOS) machinery supports heme biosynthesis by enabling optimal performance of ferrochelatase. *Redox Biology* 2021, *46*, 102125. DOI: https://doi.org/10.1016/j.redox.2021.102125.

(53) Hamza, I.; Dailey, H. A. One ring to rule them all: Trafficking of heme and heme synthesis intermediates in the metazoans. *Biochimica et Biophysica Acta (BBA) - Molecular Cell Research* 2012, *1823* (9), 1617-1632. DOI: https://doi.org/10.1016/j.bbamcr.2012.04.009.

(54) Srere, P. A. The metabolon. *Trends in Biochemical Sciences* 1985, *10* (3), 109-110. DOI: https://doi.org/10.1016/0968-0004(85)90266-X.

(55) Jørgensen, K.; Rasmussen, A. V.; Morant, M.; Nielsen, A. H.; Bjarnholt, N.; Zagrobelny, M.; Bak, S.; Møller, B. L. Metabolon

formation and metabolic channeling in the biosynthesis of plant natural products. *Current Opinion in Plant Biology* 2005, *8* (3), 280-291. DOI: https://doi.org/10.1016/j.pbi.2005.03.014.

(56) Robinson, J. B.; Srere, P. A. Organization of Krebs tricarboxylic acid cycle enzymes in mitochondria. *Journal of Biological Chemistry* 1985, *260* (19), 10800-10805. DOI: https://doi.org/10.1016/S0021-9258(19)85153-0.

(57) Campanella, M. E.; Chu, H.; Low, P. S. Assembly and regulation of a glycolytic enzyme complex on the human erythrocyte membrane. *Proceedings of the National Academy of Sciences* 2005, *102* (7), 2402-2407. DOI: 10.1073/pnas.0409741102.

(58) Cheung, C. W.; Cohen, N. S.; Raijman, L. Channeling of Urea Cycle Intermediates in Situ in Permeabilized Hepatocytes. *Journal of Biological Chemistry* 1989, *264* (7), 4038-4044. DOI: https://doi.org/10.1016/S0021-9258(19)84958-X.

(59) Deery, E.; Schroeder, S.; Lawrence, A. D.; Taylor, S. L.; Seyedarabi, A.; Waterman, J.; Wilson, K. S.; Brown, D.; Geeves, M. A.; Howard, M. J.; et al. An enzyme-trap approach allows isolation of intermediates in cobalamin biosynthesis. *Nature Chemical Biology* 2012, *8* (11), 933-940. DOI: 10.1038/nchembio.1086.

(60) Srere, P. A.; Sumegi, B. Processivity and fatty acid oxidation. *Biochemical Society Transactions* 1994, *22* (2), 446-450. DOI: 10.1042/bst0220446.

(61) Schrader, M.; Islinger, M. Editorial: Molecular mechanisms and physiological significance of organelle interactions and cooperation. *Frontiers in Cell and Developmental Biology* 2016, *4* (DEC), Editorial. DOI: 10.3389/fcell.2016.00145 Scopus.

(62) van Vliet, A. R.; Verfaillie, T.; Agostinis, P. New functions of mitochondria associated membranes in cellular signaling. *Biochimica et Biophysica Acta (BBA) - Molecular Cell Research*

2014, *1843* (10), 2253-2262. DOI: https://doi.org/10.1016/j.bbamcr.2014.03.009.

(63) Vance, J. E. MAM (mitochondria-associated membranes) in mammalian cells: Lipids and beyond. *Biochimica et Biophysica Acta (BBA) - Molecular and Cell Biology of Lipids* 2014, *1841* (4), 595-609. DOI: https://doi.org/10.1016/j.bbalip.2013.11.014.

(64) Vance, J. E. Phospholipid synthesis in a membrane fraction associated with mitochondria. *Journal of Biological Chemistry* 1990, *265* (13), 7248-7256. DOI: https://doi.org/10.1016/S0021-9258(19)39106-9.

(65) Eisenberg-Bord, M.; Shai, N.; Schuldiner, M.; Bohnert, M. A Tether Is a Tether Is a Tether: Tethering at Membrane Contact Sites. *Developmental Cell* 2016, *39* (4), 395-409. DOI: https://doi.org/10.1016/j.devcel.2016.10.022.

(66) Martinez-Guzman, O.; Willoughby, M. M.; Saini, A.; Dietz, J. V.; Bohovych, I.; Medlock, A. E.; Khalimonchuk, O.; Reddi, A. R. Mitochondrial–nuclear heme trafficking in budding yeast is regulated by GTPases that control mitochondrial dynamics and ER contact sites. *Journal of Cell Science* 2020, *133* (10), jcs237917. DOI: 10.1242/jcs.237917.

(67) Eisenberg-Bord, M.; Zung, N.; Collado, J.; Drwesh, L.; Fenech, E. J.; Fadel, A.; Dezorella, N.; Bykov, Y. S.; Rapaport, D.; Fernandez-Busnadiego, R.; et al. Cnm1 mediates nucleus–mitochondria contact site formation in response to phospholipid levels. *Journal of Cell Biology* 2021, *220* (11), e202104100. DOI: 10.1083/jcb.202104100.

(68) Bard, F.; Casano, L.; Mallabiabarrena, A.; Wallace, E.; Saito, K.; Kitayama, H.; Guizzunti, G.; Hu, Y.; Wendler, F.; DasGupta, R.; et al. Functional genomics reveals genes involved in protein secretion and Golgi organization. *Nature* 2006, *439* (7076), 604-607. DOI: 10.1038/nature04377.

(69) Mingirulli, N.; Pyle, A.; Hathazi, D.; Alston, C. L.; Kohlschmidt, N.; O'Grady, G.; Waddell, L.; Evesson, F.; Cooper, S. B. T.; Turner, C.; et al. Clinical presentation and proteomic signature of patients with TANGO2 mutations. *Journal of Inherited Metabolic Disease* 2020, *43* (2), 297-308, https://doi.org/10.1002/jimd.12156. DOI: https://doi.org/10.1002/jimd.12156.

(70) Friedman, J. R.; Mourier, A.; Yamada, J.; McCaffery, J. M.; Nunnari, J. MICOS coordinates with respiratory complexes and lipids to establish mitochondrial inner membrane architecture. *eLife* 2015, *4*, e07739. DOI: 10.7554/eLife.07739.

(71) Kozjak-Pavlovic, V. The MICOS complex of human mitochondria. *Cell and Tissue Research* 2017, *367* (1), 83-93. DOI: 10.1007/s00441-016-2433-7.

(72) Pfanner, N.; van der Laan, M.; Amati, P.; Capaldi, R. A.; Caudy, A. A.; Chacinska, A.; Darshi, M.; Deckers, M.; Hoppins, S.; Icho, T.; et al. Uniform nomenclature for the mitochondrial contact site and cristae organizing system. *Journal of Cell Biology* 2014, *204* (7), 1083-1086. DOI: 10.1083/jcb.201401006.

(73) Aaltonen, M. J.; Friedman, J. R.; Osman, C.; Salin, B.; di Rago, J.-P.; Nunnari, J.; Langer, T.; Tatsuta, T. MICOS and phospholipid transfer by Ups2–Mdm35 organize membrane lipid synthesis in mitochondria. *Journal of Cell Biology* 2016, *213* (5), 525-534. DOI: 10.1083/jcb.201602007.

(74) Subramanian, K.; Jochem, A.; Le Vasseur, M.; Lewis, S.; Paulson, B. R.; Reddy, T. R.; Russell, J. D.; Coon, J. J.; Pagliarini, D. J.; Nunnari, J. Coenzyme Q biosynthetic proteins assemble in a substrate-dependent manner into domains at ER–mitochondria contacts. *Journal of Cell Biology* 2019, *218* (4), 1353-1369. DOI: 10.1083/jcb.201808044.

(75) Stephan, T.; Brüser, C.; Deckers, M.; Steyer, A. M.; Balzarotti, F.; Barbot, M.; Behr, T. S.; Heim, G.; Hübner, W.; Ilgen, P.; et al. MICOS assembly controls mitochondrial inner membrane

remodeling and crista junction redistribution to mediate cristae formation. *The EMBO Journal* 2020, *39* (14), e104105, DOI: https://doi.org/10.15252/embj.2019104105.

(76) Hughes, A. L.; Powell, D. W.; Bard, M.; Eckstein, J.; Barbuch, R.; Link, A. J.; Espenshade, P. J. Dap1/PGRMC1 Binds and Regulates Cytochrome P450 Enzymes. *Cell Metabolism* 2007, *5* (2), 143-149. DOI: https://doi.org/10.1016/j.cmet.2006.12.009.

(77) Mallory, J. C.; Crudden, G.; Johnson, B. L.; Mo, C.; Pierson, C. A.; Bard, M.; Craven, R. J. Dap1p, a Heme-Binding Protein That Regulates the Cytochrome P450 Protein Erg11p/Cyp51p in Saccharomyces cerevisiae. *Molecular and Cellular Biology* 2005, *25* (5), 1669-1679. DOI: 10.1128/MCB.25.5.1669-1679.2005.

(78) Hand Randal, A.; Jia, N.; Bard, M.; Craven Rolf, J. Saccharomyces cerevisiae Dap1p, a Novel DNA Damage Response Protein Related to the Mammalian Membrane-Associated Progesterone Receptor. *Eukaryotic Cell* 2003, *2* (2), 306-317. DOI: 10.1128/ec.2.2.306-317.2003.

(79) Ikhlas, S. A.; Hannah, J. R.; Katherine, E. T.; Marlene, N. M.; Rolf, J. C. Progesterone Receptor Membrane Component 1 (Pgrmc1): A Heme-1 Domain Protein That Promotes Tumorigenesis and Is Inhibited by a Small Molecule. *Journal of Pharmacology and Experimental Therapeutics* 2010, *333* (2), 564. DOI: 10.1124/jpet.109.164210.

(80) Craven, R. J.; Mallory, J. C.; Hand, R. A. Regulation of Iron Homeostasis Mediated by the Heme-binding Protein Dap1 (Damage Resistance Protein 1) via the P450 Protein Erg11/Cyp51*. *Journal of Biological Chemistry* 2007, *282* (50), 36543-36551. DOI: https://doi.org/10.1074/jbc.M706770200.

(81) Li, X.; Rhee, D. K.; Malhotra, R.; Mayeur, C.; Hurst, L. A.; Ager, E.; Shelton, G.; Kramer, Y.; McCulloh, D.; Keefe, D.; et al. Progesterone receptor membrane component-1 regulates

hepcidin biosynthesis. *The Journal of Clinical Investigation* 2016, *126* (1), 389-401. DOI: 10.1172/JCI83831.

(82) Ghosh, K.; Thompson, A. M.; Goldbeck, R. A.; Shi, X.; Whitman, S.; Oh, E.; Zhiwu, Z.; Vulpe, C.; Holman, T. R. Spectroscopic and Biochemical Characterization of Heme Binding to Yeast Dap1p and Mouse PGRMC1p. *Biochemistry* 2005, *44* (50), 16729-16736. DOI: 10.1021/bi0511585.

(83) Kaluka, D.; Batabyal, D.; Chiang, B.-Y.; Poulos, T. L.; Yeh, S.-R. Spectroscopic and Mutagenesis Studies of Human PGRMC1. *Biochemistry* 2015, *54* (8), 1638-1647. DOI: 10.1021/bi501177e.

(84) Shingo, O.; Miki, N.; Yasuyuki, T.; Tatsuki, F.; Tsuyoshi, Y. Progesterone Receptor Membrane Component 1 Modulates Human Cytochrome P450 Activities in an Isoform-Dependent Manner. *Drug Metabolism and Disposition* 2011, *39* (11), 2057. DOI: 10.1124/dmd.111.040907.

(85) Thompson, A. M.; Reddi, A. R.; Shi, X.; Goldbeck, R. A.; Moënne-Loccoz, P.; Gibney, B. R.; Holman, T. R. Measurement of the Heme Affinity for Yeast Dap1p, and Its Importance in Cellular Function. *Biochemistry* 2007, *46* (50), 14629-14637. DOI: 10.1021/bi7013739.

(86) Elbaz-Alon, Y.; Rosenfeld-Gur, E.; Shinder, V.; Futerman, Anthony H.; Geiger, T.; Schuldiner, M. A Dynamic Interface between Vacuoles and Mitochondria in Yeast. *Developmental Cell* 2014, *30* (1), 95-102. DOI: https://doi.org/10.1016/j.devcel.2014.06.007.

(87) Lahiri, S.; Chao, J. T.; Tavassoli, S.; Wong, A. K. O.; Choudhary, V.; Young, B. P.; Loewen, C. J. R.; Prinz, W. A. A Conserved Endoplasmic Reticulum Membrane Protein Complex (EMC) Facilitates Phospholipid Transfer from the ER to Mitochondria. *PLOS Biology* 2014, *12* (10), e1001969. DOI: 10.1371/journal.pbio.1001969.

(88) Kornmann, B.; Currie, E.; Collins, S. R.; Schuldiner, M.; Nunnari, J.; Weissman, J. S.; Walter, P. An ER-Mitochondria Tethering Complex Revealed by a Synthetic Biology Screen. *Science* 2009, *325* (5939), 477-481. DOI: 10.1126/science.1175088.

(89) Lackner, L. L. The Expanding and Unexpected Functions of Mitochondria Contact Sites. *Trends in Cell Biology* 2019, *29* (7), 580-590. DOI: https://doi.org/10.1016/j.tcb.2019.02.009.

(90) Murley, A.; Nunnari, J. The Emerging Network of Mitochondria-Organelle Contacts. *Molecular Cell* 2016, *61* (5), 648-653. DOI: https://doi.org/10.1016/j.molcel.2016.01.031.

(91) Xue, Y.; Schmollinger, S.; Attar, N.; Campos, O. A.; Vogelauer, M.; Carey, M. F.; Merchant, S. S.; Kurdistani, S. K. Endoplasmic reticulum–mitochondria junction is required for iron homeostasis. *Journal of Biological Chemistry* 2017, *292* (32), 13197-13204. DOI: https://doi.org/10.1074/jbc.M117.784249.

(92) Desai, R.; East, D. A.; Hardy, L.; Faccenda, D.; Rigon, M.; Crosby, J.; Alvarez, M. S.; Singh, A.; Mainenti, M.; Hussey, L. K.; et al. Mitochondria form contact sites with the nucleus to couple prosurvival retrograde response. *Science Advances 6* (51), eabc9955. DOI: 10.1126/sciadv.abc9955.

(93) Heiman, P.; Mohsen, A.-W.; Karunanidhi, A.; St Croix, C.; Watkins, S.; Koppes, E.; Haas, R.; Vockley, J.; Ghaloul-Gonzalez, L. Mitochondrial dysfunction associated with TANGO2 deficiency. *Scientific Reports* 2022, *12* (1), 3045. DOI: 10.1038/s41598-022-07076-9.

(94) Lalani, Seema R.; Liu, P.; Rosenfeld, Jill A.; Watkin, Levi B.; Chiang, T.; Leduc, Magalie S.; Zhu, W.; Ding, Y.; Pan, S.; Vetrini, F.; et al. Recurrent Muscle Weakness with Rhabdomyolysis, Metabolic Crises, and Cardiac Arrhythmia Due to Bi-allelic TANGO2 Mutations. *The American Journal of Human Genetics* 2016, *98* (2), 347-357. DOI: https://doi.org/10.1016/j.ajhg.2015.12.008.

(95) Kremer, Laura S.; Distelmaier, F.; Alhaddad, B.; Hempel, M.; Iuso, A.; Küpper, C.; Mühlhausen, C.; Kovacs-Nagy, R.; Satanovskij, R.; Graf, E.; et al. Bi-allelic Truncating Mutations in TANGO2 Cause Infancy-Onset Recurrent Metabolic Crises with Encephalocardiomyopathy. *The American Journal of Human Genetics* 2016, *98* (2), 358-362. DOI: https://doi.org/10.1016/j.ajhg.2015.12.009.

(96) Milev, M. P.; Saint-Dic, D.; Zardoui, K.; Klopstock, T.; Law, C.; Distelmaier, F.; Sacher, M. The phenotype associated with variants in TANGO2 may be explained by a dual role of the protein in ER-to-Golgi transport and at the mitochondria. *Journal of Inherited Metabolic Disease* 2021, *44* (2), 426-437, DOI: https://doi.org/10.1002/jimd.12312.

(97) Powell, A. R.; Ames, E. G.; Knierbein, E. N.; Hannibal, M. C.; Mackenzie, S. J. Symptom Prevalence and Genotype-Phenotype Correlations in Patients With TANGO2-Related Metabolic Encephalopathy and Arrhythmias (TRMEA). *Pediatric Neurology* 2021, *119*, 34-39. DOI: https://doi.org/10.1016/j.pediatrneurol.2021.02.011.

(98) Asadi, P.; Milev, M. P.; Saint-Dic, D.; Gamberi, C.; Sacher, M. Vitamin B5, a coenzyme A precursor, rescues TANGO2 deficiency disease-associated defects in Drosophila and human cells. *Journal of Inherited Metabolic Disease* 2023, *46* (2), 358-368, DOI: https://doi.org/10.1002/jimd.12579.

(99) Jennions, E.; Hedberg-Oldfors, C.; Berglund, A.-K.; Kollberg, G.; Törnhage, C.-J.; Eklund, E. A.; Oldfors, A.; Verloo, P.; Vanlander, A. V.; De Meirleir, L.; et al. TANGO2 deficiency as a cause of neurodevelopmental delay with indirect effects on mitochondrial energy metabolism. *Journal of Inherited Metabolic Disease* 2019, *42* (5), 898-908, DOI: https://doi.org/10.1002/jimd.12149.

(100) Maynard, T. M.; Meechan, D. W.; Dudevoir, M. L.; Gopalakrishna, D.; Peters, A. Z.; Heindel, C. C.; Sugimoto, T. J.;

Wu, Y.; Lieberman, J. A.; LaMantia, A. S. Mitochondrial localization and function of a subset of 22q11 deletion syndrome candidate genes. *Molecular and Cellular Neuroscience* 2008, *39* (3), 439-451. DOI: https://doi.org/10.1016/j.mcn.2008.07.027.

(101) Gietz, R. D.; Schiestl, R. H. Applications of high efficiency lithium acetate transformation of intact yeast cells using single-stranded nucleic acids as carrier. *Yeast* 1991, *7* (3), 253-263, DOI: https://doi.org/10.1002/yea.320070307.

(102) Ness, F.; Achstetter, T.; Duport, C.; Karst, F.; Spagnoli, R.; Degryse, E. Sterol Uptake in Saccharomyces cerevisiae Heme Auxotrophic Mutants Is Affected by Ergosterol and Oleate but Not by Palmitoleate or by Sterol Esterification. *Journal of Bacteriology* 1998, *180* (7), 1913-1919. DOI: 10.1128/jb.180.7.1913-1919.1998.

(103) Michener, J. K.; Nielsen, J.; Smolke, C. D. Identification and treatment of heme depletion attributed to overexpression of a lineage of evolved P450 monooxygenases. *Proceedings of the National Academy of Sciences* 2012, *109* (47), 19504-19509. DOI: 10.1073/pnas.1212287109.

(104) Baureder, M.; Hederstedt, L. Genes Important for Catalase Activity in Enterococcus faecalis. *PLOS ONE* 2012, *7* (5), e36725. DOI: 10.1371/journal.pone.0036725.

(105) Hanker Jacob, S.; Rabin Albert, N. Color Reaction Streak Test for Catalase-Positive Microorganisms. *Journal of Clinical Microbiology* 1975, *2* (5), 463-464. DOI: 10.1128/jcm.2.5.463-464.1975.

(106) Espinosa, J. n. M.; Verdun, R. E.; Emerson, B. M. p53 Functions through Stress- and Promoter-Specific Recruitment of Transcription Initiation Components before and after DNA Damage. *Molecular Cell* 2003, *12* (4), 1015-1027. DOI: https://doi.org/10.1016/S1097-2765(03)00359-9.

(107) Kastan, M. B.; Onyekwere, O.; Sidransky, D.; Vogelstein, B.; Craig, R. W. Participation of p53 Protein in the Cellular Response to DNA Damage1. *Cancer Research* 1991, *51* (23_Part_1), 6304-6311.

(108) Yin, L.; Wu, N.; Curtin, J. C.; Qatanani, M.; Szwergold, N. R.; Reid, R. A.; Waitt, G. M.; Parks, D. J.; Pearce, K. H.; Wisely, G. B.; et al. Rev-erbα, a Heme Sensor That Coordinates Metabolic and Circadian Pathways. *Science* 2007, *318* (5857), 1786-1789. DOI: 10.1126/science.1150179.

(109) Gibbs, J. E.; Blaikley, J.; Beesley, S.; Matthews, L.; Simpson, K. D.; Boyce, S. H.; Farrow, S. N.; Else, K. J.; Singh, D.; Ray, D. W.; et al. The nuclear receptor REV-ERBα mediates circadian regulation of innate immunity through selective regulation of inflammatory cytokines. *Proceedings of the National Academy of Sciences* 2012, *109* (2), 582-587. DOI: 10.1073/pnas.1106750109.

(110) Chandra, V.; Mahajan, S.; Saini, A.; Dkhar, H. K.; Nanduri, R.; Raj, E. B.; Kumar, A.; Gupta, P. Human IL10 Gene Repression by Rev-erbα Ameliorates Mycobacterium tuberculosis Clearance*. *Journal of Biological Chemistry* 2013, *288* (15), 10692-10702. DOI: https://doi.org/10.1074/jbc.M113.455915.

(111) Giaever, G.; Nislow, C. The Yeast Deletion Collection: A Decade of Functional Genomics. *Genetics* 2014, *197* (2), 451-465. DOI: 10.1534/genetics.114.161620.

(112) Gietz, R. D.; Woods, R. A. Genetic Transformation of Yeast. *BioTechniques* 2001, *30* (4), 816-831. DOI: 10.2144/01304rv02.

(113) Martinez-Guzman, O. PROBING HEME TRAFFICKING USING GENETICALLY ENCODED

FLUORESCENT HEME SENSORS. Georgia Institute of Technology, 2019.

(114) Oskolkova; Leitner; Kohlwein. Yeast Protein Localization Plus Database. personal communication.
(115) Bertram, P. G.; Zeng, C.; Thorson, J.; Shaw, A. S.; Zheng, X. F. S. The 14-3-3 proteins positively regulate rapamycin-sensitive signaling. *Current Biology* 1998, *8* (23), 1259-S1251. DOI: https://doi.org/10.1016/S0960-9822(07)00535-0.
(116) Barbet, N. C.; Schneider, U.; Helliwell, S. B.; Stansfield, I.; Tuite, M. F.; Hall, M. N. TOR controls translation initiation and early G1 progression in yeast. *Molecular Biology of the Cell* 1996, *7* (1), 25-42. DOI: 10.1091/mbc.7.1.25.
(117) Stan, R.; McLaughlin, M. M.; Cafferkey, R.; Johnson, R. K.; Rosenberg, M.; Livi, G. P. Interaction between FKBP12-rapamycin and TOR involves a conserved serine residue. *Journal of Biological Chemistry* 1994, *269* (51), 32027-32030. DOI: https://doi.org/10.1016/S0021-9258(18)31592-8.
(118) Zheng, X.-F.; Fiorentino, D.; Chen, J.; Crabtree, G. R.; Schreiber, S. L. TOR kinase domains are required for two distinct functions, only one of which is inhibited by rapamycin. *Cell* 1995, *82* (1), 121-130. DOI: https://doi.org/10.1016/0092-8674(95)90058-6.
(119) Tinkelenberg, A. H.; Liu, Y.; Alcantara, F.; Khan, S.; Guo, Z.; Bard, M.; Sturley, S. L. Mutations in Yeast ARV1 Alter Intracellular Sterol Distribution and Are Complemented by Human ARV1*. *Journal of Biological Chemistry* 2000, *275* (52), 40667-40670. DOI: 10.1074/jbc.C000710200.
(120) Brandriss, M. C.; Magasanik, B. Genetics and physiology of proline utilization in Saccharomyces cerevisiae: enzyme induction by proline. *Journal of Bacteriology* 1979, *140* (2), 498-503. DOI: 10.1128/jb.140.2.498-503.1979.
(121) Brandriss, M. C. Evidence for Positive Regulation of the Proline Utilization Pathway in Saccharomyces cerevisiae. *Genetics* 1987, *117* (3), 429-435. DOI: 10.1093/genetics/117.3.429.

(122) Teng, X.; Hardwick, J. M. Genome evolution in yeast reveals connections between rare mutations in human cancers. *Microb Cell* 2014, *1* (6), 206-209. DOI: 10.15698/mic2014.06.153 From NLM.
(123) Gietz, R. D.; Schiestl, R. H. Microtiter plate transformation using the LiAc/SS carrier DNA/PEG method. *Nature Protocols* 2007, *2* (1), 5-8. DOI: 10.1038/nprot.2007.16.
(124) Liu, G.; Lanham, C.; Buchan, J. R.; Kaplan, M. E. High-throughput transformation of Saccharomyces cerevisiae using liquid handling robots. *PLOS ONE* 2017, *12* (3), e0174128. DOI: 10.1371/journal.pone.0174128.
(125) Sawicki, K. T.; Chang, H. C.; Ardehali, H. Role of Heme in Cardiovascular Physiology and Disease. *Journal of the American Heart Association* 2015, *4* (1), e001138. DOI: 10.1161/JAHA.114.001138.
(126) Bastide, N. M.; Pierre, F. H. F.; Corpet, D. E. Heme Iron from Meat and Risk of Colorectal Cancer: A Meta-analysis and a Review of the Mechanisms Involved. *Cancer Prevention Research* 2011, *4* (2), 177-184. DOI: 10.1158/1940-6207.CAPR-10-0113.
(127) Chambers, I. G.; Willoughby, M. M.; Hamza, I.; Reddi, A. R. One ring to bring them all and in the darkness bind them: The trafficking of heme without deliverers. *Biochimica et Biophysica Acta (BBA) - Molecular Cell Research* 2021, *1868* (1), 118881. DOI: https://doi.org/10.1016/j.bbamcr.2020.118881.
(128) Medlock, A. E.; Shiferaw, M. T.; Marcero, J. R.; Vashisht, A. A.; Wohlschlegel, J. A.; Phillips, J. D.; Dailey, H. A. Identification of the Mitochondrial Heme Metabolism Complex. *PLOS ONE* 2015, *10* (8), e0135896. DOI: 10.1371/journal.pone.0135896.
(129) Pfeifer, K.; Kim, K.-S.; Kogan, S.; Guarente, L. Functional dissection and sequence of yeast HAP1 activator. *Cell* 1989, *56*

(2), 291-301. DOI: https://doi.org/10.1016/0092-8674(89)90903-3.
(130) Hach, A.; Hon, T.; Zhang, L. A New Class of Repression Modules Is Critical for Heme Regulation of the Yeast Transcriptional Activator Hap1. *Molecular and Cellular Biology* 1999, *19* (6), 4324-4333. DOI: 10.1128/MCB.19.6.4324.
(131) Zhang, L.; Hach, A.; Wang, C. Molecular Mechanism Governing Heme Signaling in Yeast: a Higher-Order Complex Mediates Heme Regulation of the Transcriptional Activator HAP1. *Molecular and Cellular Biology* 1998, *18* (7), 3819-3828. DOI: 10.1128/MCB.18.7.3819.
(132) Zhang, L.; Guarente, L. The C6 zinc cluster dictates asymmetric binding by HAP1. *The EMBO Journal* 1996, *15* (17), 4676-4681, DOI: https://doi.org/10.1002/j.1460-2075.1996.tb00844.x.
(133) Zhang, L.; Guarente, L. HAP1 is nuclear but is bound to a cellular factor in the absence of heme. *Journal of Biological Chemistry* 1994, *269* (20), 14643-14647. DOI: https://doi.org/10.1016/S0021-9258(17)36673-5.
(134) Creusot, F.; Verdière, J.; Gaisne, M.; Slonimski, P. P. CYP1 (HAP1) regulator of oxygen-dependent gene expression in yeast: I. Overall organization of the protein sequence displays several novel structural domains. *Journal of Molecular Biology* 1988, *204* (2), 263-276. DOI: https://doi.org/10.1016/0022-2836(88)90574-8.
(135) Hon, T.; Hach, A.; Lee, H. C.; Cheng, T.; Zhang, L. Functional Analysis of Heme Regulatory Elements of the Transcriptional Activator Hap1. *Biochemical and Biophysical Research Communications* 2000, *273* (2), 584-591. DOI: https://doi.org/10.1006/bbrc.2000.2995.
(136) Hon, T.; Hach, A.; Tamalis, D.; Zhu, Y.; Zhang, L. The Yeast Heme-responsive Transcriptional Activator Hap1 Is a Preexisting Dimer in the Absence of Heme*. *Journal of*

Biological Chemistry 1999, *274* (32), 22770-22774. DOI: https://doi.org/10.1074/jbc.274.32.22770.

(137) Lee, H. C.; Hon, T.; Lan, C.; Zhang, L. Structural Environment Dictates the Biological Significance of Heme-Responsive Motifs and the Role of Hsp90 in the Activation of the Heme Activator Protein Hap1. *Molecular and Cellular Biology* 2003, *23* (16), 5857-5866. DOI: 10.1128/MCB.23.16.5857-5866.2003.

(138) Mense, S. M.; Zhang, L. Heme: a versatile signaling molecule controlling the activities of diverse regulators ranging from transcription factors to MAP kinases. *Cell Research* 2006, *16* (8), 681-692. DOI: 10.1038/sj.cr.7310086.

(139) Becerra, M.; Lombardía-Ferreira, L. J.; Hauser, N. C.; Hoheisel, J. D.; Tizon, B.; Cerdán, M. E. The yeast transcriptome in aerobic and hypoxic conditions: effects of hap1, rox1, rox3 and srb10 deletions. *Molecular Microbiology* 2002, *43* (3), 545-555, DOI: https://doi.org/10.1046/j.1365-2958.2002.02724.x.

(140) Kwast, K. E.; Burke, P. V.; Poyton, R. O. Oxygen Sensing and the Transcriptional Regulation of Oxygen-Responsive Genes in Yeast. *Journal of Experimental Biology* 1998, *201* (8), 1177-1195. DOI: 10.1242/jeb.201.8.1177.

(141) Ter Linde, J. J. M.; Steensma, H. Y. A microarray-assisted screen for potential Hap1 and Rox1 target genes in Saccharomyces cerevisiae. *Yeast* 2002, *19* (10), 825-840, DOI: https://doi.org/10.1002/yea.879.

(142) Hickman, M. J.; Winston, F. Heme Levels Switch the Function of Hap1 of Saccharomyces cerevisiae between Transcriptional Activator and Transcriptional Repressor. *Molecular and Cellular Biology* 2007, *27* (21), 7414-7424. DOI: 10.1128/MCB.00887-07.

(143) Harbison, C. T.; Gordon, D. B.; Lee, T. I.; Rinaldi, N. J.; Macisaac, K. D.; Danford, T. W.; Hannett, N. M.; Tagne, J.-B.; Reynolds, D. B.; Yoo, J.; et al. Transcriptional regulatory code of a eukaryotic

genome. *Nature* 2004, *431* (7004), 99-104. DOI: 10.1038/nature02800.

(144) Teixeira, M. C.; Viana, R.; Palma, M.; Oliveira, J.; Galocha, M.; Mota, M. N.; Couceiro, D.; Pereira, M. G.; Antunes, M.; Costa, I. V.; et al. YEASTRACT+: a portal for the exploitation of global transcription regulation and metabolic model data in yeast biotechnology and pathogenesis. *Nucleic Acids Research* 2023, *51* (D1), D785-D791. DOI: 10.1093/nar/gkac1041.

(145) Hon, T.; Lee, H. C.; Hu, Z.; Iyer, V. R.; Zhang, L. The Heme Activator Protein Hap1 Represses Transcription by a Heme-Independent Mechanism in Saccharomyces cerevisiae. *Genetics* 2005, *169* (3), 1343-1352. DOI: 10.1534/genetics.104.037143.

(146) Zhu, H.; Riggs, A. F. Yeast Flavohemoglobin is an Ancient Protein Related to Globins and a Reductase Family. *Proceedings of the National Academy of Sciences of the United States of America* 1992, *89* (11), 5015-5019.

(147) Zhao, X.-J.; Raitt, D.; Burke, P. V.; Clewell, A. S.; Kwast, K. E.; Poyton, R. O. Function and Expression of Flavohemoglobin in Saccharomyces cerevisiae: EVIDENCE FOR A ROLE IN THE OXIDATIVE STRESS RESPONSE*. *Journal of Biological Chemistry* 1996, *271* (41), 25131-25138. DOI: https://doi.org/10.1074/jbc.271.41.25131.

(148) Liu, L.; Zeng, M.; Hausladen, A.; Heitman, J.; Stamler, J. S. Protection from nitrosative stress by yeast flavohemoglobin. *Proceedings of the National Academy of Sciences* 2000, *97* (9), 4672-4676. DOI: 10.1073/pnas.090083597.

(149) Dastoor, Z.; Dreyer, J.-L. Potential role of nuclear translocation of glyceraldehyde-3-phosphate dehydrogenase in apoptosis and oxidative stress. *Journal of Cell Science* 2001, *114* (9), 1643-1653. DOI: 10.1242/jcs.114.9.1643.

(150) Zheng, L.; Roeder, R. G.; Luo, Y. S Phase Activation of the Histone H2B Promoter by OCA-S, a Coactivator Complex that

Contains GAPDH as a Key Component. *Cell* 2003, *114* (2), 255-266. DOI: https://doi.org/10.1016/S0092-8674(03)00552-X.

(151) Sundararaj, K. P.; Wood, R. E.; Ponnusamy, S.; Salas, A. M.; Szulc, Z.; Bielawska, A.; Obeid, L. M.; Hannun, Y. A.; Ogretmen, B. Rapid Shortening of Telomere Length in Response to Ceramide Involves the Inhibition of Telomere Binding Activity of Nuclear Glyceraldehyde-3-phosphate Dehydrogenase*. *Journal of Biological Chemistry* 2004, *279* (7), 6152-6162. DOI: https://doi.org/10.1074/jbc.M310549200.

(152) Gaisne, M.; Bécam, A. M.; Verdière, J.; Herbert, C. J. A 'natural' mutation in Saccharomyces cerevisiae strains derived from S288c affects the complex regulatory gene HAP1 (CYP1). *Current Genetics* 1999, *36* (4), 195-200. DOI: 10.1007/s002940050490.

(153) Kathiresan, M.; Martins, D.; English, A. M. Respiration triggers heme transfer from cytochrome c peroxidase to catalase in yeast mitochondria. *Proceedings of the National Academy of Sciences* 2014, *111* (49), 17468-17473. DOI: 10.1073/pnas.1409692111.

Vita

Mathilda Marie Willoughby was born April 18, 1995 in Fuzhou, China. She was adopted by Ross and Mary Ellen Willoughby at the age of eight months, and grew up in Pittsburgh, PA. In September 2013, she started undergraduate studies at Westminster College in New Wilmington, PA, where she received a B.S. degree in Biochemistry in May 2017.

During her undergraduate career, she conducted summer research in 2015 at the University of Delaware under Professor Sharon Rozovsky, and in 2017 at the Georgia Institute of Technology under Professor Loren Williams.

In the fall of 2017, she entered the Georgia Institute of Technology and was appointed as a Graduate Teaching Assistant for the undergraduate biochemistry II labs, under the direction of Dr. Mary Peek.

In January 2018, she met Matthew Richardson of Philadelphia, PA and they wed in September 2022 in New Wilmington, PA.

In June 2023, she accepted a Post Doctoral position at the University of Nebraska Medical Center in the lab of Professor Micah Schott in Omaha, Nebraska.